

# **Guidelines to achieving high selectivity for the hydrogenation of $\alpha,\beta$ -unsaturated aldehydes with bimetallic and dilute alloy catalysts**

**– A review**

Mathilde Luneau,<sup>†,a</sup> Jin Soo Lim,<sup>†,a</sup> Dipna A. Patel,<sup>‡,a</sup>

E. Charles H. Sykes,<sup>‡</sup> Cynthia M. Friend,<sup>†</sup> and Philippe Sautet<sup>\*,¶§</sup>

<sup>†</sup> Department of Chemistry and Chemical Biology, Harvard University, Cambridge, MA 02138, USA

<sup>‡</sup> Department of Chemistry, Tufts University, Medford, MA 02155, USA

<sup>¶</sup> Department of Chemical and Biomolecular Engineering, University of California, Los Angeles, Los Angeles, CA 90095, USA

<sup>§</sup> Department of Chemistry and Biochemistry, University of California, Los Angeles, Los Angeles, CA 90095, USA

\* Email: [sautet@ucla.edu](mailto:sautet@ucla.edu)

---

<sup>a</sup> These three authors contributed equally to this review.

## Abstract

Selective hydrogenation of  $\alpha,\beta$ -unsaturated aldehydes to unsaturated alcohols is a challenging class of reactions, yielding valuable intermediates for the production of pharmaceuticals, perfumes, and flavorings. On monometallic heterogeneous catalysts, the formation of the unsaturated alcohols is thermodynamically disfavored over the saturated aldehydes. Hence, new catalysts are required to achieve the desired selectivity. Herein, the literature of three major research areas in catalysis is integrated as a step toward establishing the guidelines for enhancing the selectivity: reactor studies of complex catalyst materials at operating temperature and pressure; surface science studies of crystalline surfaces in ultrahigh vacuum; and first-principles modeling using density functional theory calculations. Aggregate analysis shows that bimetallic and dilute alloy catalysts significantly enhance the selectivity to the unsaturated alcohols compared to monometallic catalysts. This comprehensive review focuses primarily on the role of different metal surfaces as well as the factors that promote the adsorption of the unsaturated aldehyde via its C=O bond, most notably by electronic modification of the surface and formation of the electrophilic sites. Furthermore, challenges, gaps, and opportunities are identified to advance the rational design of efficient catalysts for this class of reactions, including the need for systematic studies of catalytic processes, theoretical modeling of complex materials, and model studies under ambient pressure and temperature.

## **Table of Contents**

1. Introduction
2. Experiment overview
  - 2.1. Major strategies for selectivity enhancement
3. Theory overview
  - 3.1. Categories of DFT investigations
  - 3.2. Limitations of DFT modeling
  - 3.3. Major trends in thermodynamics and kinetics
    - 3.3.1. Adsorption and reactivity
    - 3.3.2. Hydrogenation mechanism
    - 3.3.3. Furfural reduction
4. Discussions
  - 4.1. Active electronegative metals
    - 4.1.1. Pt and Pt alloys
      - 4.1.1.1. Electrophilic sites from promoters
      - 4.1.1.2. Electron transfer to Pt
      - 4.1.1.3. Concurrent electron transfer and electrophilic site formation
    - 4.1.2. Ru and Ru alloys
      - 4.1.2.1. Concurrent electron transfer and electrophilic site formation
      - 4.1.2.2. Ru as the Lewis acid site
    - 4.1.3. Ir and Ir alloys
      - 4.1.3.1. Electrophilic sites from promoters

- 4.1.3.2. Other effects
  - 4.1.4. Rh and Rh alloys
    - 4.1.4.1. Concurrent electron transfer and electrophilic site formation
  - 4.1.5. Pd and Pd alloys
    - 4.1.5.1. Concurrent electron transfer and electrophilic site formation
    - 4.1.5.2. Other effects
- 4.2. Active electropositive metals
  - 4.2.1. Co and Co alloys
    - 4.2.1.1. Electron transfer from Co
  - 4.2.2. Ni and Ni alloys
    - 4.2.2.1. Electron transfer to Ni
    - 4.2.2.2. Concurrent electron transfer and other effects
- 4.3. More noble and selective metals
  - 4.3.1. Au and Au alloys
    - 4.3.1.1. Promotion of activity
    - 4.3.1.2. Other effects
  - 4.3.2. Ag and Ag alloys
    - 4.3.2.1. Promotion of activity
    - 4.3.2.2. Electrophilic sites from promoters
  - 4.3.3. Cu and Cu alloys
    - 4.3.3.1. Promotion of activity
    - 4.3.3.2. Other effects
- 5. Conclusions and prospects
- 6. Supporting information available

Acknowledgments

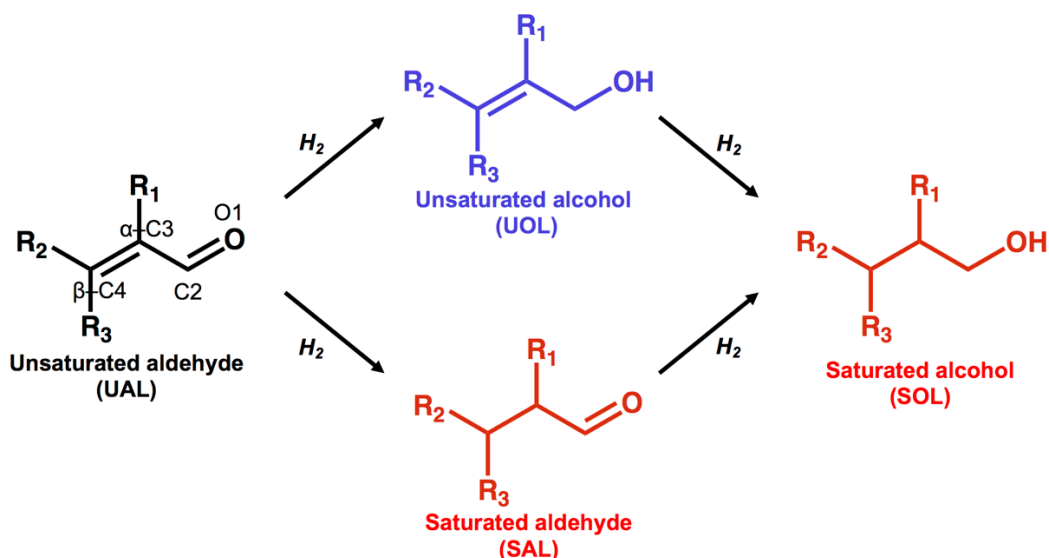
References

## **1. Introduction**

Selective hydrogenation of unsaturated oxygenates remains a challenging and unsolved problem that requires the study and development of new catalysts. In particular, allylic alcohols – a subclass of naturally occurring terpenoid alcohols – comprise an important class of chemicals in the fine chemical industry, serving as valuable intermediates in the production of pharmaceuticals, perfumes, and flavorings.<sup>1–5</sup> Allylic alcohols are primarily synthesized by the reduction of the carbonyl group of  $\alpha,\beta$ -unsaturated aldehydes. Typically, the chemoselective reduction of the carbonyl group is achieved using reducing agents,<sup>6</sup> Meerwein-Ponndorf-Verley reagents,<sup>7</sup> or organometallic catalysts.<sup>8–15</sup> These processes often use costly chemicals and solvents which require separations. In this context, heterogeneous catalysis is viewed as an alternative, more sustainable route for the production of these high-value chemicals at an industrial scale.<sup>16–26</sup> Simple heterogeneous catalyst preparation and recovery are desirable features for the chemical industry.

The major challenge in developing a catalytic process is that the desired products, unsaturated alcohols, are not the most thermodynamically favored, as indicated by the enthalpy of formation values in Table 1. Partial hydrogenation of  $\alpha,\beta$ -unsaturated aldehydes leads to two main products (Fig. 1): the unsaturated (allylic) alcohol via 1,2-addition; and the saturated aldehyde via 4,3-addition. 1,4-addition leads to the enol, but it quickly isomerizes to its keto form, the saturated aldehyde. The saturated aldehydes are undesirable, as they are readily produced via alkene hydroformylation. Further hydrogenation leads to the saturated alcohols which are lower value products.

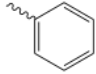
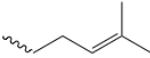
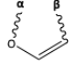
The functional groups present at the  $\alpha$ - and  $\beta$ -carbon determine the identity of the compound (Table 1).



**Figure 1.** Primary reaction scheme for the hydrogenation of  $\alpha,\beta$ -unsaturated aldehydes (UAL) showing the three main products: unsaturated alcohol (UOL), saturated aldehyde (SAL), and saturated alcohol (SOL). The unsaturated alcohol (blue) is the desired non-thermodynamic product; the undesired products are labeled in red. The backbone atoms are numbered starting with the carbonyl oxygen (O1). Functional groups (-R) at the  $\alpha$ - and  $\beta$ -carbon determine the identity of the compound (Table 1).

**Table 1:** Names of the representative compounds considered in the hydrogenation of  $\alpha,\beta$ -unsaturated aldehydes, according to the functional groups (-R) at the  $\alpha$ - and  $\beta$ -carbon (Fig. 1), as adopted in this paper. *E*-isomers are shown when stereochemically applicable. Experimental values of gas-phase enthalpy of formation (kJ/mol) (liquid-phase for furfural) are listed below each compound;<sup>27–29</sup> values in italics are estimations from the Joback method.<sup>30</sup>

R <sub>1</sub>	R <sub>2</sub>	R <sub>3</sub>	Unsaturated aldehyde	Unsaturated alcohol	Saturated aldehyde	Saturated alcohol
H	H	H	Acrolein	Allyl alcohol	Propanal	n-Propanol
			-87.7	-123.6	-188.7	-256

CH <sub>3</sub>	H	H	Methacrolein -106.4	Methallyl alcohol -162.5	Isobutanal -215.8	Isobutanol -283.8
H	CH <sub>3</sub>	H	Crotonaldehyde -109.7	Crotyl alcohol -160.9	Butanal -211.8	n-Butanol -277
H	CH <sub>3</sub>	CH <sub>3</sub>	Prenal -124.7	Prenol -191.3	Isovaleraldehyde -237.4	Isoamyl alcohol -300.8
H		H	Cinnamaldehyde 39.1	Cinnamyl alcohol -27.6	Hydro-cinnamaldehyde -78.1	Hydro-cinnamyl alcohol -144.8
H		CH <sub>3</sub>	Citral E = Geraniol Z = Neral -120.5	E = Geraniol Z = Nerol -187.1	Citronellal -233.2	Citronellol -299.8
		H	Furfural -200.2	Furfuryl alcohol -276.4	Tetrahydro-furfural -301.6	Tetrahydro-furfuryl alcohol -435.6

Despite widespread investigations, obstacles remain in the development of efficient heterogeneous catalytic processes for the selective hydrogenation of unsaturated oxygenates. Conventional monometallic catalysts favor hydrogenation of the C=C bond over the C=O bond due to the underlying adsorption and reaction thermodynamics.<sup>31-33</sup> The selectivity is further degraded due to other competing reactions, including dehydrogenation, isomerization, and coupling among the hydrogenation intermediates. Bond-breaking reactions, such as hydrodeoxygenation, decarbonylation, and ring opening, are also observed with e.g. furfural, a popular biomass-derived compound. As such, the selective hydrogenation of  $\alpha,\beta$ -unsaturated aldehydes is also an ideal case for the study of structure-activity relationships in heterogeneous catalysis.<sup>34-47</sup>

Recent works indicate that bimetallic catalysts have the potential to enhance the selectivity in the hydrogenation of many different classes of chemicals, such as alkynes, alkenes, imines, and carbonyl compounds,<sup>21,26,39,46,48-66</sup> as well as biomass-derived molecules.<sup>67-73</sup> In particular, single-atom alloys, in which dilute amounts of catalytically active elements, e.g. Group 8-10 (VIII B), are

embedded as well-dispersed single atoms in a more inert host, e.g. Group 11 (IB), have gained much attention as bifunctional catalysts capable of achieving an optimal activity-selectivity balance.<sup>74–77</sup> In general, the presence of a secondary metal can enhance the selectivity by various electronic (ligand) and geometric (ensemble) effects (see section 2.1 and 3.3). Fundamental understanding and engineering of these variables, however, remain challenging due to the structural and chemical complexities intrinsic to bimetallic systems. Further complications arise from the dynamic nature of the surface composition and morphology under reaction conditions, such as reverse surface segregation in response to different pretreatments and reactive environments.<sup>78–84</sup>

This review aims to present a compelling set of guidelines for the selective hydrogenation of  $\alpha,\beta$ -unsaturated aldehydes in heterogeneous catalysis with a focus on the role of different metal surfaces. The numerous studies of powder catalysts, single crystal models, and theoretical calculations are integrated into a comprehensive picture based on the knowledge garnered from the literature of the past 20 years. An aggregate analysis of the published data is presented to establish key factors that influence the selectivity and to identify gaps that need to be addressed in future research, in particular concerning bimetallic alloys. A systematic approach was employed, bridging the basic knowledge from monometallic systems with the observations from bimetallic and dilute alloy catalysts.

This review is organized by summarizing the literature, culminating in an analysis of the catalytic performance in terms of key factors that suggest the guidelines for improving the selectivity and the directions for future research. In sections 2 and 3, critical overviews of experimental and theoretical studies are given, respectively, identifying physical and chemical factors for the selectivity by analyzing trends in the published data. In section 4, we present a detailed discussion of the literature organized by electronegativity and activity, bridging from monometallic to bimetallic cases whenever possible. In section 5, we summarize the established guidelines for catalysis and



identify gaps and implications for future research. The synergy of this review across theoretical and single-crystal studies to catalytic studies under reaction conditions presents a collaborative effort toward a more comprehensive understanding of the selective hydrogenation of unsaturated aldehydes.

## 2. Experiment overview

### 2.1. Major strategies for selectivity enhancement

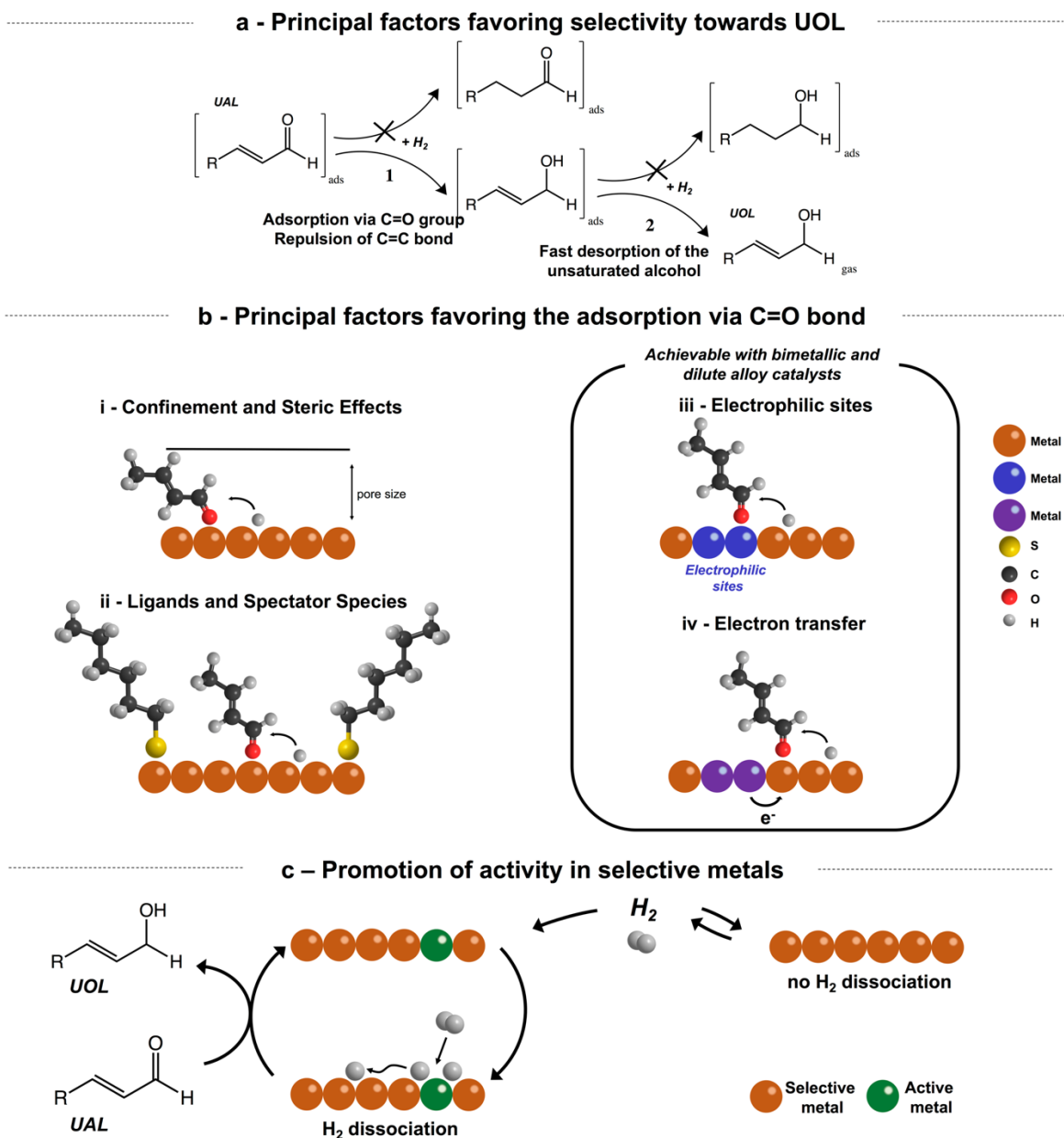


**Figure 2.** Schematic showing the principal factors and strategies that influence the selectivity to the unsaturated alcohol. **(a)** The adsorption mode of the unsaturated aldehyde (UAL) and the desorption of the unsaturated alcohol (UOL) influence the hydrogenation selectivity. **(b)** Favorable adsorption of the unsaturated

aldehyde via its C=O bond can be achieved by four main strategies: (i) confinement and steric effects; (ii) ligands and spectator species; (iii) formation of the electrophilic sites; and (iv) electron transfer. Bimetallic and dilute alloy catalysts have generally been used to achieve (iii) and (iv). (c) Promotion of the catalytic activity of less reactive but more selective metals can be achieved by adding a dilute amount of a more reactive metal.

Two major factors influence the selectivity in the hydrogenation of the unsaturated aldehydes (Fig. 2a): (i) the adsorption mode of the unsaturated aldehyde and (ii) the desorption of the unsaturated alcohol. First, in general, the adsorption of the C=C bond is thermodynamically favored over that of the C=O bond, which can lead to the undesired saturated aldehyde. As such, various strategies have been employed to promote the C=O bond adsorption. Second, facile desorption of the desired unsaturated alcohol is necessary to prevent over-hydrogenation to the saturated alcohol.

The desorption of the unsaturated alcohol has rarely been investigated in bimetallic systems, in both surface science and catalytic experiments.<sup>85</sup> The majority of experimental studies have focused on the adsorption of the unsaturated aldehyde as a key parameter for tuning the selectivity. Several approaches can be used to engineer the adsorption mode of the unsaturated aldehydes (Fig. 2b): (i) confinement and steric effects; (ii) ligands and spectator species; (iii) formation of the electrophilic sites; and (iv) electronic modification of the surface.

The confinement strategy relies on complete or partial inhibition of the C=C bond adsorption by impeding its contact with the surface (Fig. 2b i).<sup>86-89</sup> In unsaturated aldehydes, the C=C bond is typically located in the middle of the molecule, whereas the C=O bond is always terminal and geometrically unconstrained. By creating catalysts in which the active sites (i.e. metal nanoparticles) are confined in the pores or the cavities of the support, the C=C bond can be sterically pushed away from the surface, allowing the C=O bond to preferentially adsorb and react. Over the

years, tuning the size of the pores and the nanoparticles themselves has led to success, as demonstrated for zeolites and metal organic frameworks.<sup>86–89</sup>

The usage of ligands is a strategy that builds on the same principle of partial or complete inhibition of the C=C bond adsorption (Fig. 2b ii). A high coverage of ligands or strongly bound spectator species can sterically prevent the C=C bond from adsorbing on the active sites and has resulted in higher selectivity in reactor studies.<sup>90,91</sup> Controlling the reactant pressure can similarly induce surface crowding. For example, by increasing the H<sub>2</sub> pressure, the vertical adsorption mode of the C=O bond can be promoted. However, the saturated aldehydes have remained the major product in most surface science studies.<sup>92–96</sup>

Electronic modification of the surface is another strategy for improving the selectivity (Fig. 2b iv). For example, the modification of monometallic metals has been achieved by the addition of sulfur<sup>97,98</sup> and the use of various supports, such as carbon nanotubes and nanofibers,<sup>99–101</sup> which have been reviewed previously.<sup>20,102</sup> In bimetallic catalysts, the electronic properties of the active metal are modified via an electron transfer from a promoter metal. Because the C=C bond adsorption occurs via electron donation to the metal atoms, it is weakened when the electron density of the active metal increases. This decreases the probability of the C=C bond reduction relative to that of the C=O bond reduction, promoting the formation of the unsaturated alcohol.<sup>103,104</sup> In low pressure surface science experiments, the decomposition of the unsaturated aldehyde has predominated on reactive monometallic surfaces, such as Pt(111) and Pd(111), in the absence of H<sub>2</sub>.<sup>93–95,105–112</sup> In contrast, such C-C bond breaking is tempered significantly on bimetallic surfaces due to the electronic modification of the surface.<sup>113,114</sup>

In monometallic catalysts, formation of the electrophilic sites for the preferential adsorption of the C=O bond via its O lone pair (Fig. 2b iii) has been achieved most notably by increasing the Lewis acidity of supports,<sup>115</sup> creating O vacancies in reducible metal oxide supports (e.g. Pt/TiO<sub>2</sub>;

Pt/Ce<sub>x</sub>Zr<sub>1-x</sub>O<sub>2</sub>),<sup>116,117</sup> or using promoters (e.g. chloride; bromide).<sup>20,102</sup> In bimetallic catalysts, the promoter can act as an electrophilic/oxophilic site by presenting a local positive charge where the C=O bond adsorption is favored. The active metal, in close proximity to the promoter, provides the overall activity by functioning as the active site for H<sub>2</sub> dissociation and thereby initiating the catalytic cycle (Fig. 2c).

Many monometallic surfaces that have high selectivity—Cu, Ag, and Au—have a limited ability to dissociate H<sub>2</sub>, as shown by surface science studies in ultrahigh vacuum.<sup>45,118–121</sup> Furthermore, H atoms are bound weakly on these metals, so the desorption of H<sub>2</sub> often occurs at temperatures below those required for hydrogenation. A few studies have employed atomic hydrogen sources to study hydrogen adsorption and hydrogenation in ultrahigh vacuum.<sup>45,92,122,123</sup> For example, Mullins *et al.* used an atomic hydrogen source to study the hydrogenation of acetaldehyde and propanal on Au(111). However, to the best of our knowledge, no surface science studies have been reported on the hydrogenation of the unsaturated aldehydes on Au(111).<sup>123,124</sup> On the other hand, reactive but less selective metals, such as Pt and Pd, can readily dissociate H<sub>2</sub>, and the temperature for the recombination and the desorption of H<sub>2</sub> is higher as a result.<sup>125–127</sup> As such, the majority of the surface science studies reviewed here have focused on these monometallic surfaces. In reactor studies, it is possible to achieve H<sub>2</sub> dissociation on monometallic Cu, Ag, and Au catalysts, most notably via strong interaction with metal oxide supports or at very high pressures.<sup>46,128–130</sup> However, their activity remains limited compared to other metals, and their promotion with more reactive metals has been considered as a strategy to enhance the activity (Fig. 2c).

In this manuscript, recent literature on the selective hydrogenation of  $\alpha,\beta$ -unsaturated aldehydes on bimetallic and dilute alloy catalysts is systematically reviewed, focusing on studies in which monometallic and bimetallic catalysts were tested under identical conditions. As such, the

influence of reaction conditions (temperature, pressure, and solvent) will not be addressed comprehensively, but instead has been well-described in the previous literature.<sup>18,20</sup> As mentioned above, the support plays an important role, e.g. by electronic modifications from carbon supports or the creation of electrophilic sites when reducible metal oxide supports are used. Recent reviews have addressed the challenges and opportunities related to these support effects in the hydrogenation of unsaturated aldehydes.<sup>20,102</sup> The role of the support is beyond the scope of our work, as both monometallic and bimetallic nanoparticles were supported on the same set of materials within a given study. Moreover, investigation of support effects remains challenging using theoretical modeling and surface science studies alone.<sup>131</sup>

With this in mind, the catalytic performance from reactor studies are summarized in figures that plot the selectivity to the unsaturated alcohol as a function of the unsaturated aldehyde conversion (e.g. Fig. 3). An ideal catalyst would be located in the upper right quadrant of such a plot, where both the selectivity and the activity are high (>50%). A clear trend emerges from such analysis when comparing monometallics and bimetallics: while monometallic catalysts rarely achieve high selectivity at high conversion, the addition of a secondary metal greatly improves the selectivity and in ideal cases also promotes the activity (Fig. 3). Detailed analysis of the promotion effects is presented in section 4.

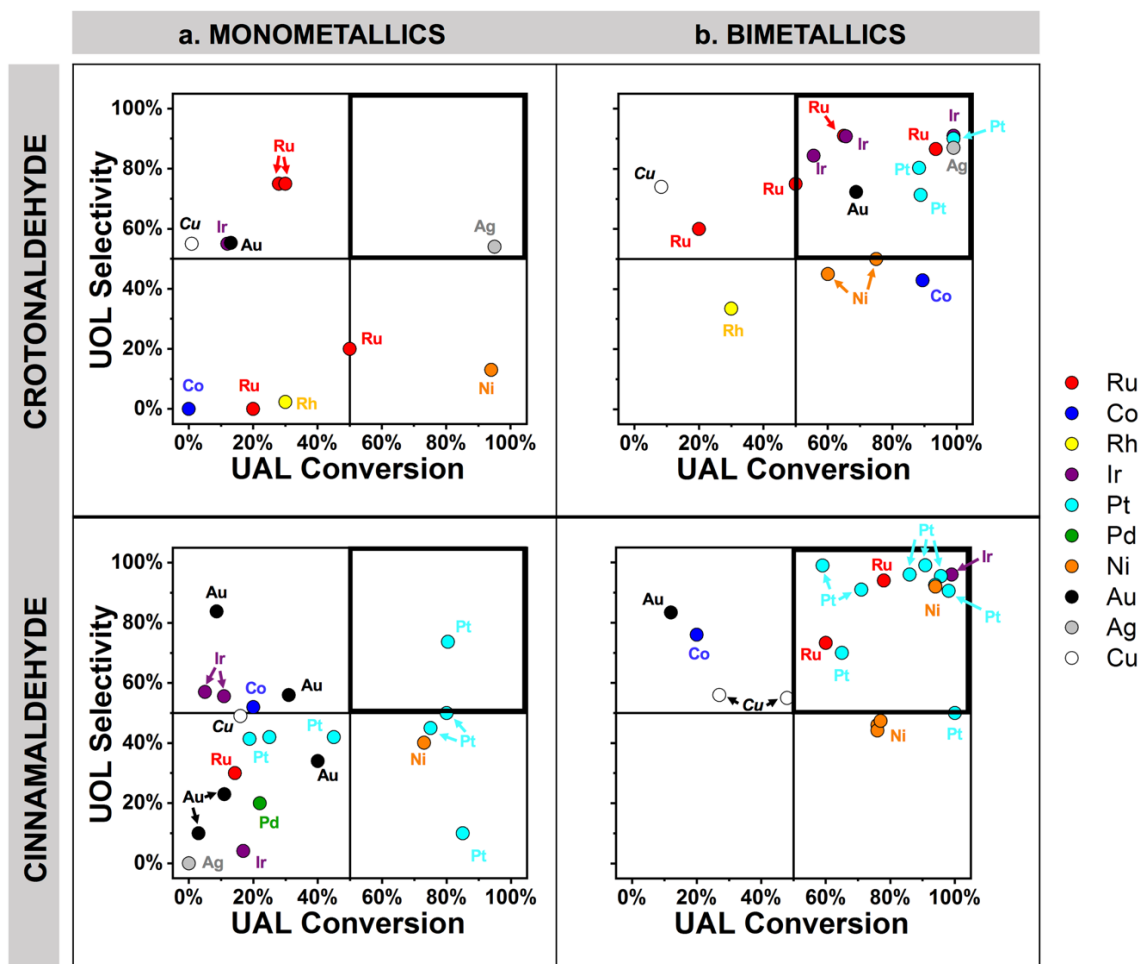


**Figure 3.** A compilation of the reported selectivity to the unsaturated alcohol (UOL) as a function of the unsaturated aldehyde (UAL) conversion for the hydrogenation of crotonaldehyde<sup>85,132–147</sup> and cinnamaldehyde<sup>133,134,136,141,142,147–159</sup> on: **(a)** monometallic catalysts, showing only the ones that were directly compared to a bimetallic composition in a given study; **(b)** bimetallic and dilute alloy catalysts, with the majority metal labeled and indicated in the legend. Specific dopants are discussed in section 4. High selectivity at high conversion is desirable, as emphasized by the bold box in the upper right quadrant of each plot.

### **3. Theory overview**

Several aspects of DFT studies warrant careful consideration when interpreting the published results on the hydrogenation of the unsaturated aldehydes, and they are discussed prior to presenting the key results from the theory literature.

#### **3.1. Categories of DFT investigations**

The DFT studies considered in this review fall into two main categories. The most common type of investigation is the modeling of the adsorption energetics and geometries, which involves ionic relaxation, or energy minimization, of adsorbates on metal surfaces. Most of these studies have focused on the unsaturated aldehydes, correlating the experimentally observed selectivity trends with the adsorption thermodynamics of different binding modes. The adsorption strength is quantified by the adsorption energy  $E_{\text{ads}}$ , typically defined as the change in energy as the system goes from an isolated surface and a gas-phase molecule into a combined system of the adsorbate interacting with the surface. As such, the more negative the adsorption energy, the stronger the adsorption. For an unsaturated aldehyde UAL on a metal surface M,

$$E_{\text{ads}} = E(\text{UAL}_{(\text{ads})}/\text{M}) - E(\text{M}) - E(\text{UAL}_{(\text{g})}). \quad (1)$$

The second type of investigation involves the modeling of the reactivity, which goes beyond adsorption by mapping out the transition state pathways for the elementary reaction steps. To do so, transition state modeling techniques are employed, which are computationally more involved than simple relaxations. The resulting energy barriers, or activation energies  $E_{\text{a}}$ , allow identification



of the rate-limiting steps and the reaction kinetics according to the Arrhenius expression of the rate constant  $k$ :

$$k = \nu \exp\left(\frac{-E_a}{k_B T}\right), \quad (2)$$

where  $\nu$  is the pre-exponential factor containing the entropy change  $S_a$  associated with the activation:

$$\nu = \frac{k_B T}{h} \exp\left(\frac{S_a}{k_B}\right), \quad (3)$$

thereby recovering the Eyring equation in terms of the activation free energy  $F_a = E_a - TS_a$ :

$$k = \frac{k_B T}{h} \exp\left(\frac{-F_a}{k_B T}\right). \quad (4)$$

A few studies of crotonaldehyde<sup>160,161</sup> and furfural<sup>162–164</sup> have used the calculated rate constants as inputs for microkinetic modeling to obtain macroscopic insights on the activity and the selectivity.

The majority of the DFT studies do not investigate the thermal effects beyond the internal energy  $E$ . To do so, entropic contributions must be evaluated using the partition functions  $Q$  of the relevant degrees of freedom:

$$\Delta S = k_B \ln \frac{Q_{\text{final}}}{Q_{\text{initial}}}. \quad (5)$$

Here, the initial and the final state may refer to: (i) an adsorption process, from gas phase to the adsorbed state, to provide adsorption phase diagrams from *ab initio* thermodynamics, as done for acrolein;<sup>165,166</sup> or (ii) an activation process, from the initial state to the transition state, to provide free energy diagrams of the elementary reaction steps, as done for crotonaldehyde<sup>31,160</sup> and furfural.<sup>167–169</sup>

### 3.2. Limitations of DFT modeling

Several factors influence the results obtained from DFT calculations to varying degrees:

(i) The inherent limitation in the approximations of the exchange-correlation functional poses a fundamental challenge to accurate prediction of a range of properties, most notably the electronic structures of insulators and semiconductors,<sup>170</sup> as well as the adsorption of organic molecules on metals.<sup>171</sup> The latter issue is particularly relevant for computational catalysis. The adsorption energies calculated by DFT can deviate significantly from the experimental benchmarks, if rare microcalorimetry data is available.<sup>171</sup> Qualitative or semi-quantitative insights can be established, however, with the exception of pathological cases such as CO/Pt(111).<sup>172</sup> Typically, DFT uncertainties in the relative energies span  $\sim 0.15$  eV for the adsorbates and  $\sim 0.2$ - $0.3$  eV for the transition state species.<sup>173</sup>

A few studies have investigated the effect of van der Waals (vdW) corrections/functionals on the adsorption and/or reactivity of acrolein<sup>174–177</sup> and furfural.<sup>168,178</sup> Qualitative observations remained largely unaffected for a given molecule, with systematic shifts in the magnitude of the adsorption energy. However, no systematic comparisons were made across different unsaturated aldehyde species. Recent works have demonstrated that vdW interactions are needed to accurately

describe the relative interactions of different substituents with the surface that ultimately influence the overall selectivity.<sup>179–183</sup>

(ii) In the evaluation of free energies and/or rates, entropic contributions [Eq. (5)] contain the vibrational entropy. The vibrational frequencies are obtained from DFT calculation of the Hessian matrix using the harmonic approximation. However, low-frequency vibrational modes, so-called “soft” modes such as frustrated molecular rotation on the surface, are largely anharmonic. As a result, harmonic treatment of these modes can eventually lead to order-of-magnitude errors in the pre-exponential factors, highlighting the need for accurate and efficient modeling of anharmonic effects.<sup>184</sup>

(iii) Validation of the physical model used in DFT is limited by the static nature of the method, meaning a certain surface structure and reaction mechanism must be assumed. As such, multiple computations are needed to discover the most relevant sets of structures and mechanisms. The corresponding configurational space becomes especially large for bimetallic systems with strong tendencies for surface segregation.<sup>83,185</sup> Because of the large underlying degrees of freedom, the majority of the DFT studies considered in this review have focused on monometallic systems, with bimetals limited to known ordered structures such as SnPt,<sup>103,109,110,186–189</sup> or simple monolayer on bulk structures such as M/Pt(111) (M = Fe, Co, Ni, Cu).<sup>94,190,191</sup> To the best of our knowledge, only one study investigated the effect of surface segregation in the presence of acrolein and prenal on Pt<sub>4</sub>Fe(111),<sup>104</sup> highlighting the need for model validation of bimetallic systems with dynamic surface composition and morphology.

### 3.3. Major trends in thermodynamics and kinetics

Here, we present an aggregate analysis of the key observations from the theory literature to establish major trends in the thermodynamics and kinetics of the hydrogenation of the unsaturated aldehydes. DFT modeling of the adsorption energetics and geometry is discussed first in relation to the reactivity, followed by the reaction mechanisms. Further details can be found in section 4 for each host metal.

#### 3.3.1. Adsorption and reactivity

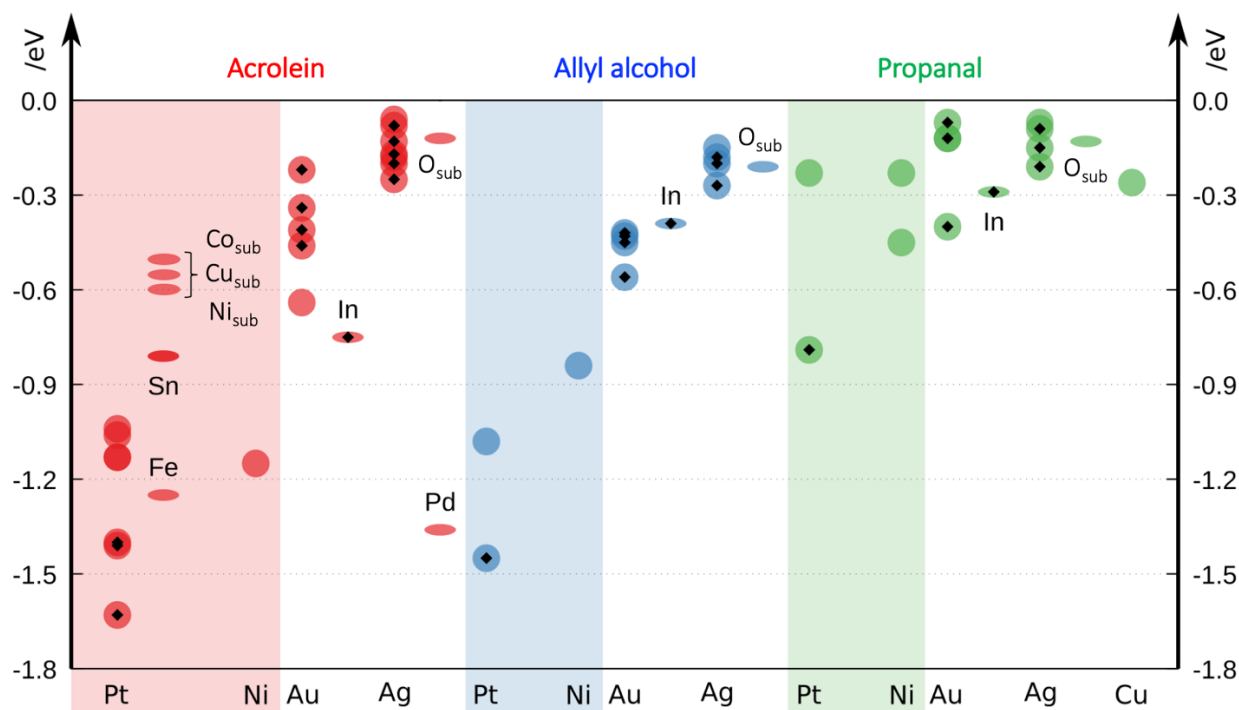


**Figure 4.** A summary of the adsorption energies (eV) of acrolein (unsaturated aldehyde; red), allyl alcohol (unsaturated alcohol; blue), and propanal (saturated aldehyde; green), on transition metal surfaces as reported by 19 DFT studies,<sup>32,103,104,165,166,176,190,192–203</sup> selecting the most negative value in a given study (see Table S1 for full tabulation of the data). Data from 5 vdW-DFT studies<sup>174–177,204</sup> are omitted for consistency; vdW corrections/functionals introduce systematic discrepancies. Each metal host consists of a column for the monometallic case (circular points) and an adjacent column for the bimetallic cases (elliptical points)

with the promoters labeled. Shaded regions indicate Group 10 hosts (Pt, Pd, Ni); non-shaded regions indicate Group 11 hosts (Au, Ag, Cu). Data points indicate the face centered cubic (111) facet, unless labeled with a black diamond for non-(111) facets or nanoclusters. All promoters interacting with the adsorbate reside in the surface layer, unless labeled with a subscript “sub” for the subsurface layer.  $O_{\text{sub}}$  refers to the subsurface oxygen species.

The adsorption energies of acrolein and its partially hydrogenated products, allyl alcohol and propanal, from DFT calculations indicate that the selectivity is controlled by the adsorption thermodynamics on Group 10 metals but not on Group 11 metals (Fig. 4).

On Group 10 metals (Pt, Pd, Ni), the selectivity is thermodynamically controlled. On Pt(111), the adsorption energy of acrolein is around  $-1.1$  eV. Comparison of the different adsorption geometries (Fig. 5) shows that acrolein binds mainly via planar  $\eta^3$  and  $\eta^4$  configurations on Pt facets (Table 2), with the C=C bond binding more strongly than the C=O bond. Vertical  $\eta^1$  configuration via the carbonyl O can potentially be stabilized at the edge sites, however.<sup>201</sup>

Upon hydrogenation, allyl alcohol has essentially the same adsorption strength as acrolein, whereas the adsorption of propanal is significantly weaker. The same trend holds on Ni(111),<sup>193</sup> as well as Pd(111) (not shown in Fig. 4 due to a large offset associated with the functional).<sup>174</sup> As a result, allyl alcohol becomes further hydrogenated into n-propanol instead of undergoing desorption. The adsorption thermodynamics of allyl alcohol hence determines the selectivity.

In the presence of substituents at the  $\beta$ -carbon, the C=C bond adsorption is sterically weakened. In fact, prenal shifts to a vertical  $\eta^1$ - $\sigma(\text{O})$  configuration (analogous to Fig. 5a) at high coverages, promoting the desired chemoselective reduction of the carbonyl group. Furthermore, more

highly substituted unsaturated alcohols, with a larger number of substituents or more bulky substituents, have weaker adsorption, thereby favoring their desorption over further hydrogenation to the saturated alcohols.

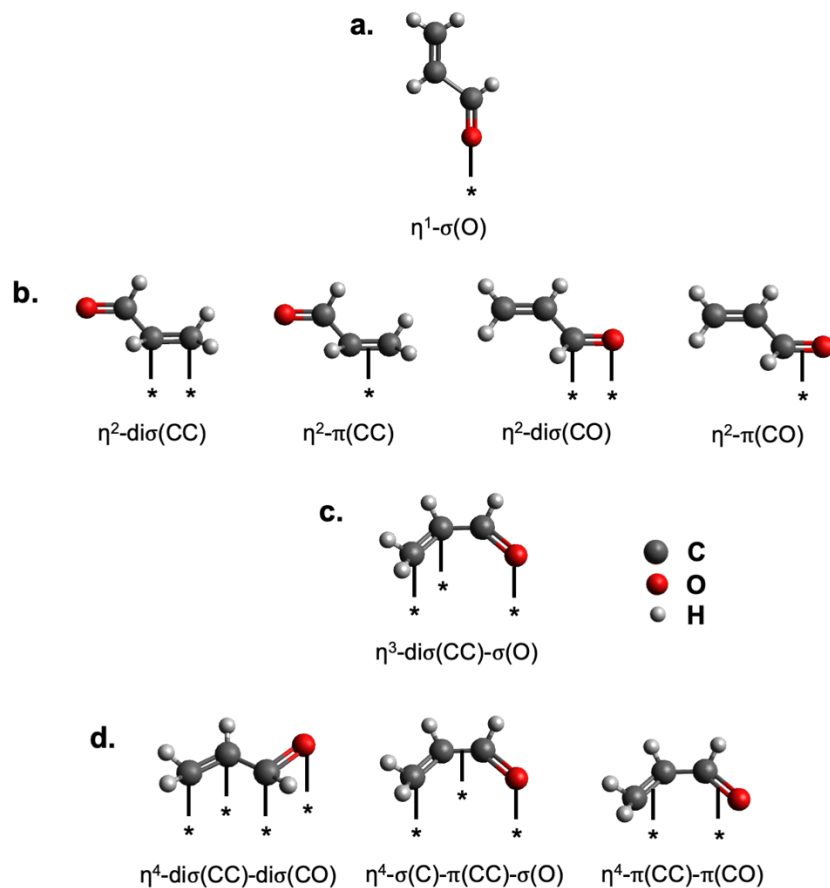


**Figure 5.** The adsorption modes of acrolein: **(a)**  $\eta^1$ -mode (atop) via the carbonyl O; **(b)**  $\eta^2$ -modes via either the C=C or the C=O bond, as well as a metallocycle via the terminal atoms; **(c)**  $\eta^3$ -mode via the C=C bond and the carbonyl O; **(d)**  $\eta^4$ -modes involving all backbone atoms.

**Table 2:** Stable adsorption modes of acrolein (Fig. 5), as reported by 22 DFT studies,<sup>32,103,104,165,166,174–177,190,193–204</sup> organized by host metal (Group 10 vs. 11). Nanoclusters are indicated as “NC,” with the number of atoms in parentheses. Cases with a monolayer of promoter on a given metal are indicated as “ML.” All promoters interacting with the adsorbate reside in the surface layer, unless specified with a subscript “sub” for the subsurface layer. See sections 2-5, SI for the adsorption modes of other unsaturated aldehydes.

Host	Promoter	Facet	Adsorption mode	Ref.
<b>Group 10 hosts (Pt, Pd, Ni)</b>				
Pt		NC (24-40)	$\eta^1\text{-}\sigma(\text{O})$	201
		(111)	$\eta^2\text{-di}\sigma(\text{CC})$	32,165,174
		(110)	$\eta^3\text{-di}\sigma(\text{CC})\text{-}\sigma(\text{O})$	32,165,175
		(211)	$\eta^4\text{-di}\sigma(\text{CC})\text{-di}\sigma(\text{CO})$	32,104,165,190,203
			$\eta^2\text{-di}\sigma(\text{CC})$	166
			$\eta^4\text{-}\sigma(\text{C})\text{-}\pi(\text{CC})\text{-}\sigma(\text{O})$	202
Pt	Sn	(111)	$\eta^2\text{-}\sigma(\text{C4})\text{-}\sigma(\text{O})\text{-OSn}$	103
			$\eta^3\text{-di}\sigma(\text{CC})\text{-}\sigma(\text{O})\text{-OSn}$	103
Pt	Fe Fe <sub>sub</sub>	(111)	$\eta^3\text{-di}\sigma(\text{CC})\text{-}\sigma(\text{O})\text{-OFe}$	104
			$\eta^3\text{-di}\sigma(\text{CC})\text{-}\sigma(\text{O})$	104
Pt	Co ML Co <sub>sub</sub> ML	(111)	$\eta^4\text{-di}\sigma(\text{CC})\text{-di}\sigma(\text{CO})$	190
			$\eta^2\text{-di}\sigma(\text{CC})$	190
Pt	Ni ML Ni <sub>sub</sub> ML	(111)	$\eta^4\text{-di}\sigma(\text{CC})\text{-di}\sigma(\text{CO})$	190
			$\eta^4\text{-di}\sigma(\text{CC})\text{-di}\sigma(\text{CO})$	190
Pt	Cu ML Cu <sub>sub</sub> ML	(111)	$\eta^4\text{-di}\sigma(\text{CC})\text{-di}\sigma(\text{CO})$	190
			$\eta^2\text{-di}\sigma(\text{CC})$	190
Pd		(111)	$\eta^2\text{-di}\sigma(\text{CC})$	174
Ni		(111)	$\eta^4\text{-di}\sigma(\text{CC})\text{-di}\sigma(\text{CO})$	193
<b>Group 11 hosts (Au, Ag, Cu)</b>				
Au		NC (55)	$\eta^2\text{-}\pi(\text{CC})$	195,204
		(110)	$\eta^2\text{-}\pi(\text{CC})$	166
		(211)	$\eta^2\text{-di}\sigma(\text{CO})$	195
			$\eta^2\text{-}\pi(\text{CC})$	194,202
Au	In	(110)	$\eta^2\text{-di}\sigma(\text{CO})\text{-OIn}$	195
Ag		(111)	$\eta^2\text{-}\pi(\text{CC})$	176,177,197
			$\eta^2\text{-}\pi(\text{CC}) + \eta^1\text{-}\sigma(\text{O})$	177,197
		(110)	$\eta^4\text{-}\pi(\text{CC})\text{-}\pi(\text{CO})$	198
			$\eta^2\text{-di}\sigma(\text{CC})$	199
		(100)	$\eta^4\text{-}\pi(\text{CC})\text{-}\pi(\text{CO})$	176
		(211)	$\eta^4\text{-}\pi(\text{CC})\text{-}\pi(\text{CO})$	176

		(221)	$\eta^4\text{-}\pi(\text{CC})\text{-}\pi(\text{CO})$	199
Ag	Pd	(111)	$\eta^2\text{-}\pi(\text{CC})\text{-Pd}$	200
Ag	O <sub>sub</sub>	(111)	$\eta^4\text{-}\pi(\text{CC})\text{-}\pi(\text{CO})$	198

Promotion of Pt with electropositive metals Sn and Fe has been modeled, showing that a charge transfer from the promoter to Pt weakens the C=C bond adsorption. This effect is discussed in section 2.1 as one of the strategies for enhancing the selectivity (Fig. 2b iv). Furthermore, oxophilic promoters enable the C=O bond activation via coordination with the carbonyl O (Fig. 2b iii). In turn, such preferential adsorption allows Fe to segregate to the surface.<sup>104</sup>

The effects of 3d metal monolayer (M = Co, Ni, Cu) on Pt(111) has also been modeled. Compared to Pt(111), a subsurface metal monolayer (Pt/M/Pt) weakens the adsorption of acrolein, thereby promoting the formation of allyl alcohol, whereas the opposite holds for a surface metal monolayer (M/Pt) (not shown in Fig. 4 due to scaling). The issue of surface segregation was not addressed in the study, however.<sup>190</sup>

In addition to the charge transfer effect discussed in section 2.1, the presence of a secondary metal can alter the local chemical reactivity by other microscopic effects of electronic and geometric nature.<sup>205</sup> DFT calculations have enabled quantitative investigation of how the following effects change the surface *d*-band.<sup>206,207</sup> (i) Ligand effect: the *d*-band width and center of the host metal are altered by its hybridization with the localized *d*-state of the promoter that is energetically misaligned. (ii) Strain effect: lattice mismatch between the host and the promoter introduces strain, which alters the bond distances, the orbital overlap, and hence the *d*-band center. (iii) Ensemble effect: due to the aforementioned differences in the energetics and lattice constants, the reactivity of an active site is determined by its local composition and size (e.g. monomer vs. dimer, trimer, etc., of the promoter in the surface layer of the host metal).<sup>208</sup>



On Group 11 metals (Au, Ag, Cu), the activity for H<sub>2</sub> dissociation is low because of the full *d*-shell, and the selectivity to the unsaturated alcohols is kinetically controlled. Compared to Group 10 metals, the adsorption of acrolein is significantly weaker on Au and Ag, as evidenced by a shift from diσ to predominantly π binding modes (Table 2). Furthermore, the adsorption of allyl alcohol and propanal remain similarly weak. As a result, the desorption of allyl alcohol no longer determines the selectivity. In general, the reduction of the C=O bond is kinetically favored on Au facets as well as on Ag(111) in the presence of subsurface O.<sup>198</sup> Promotion of Group 11 metals with a secondary metal has not been investigated systematically with DFT.

### 3.3.2. Hydrogenation mechanism

The hydrogenation mechanisms have been modeled almost exclusively on monometallic systems. The stepwise addition of H results in two possible pathways leading to each of the partially hydrogenated products (Fig. 6); further hydrogenation to the saturated alcohol can occur via twelve pathways. Full tabulation of the energy barriers associated with the dominant pathways can be found in the SI.

In general, the first hydrogenation step is the rate-limiting step, with the hydrogenation of the terminal atoms (O1 and C4) kinetically favored in a Markovnikov fashion. Despite the stronger adsorption of the C=C bond on Group 10 metals, the reduction of the C=O bond is associated with lower energy barriers in most cases. Nonetheless, the desorption of the resulting unsaturated alcohol remains difficult. On the other hand, the formation of the saturated aldehyde has been shown to proceed by an indirect pathway in many cases via isomerization of the enol.<sup>160,161,202,209</sup>

On Group 11 metals, because of their low activity for H<sub>2</sub> dissociation, the non-Horiuti-Polyani mechanisms involving weakly bound molecular H<sub>2</sub> have been proposed to be kinetically

favored. However, the entropic contributions have not been assessed in these studies.<sup>176,194</sup> In particular, the participation of molecular H<sub>2</sub>, which is very weakly bound, is expected to be severely hindered by low surface residence time at the reaction temperatures and pressures.

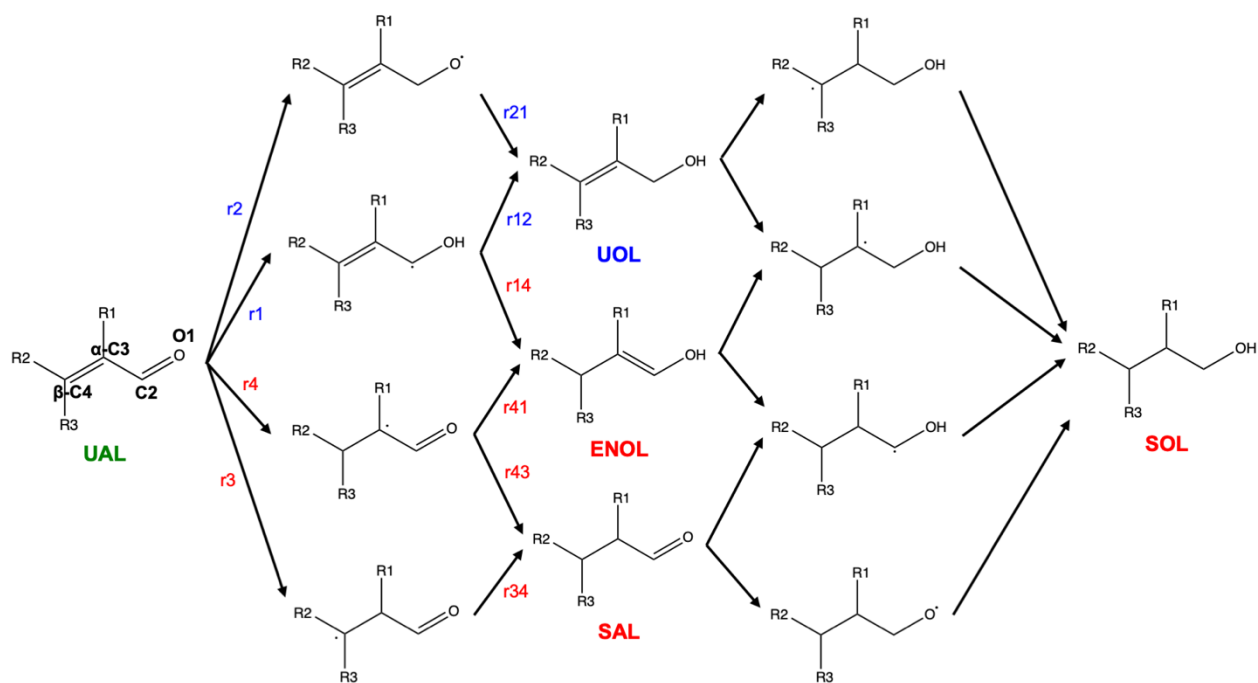


**Figure 6.** The Horiuti-Polyani mechanism for the hydrogenation of the unsaturated aldehyde (UAL), in which one H atom is added in each step. Partial hydrogenation (adding 2H) can result in the unsaturated alcohol (UOL), the enol (ENOL), or the saturated aldehyde (SAL), whereas complete hydrogenation (adding 4H) produces the saturated alcohol (SOL). Reaction pathways are indicated by “r” with the sequence of the IDs of the backbone atoms that are hydrogenated in order. Only 1,2- or 2,1-addition leads to the desired unsaturated alcohol.

### 3.3.3. Furfural reduction

The reduction of furfural is more complex due to the presence of reactions alternative to hydrogenation (Fig. 7). The main competitive pathways are (1) hydrodeoxygenation to methylfuran; (2) decarbonylation to furan; and (3) the furanyl ring opening to linear-chain species.

In general, hydrogenation to furfuryl alcohol is kinetically favored over both decarbonylation and hydrodeoxygenation. An increase in the H coverage weakens the adsorption of furfural by tilting the furanyl ring away from the surface, thereby shifting the reactivity away from decarbonylation and ring opening toward the formation of furfuryl alcohol.

The situation is complicated by the possible dehydration of furfuryl alcohol to methylfuran, which is promoted on Group 10 metals where the furanyl ring interacts strongly with the surface. On Group 11 metals, the desorption of furfuryl alcohol is facile, and the dehydration becomes kinetically feasible only at high temperatures.

The effects of 3d metal monolayers (M = Fe, Co, Ni, Cu) on Pt(111) have also been considered for the reduction of furfural. Compared to Pt(111), surface deposition (M/Pt) of the more oxophilic metals (Fe, Co) strengthens the adsorption of furfural, thereby promoting hydrodeoxygenation with furfuryl alcohol as the likely intermediate.<sup>191</sup> On the other hand, decarbonylation requires the formyl C-H bond scission. As such, it depends on the interaction of the carbonyl C with the surface, which has been shown to be weakened by Cu promoters on Pd(111).<sup>210</sup>

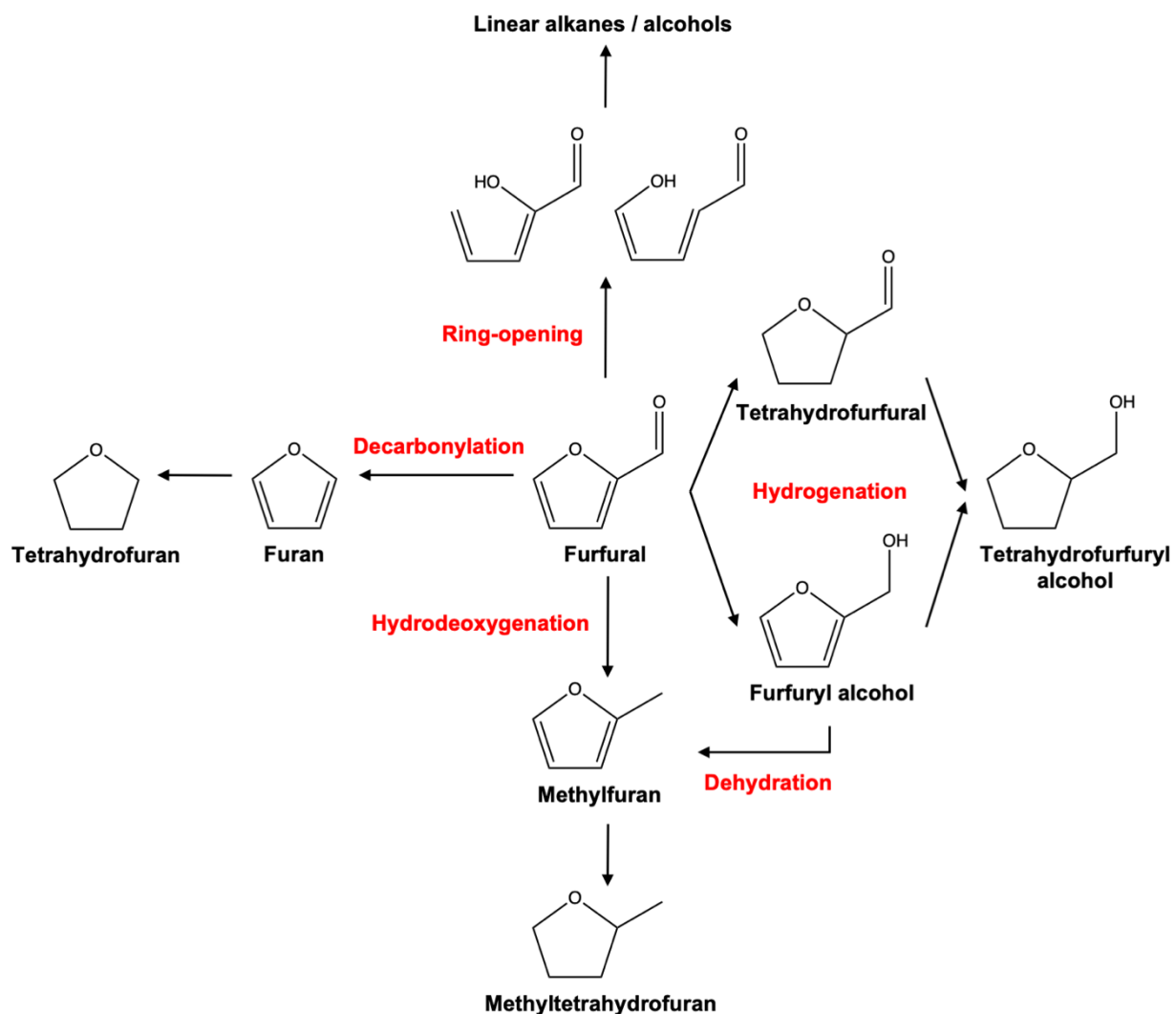


**Figure 7.** Four main types of reaction considered in the reduction of furfural, a biomass-derived compound: (1) hydrogenation of the carbonyl or the furanyl double bond; (2) the furanyl ring opening via the C-O bond scission to form aliphatic compounds; (3) hydrodeoxygenation, removal of the carbonyl O to form methylfuran, which can occur via the dehydration of furfuryl alcohol; (4) decarbonylation, removal of the carbonyl group to form furan.

## 4. Discussions

The metals used for the selective hydrogenation of the unsaturated aldehydes can be classified into three main categories (Fig. 8): (i) the electronegative metals in Groups 8-10 (Ru, Rh, Pd, Ir, Pt) showing high activity but low selectivity (section 4.1); (ii) the electropositive metals (Co, Ni) showing high activity but low selectivity (section 4.1); (iii) the more noble and selective metals in Group 11 (Au, Ag, Cu) showing low to moderate activity (section 4.3).

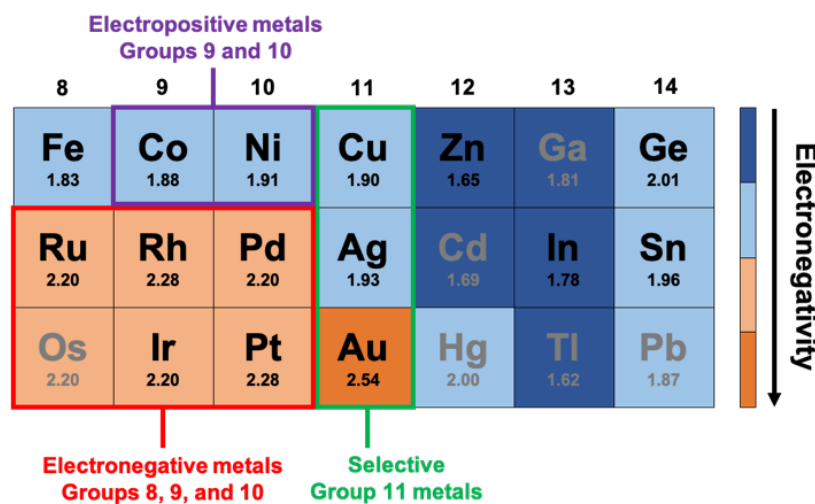


**Figure 8.** The metals reviewed in this work (indicated in black) can be classified into three main categories: the electronegative metals in Groups 8-10 (red box); the electropositive metals in Groups 9-10 (purple box); and the more noble metals in Group 11 (green box). The electronegativity values are indicated for each element, colored from blue to orange according to the magnitude of the value. Zn, In, Ge and Sn are considered as promoters.

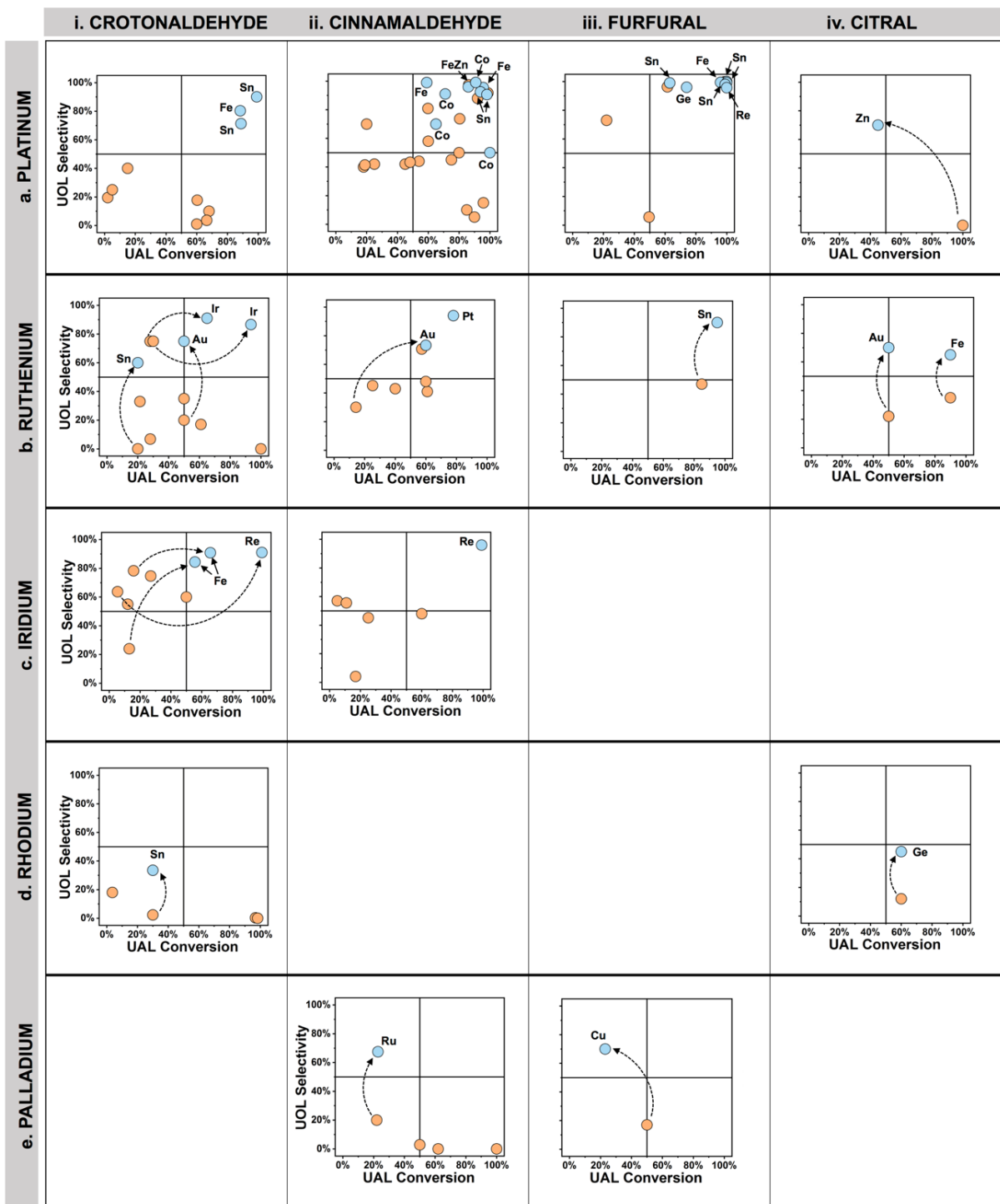
### 4.1. Active electronegative metals

The electronegative metals in Groups 8-10 include Ru, Rh, Pd, Ir, and Pt, which are conventionally used in hydrogenation reactions because of their high activity for H<sub>2</sub> dissociation. In

general, these metals have led to the formation of the saturated aldehyde or the saturated alcohol as the main product in catalytic studies. The selectivity to the unsaturated alcohol has been increased successfully by promotion with more electropositive metals (Fig. 9), which induce a charge transfer from the promoter to the active metal (e.g. Sn to Pt, Pd, Ru, or Rh; Co to Pt; Fe to Pt), or via oxidized species functioning as the Lewis acid sites (e.g. FeO<sub>x</sub> to Ir; ReO<sub>x</sub> to Pt; ZnO<sub>x</sub> to Pt; GeO<sub>x</sub> to Pt). Combinations of these effects have also been reported, as well as other effects which are described in this section.

#### 4.1.1. Pt & Pt alloys

Monometallic Pt catalysts have been investigated the most for the hydrogenation of the unsaturated aldehydes. The nature of the reactant strongly influences the degree of selectivity to the unsaturated alcohol (Fig. 9a). While moderate to high selectivity was generally reported at high conversions of cinnamaldehyde<sup>86,100,147-149,157-159,211-219</sup> and furfural,<sup>213,220</sup> the hydrogenation of citral<sup>221</sup> and smaller aldehydes, such as crotonaldehyde<sup>85,116,142,214,222,223</sup> and acrolein,<sup>213</sup> have usually exhibited very low selectivity to the unsaturated alcohols.



monometallic catalysts

bimetallic catalysts

**Figure 9.** Aggregated data reporting the selectivity to the unsaturated alcohol (UOL) as a function of the unsaturated aldehyde (UAL) conversion, illustrating the effects of a secondary metal on: **(a)** Pt and Pt-rich

bimetallics for the hydrogenation of crotonaldehyde,<sup>85,100,116,133,134,142,147,214,222,223</sup> cinnamaldehyde,<sup>86,100,133,134,147–149,155,157–159,211–219</sup> furfural,<sup>133,134,147,213,220,221,224–227</sup> and citral;<sup>221</sup> **(b)** Ru and Ru-rich bimetallics for the hydrogenation of crotonaldehyde,<sup>132,140–142,214,228–231</sup> cinnamaldehyde,<sup>101,141,156,214,228,232</sup> furfural,<sup>233</sup> and citral;<sup>141,234</sup> **(c)** Ir and Ir-rich bimetallics for the hydrogenation of crotonaldehyde<sup>142,145,146,229,235,236</sup> and cinnamaldehyde;<sup>142,153,237,238</sup> **(d)** Rh and Rh-rich bimetallics for the hydrogenation of crotonaldehyde<sup>139,142,143</sup> and citral;<sup>239</sup> **(e)** Pd and Pd-rich bimetallics for the hydrogenation of cinnamaldehyde<sup>151,214,240–242</sup> and furfural.<sup>210</sup> Dotted arrows indicate that the data are derived from the same study.

Surface science studies of Pt(111) have demonstrated the challenge of linking ultrahigh vacuum studies with catalysis. Hydrogenation products were not observed for acrolein,<sup>94,95,106,107,243,244</sup> crotonaldehyde,<sup>106,108,109,187,243,245–247</sup> and prenal.<sup>110,248</sup> Instead, decarbonylation dominated, yielding CO, H<sub>2</sub>, and propylene. Using DFT, the decomposition pathway was modeled for prenal, which proceeded by the formyl C-H bond scission, decarbonylation, and isomerization to the highly stable  $\eta^1$ -isobutylidyne species.<sup>248</sup> Furfural was an exception, which underwent hydrogenation on Pt(111) when H atoms were adsorbed first, followed by furfural.<sup>93,111</sup> The selectivity to furfuryl alcohol could be enhanced by sterically limiting the adsorption with coverage effects. By first depositing high coverage of H, followed by a low coverage of furfural (i.e. a high ratio of H<sub>(ads)</sub>:furfural), a sufficient concentration of H atoms was made available, which led to the formation of the desired furfuryl alcohol and methylfuran with 50% and 45% selectivity, respectively.<sup>93</sup>

To determine whether crotonaldehyde hydrogenation occurs stepwise via partially hydrogenated intermediates, or directly to the fully hydrogenated product, an effusive collimated molecular beam was used to direct the molecules onto a Pt polycrystalline film in ultrahigh vacuum.<sup>247</sup> All hydrogenation products were obtained, with butanal as the major product and 20% selectivity



to crotyl alcohol. Dehydrogenation products such as CO and propylene were not observed, in contrast to the previous reports on clean Pt(111).<sup>106</sup> In temperature programmed desorption experiments, steady state is not achieved. As such, even if the surfaces are pre-dosed with H<sub>2</sub>, it recombines and desorbs at low temperatures (~300 K), preventing hydrogenation.<sup>125,126</sup> In contrast, the molecular beam provided a high H coverage under steady-state conditions, thereby promoting the hydrogenation.

The adsorption energetics and reactivity on Pt(111) have been investigated extensively using DFT for acrolein,<sup>32,104,165,174,175,190,203</sup> crotonaldehyde,<sup>31,32,109,160,161,186–188</sup> and prenal.<sup>31,32,104,110,188,248</sup> The experimentally observed selectivity trends were attributed to the adsorption geometry of the unsaturated aldehyde in key comparative studies of the three species.<sup>31–33</sup> Initial results from the semi-empirical extended Hückel theory,<sup>33</sup> followed by first-principles calculations,<sup>31,32,160,161,165,174,175,203,248</sup> have established the following. Acrolein adsorbed mainly via its C=C bond over a large range of coverage, promoting the formation of propanal. From *ab initio* thermodynamics,<sup>165</sup> a mixture of *cis*- $\eta^3$  and *trans*- $\eta^4$  configurations were identified at low coverages and finite temperatures, in agreement with sum frequency generation vibrational spectroscopy.<sup>243</sup> This was also the case for crotonaldehyde,<sup>243</sup> whose C=C bond remained parallel to the surface at all coverages, based on near edge X-ray absorption fine structure spectroscopy.<sup>246</sup> Substituents at the  $\beta$ -carbon sterically weakened the adsorption, especially for prenal.<sup>110,187</sup> Due to the geometric constraints, the planar  $\eta^4$ -di $\sigma$ (CC)-di $\sigma$ (CO) configuration was favored only at low coverages, eventually shifting to a vertical  $\eta^1$ - $\sigma$ (O) configuration at high coverages (Fig. 10). As such, the chemoselective reduction of the C=O bond became much more feasible for prenal.

Structure sensitivity of the hydrogenation of the unsaturated aldehydes has been investigated in both single-crystal surface science experiments and DFT modeling of non-close-packed

facets and Pt nanoclusters. From *ab initio* thermodynamics,<sup>166</sup> the adsorption of acrolein on Pt(110)-(1×2) remained stable in the considered temperature range of 100-400 K at 0.15 atm. At the step edges of Pt(211), the formation of 1-propenol was kinetically favored.<sup>202</sup> Similar to crotonaldehyde on Pt(111),<sup>160,161</sup> propanal formed indirectly via isomerization of 1-propenol. From surface science experiments of crotonaldehyde hydrogenation,<sup>243</sup> crotyl alcohol formed with 60% and 30% selectivity on Pt(111) and Pt(100) at 35 °C, respectively. At higher temperatures, however, butanal was the major product, with 80% selectivity on both surfaces at steady state.

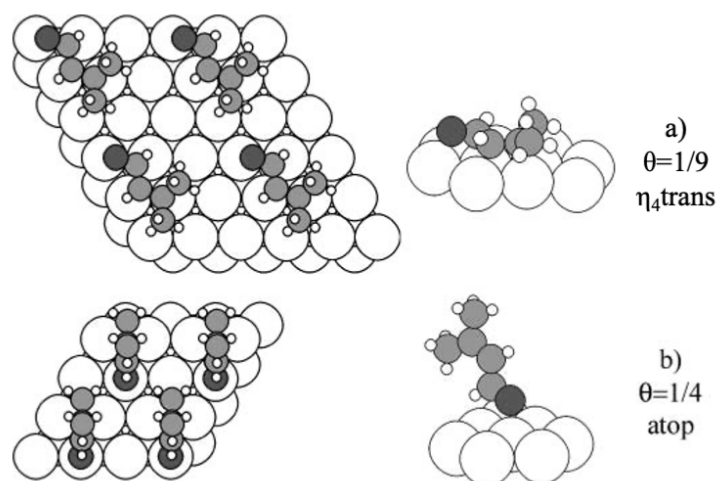


**Figure 10.** Based on DFT modeling, the most stable adsorption geometry of prenal on Pt(111) undergoes a change as a function of coverage, from (a) the flat  $\eta^4$  mode at a low coverage of 1/9 to (b) the vertical atop mode at a high coverage of 1/4 (Pt = big white; H = small white; C = grey; O = black). Adapted with permission from ref. 32 (Copyright 2002, Elsevier, Amsterdam).

Significant thermodynamic and kinetic effects have been observed from modeling the low-coordination sites and the metal-support interaction in Pt<sub>13</sub>/CeO<sub>2</sub>(111) for crotonaldehyde hydrogenation.<sup>131</sup> Compared to Pt(111), the adsorption of crotonaldehyde was strengthened on the Pt

clusters. The computed energy barriers for the reduction of the C=O bond increased on the nanocluster but decreased at the CeO<sub>2</sub> interface (Fig. 11). The authors concluded that the following model limitations must be addressed to fully explain the selectivity to crotyl alcohol reported by reactor studies: (1) larger Pt nanocluster sizes; (2) reducibility of CeO<sub>2</sub>, i.e. the presence of O vacancies; and (3) the role of H atom spillover onto CeO<sub>2</sub>. On the other hand, strain engineering was proposed as a strategy to enhance the selectivity to allyl alcohol, using Pt supported on Ba<sub>x</sub>Sr<sub>1-x</sub>TiO<sub>3</sub> nanocuboids (x = 0, 0.5, 1).<sup>201</sup> The effect of strain on acrolein adsorption was modeled using Pt<sub>N</sub> (N = 24-40) clusters, where the vertical  $\eta^1$ - $\sigma$ (O) configuration was shown to be favored at the edge sites.

Pt supported on Mn oxide octahedral molecular sieve catalysts exhibited high selectivity to cinnamyl alcohol in cinnamaldehyde hydrogenation.<sup>249,250</sup> Using DFT, the selectivity was attributed to the preferential adsorption of the C=O bond at the step edges of Pt(211). The hydrogenation pathways were further mapped out on Pt<sub>N</sub> (N = 6-18).<sup>216,251-253</sup> Pt/graphene showed high selectivity to cinnamyl alcohol,<sup>216</sup> which was attributed to (i) an increased concentration of Pt<sup>0</sup> sites promoting the adsorption of the C=O bond; and (ii) enhanced  $\pi$ - $\pi$  interaction between graphene and the phenyl group of cinnamaldehyde. The most stable adsorption mode depended on the nanocluster size, changing from  $\eta^2$ - $\pi$ (CC) on Pt<sub>6</sub> and Pt<sub>10</sub>,<sup>216,253</sup> to  $\eta^2$ - $\pi$ (CO) and  $\eta^2$ -di $\sigma$ (CO) on Pt<sub>13</sub> and Pt<sub>14</sub>.<sup>216,251,252</sup> However, arguments were made for the kinetic control of selectivity, where the computed energy barriers for the C=O bond reduction were always lower than those of the C=C bond reduction on both Pt<sub>6</sub> and Pt<sub>14</sub>.<sup>252,253</sup>

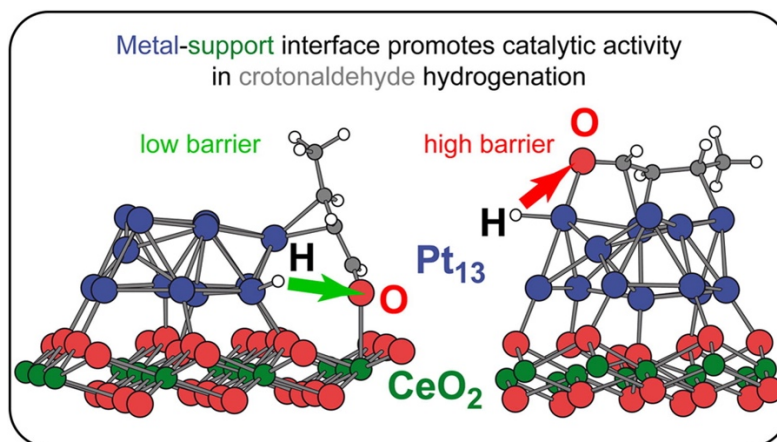


**Figure 11.** Based on DFT modeling, the reduction of the C=O bond in crotonaldehyde is kinetically facilitated at the metal-support interface of Pt<sub>13</sub>/CeO<sub>2</sub>(111), compared to the Pt cluster facet. Reprinted with permission from ref. 131 (Copyright 2015, Elsevier, Amsterdam).

In reactor studies, promotion of Pt with a secondary metal, such as Re,<sup>225</sup> Fe,<sup>147,159</sup> Co,<sup>148,149,158</sup> Zn,<sup>159,221</sup> Sn,<sup>133,134,224,227</sup> and Ge,<sup>224</sup> has led to high selectivity at high conversion, even for crotonaldehyde hydrogenation, due to an electron transfer and/or the formation of the electrophilic sites (Fig. 9a). As noted in section 2.1, multiple factors can influence the selectivity, such as strong interaction with the support, as well as changes in the catalyst structure and the particle size. However, these factors are not discussed in detail below, instead focusing on the promotion effect by a secondary metal.

#### 4.1.1.1. Electrophilic sites from promoters

In reactor studies, promotion of Pt with Re, Ge, and Zn has resulted in the formation of the oxidized species functioning as the electrophilic sites in close contact with Pt. The preferential adsorption of the C=O bond has led to higher selectivity to the unsaturated alcohols, compared to monometallic Pt catalysts.

$\text{Re}_{0.34}\text{Pt}_{0.66}/\text{TiO}_2\text{-ZrO}_2$  had higher selectivity (95.7%) to furfuryl alcohol in furfural hydrogenation, compared to  $\text{In}_{0.63}\text{Pt}_{0.37}/\text{TiO}_2\text{-ZrO}_2$ ,  $\text{Sn}_{0.62}\text{Pt}_{0.38}/\text{TiO}_2\text{-ZrO}_2$ , and monometallic  $\text{Pt}/\text{TiO}_2\text{-ZrO}_2$ , due to the presence of surface  $\text{ReO}_x$  species that promoted the C=O bond activation.<sup>225</sup> Similarly,  $\text{Ge}_{0.38}\text{Pt}_{0.62}/\text{SiO}_2$  had higher activity and selectivity (96%) to furfuryl alcohol, compared to monometallic  $\text{Pt}/\text{SiO}_2$ .<sup>224</sup> No Pt-Ge alloy phase was observed. Instead, Pt remained metallic and Ge remained fully oxidized, thereby promoting the C=O bond activation.

$\text{Zn}_{0.34}\text{Pt}_{0.66}/\text{SBA-15}$  showed high selectivity to geraniol/nerol in citral hydrogenation, in contrast to monometallic  $\text{Pt}/\text{SBA-15}$  that exhibited no selectivity.<sup>221</sup> The enhancement was attributed to the presence of oxidized Zn species. The higher the Zn content, the lower the conversion, as the surface Zn decreases the number of the Pt active sites. The trend is in agreement with surface science studies showing decreased desorption of furfural on  $\text{ZnPt}(111)$  compared to  $\text{Pt}(111)$ .<sup>111</sup> From high resolution electron energy loss spectroscopy, furfural was found to adsorb via the carbonyl group, with its O coordinated to Zn and C to Pt. Addition of Zn weakened the interaction of the furanyl ring with Pt, and the surface intermediate was stabilized, thereby decreasing the activity toward hydrogenation.

#### **4.1.1.2. Electron transfer to Pt**

Because Co, Fe, and Ni are more electropositive than Pt, these promoters are expected to donate electron to Pt, thereby weakening the C=C bond adsorption and promoting the chemoselective reduction of the C=O bond as described in section 2.1 (Fig. 2b iv).

Unsupported  $\text{Co}_{0.15}\text{Pt}_{0.85}$  nanoparticles had higher selectivity (99.1%) to cinnamyl alcohol in cinnamaldehyde hydrogenation, compared to unsupported monometallic Pt nanoparticles of the same size (41.4%).<sup>148</sup> CoPt nanoparticles were more selective than FePt and MnPt nanoparticles, but the latter two compositions were not studied in detail. Co atoms preferentially segregated at the

low-coordination sites on Pt nanoparticles, and the C=C bond reduction was favored in the absence of Co based on infrared spectroscopy measurements. A charge transfer was observed from Co to Pt, which weakened the C=C bond adsorption and increased the Pt back-donation to the C=O  $\pi^*$  orbital. This is consistent with DFT calculations showing lower energy barriers for the C=O bond reduction on CoPt<sub>5</sub> compared to Pt<sub>6</sub>.<sup>253</sup> As such, the local electronic properties of Pt were influenced by increasing the Co content, much more so in smaller particles; larger particles led to a loss of the selectivity.

However, a charge transfer from Co to Pt was not observed in other studies of Pt-rich CoPt catalysts. Co<sub>0.4</sub>Pt<sub>0.6</sub>/SBA-15 had higher selectivity (91%) to cinnamyl alcohol in cinnamaldehyde hydrogenation, compared to monometallic Pt/SBA-15 (42%).<sup>149</sup> Co<sub>0.4</sub>Pt<sub>0.6</sub> was found to be the optimal composition; lower Co content led to decreased activity and selectivity, whereas higher Co content led to decreased selectivity. The enhancement was attributed to an increase in the surface concentration of Pt<sup>0</sup> species, as X-ray photoelectron spectroscopy indicated no charge transfer. Similarly, no notable difference was observed in the electronic structure of shaped Co<sub>0.33</sub>Pt<sub>0.67</sub> nanoparticles (multicubes), which had higher selectivity (50%) to cinnamyl alcohol, compared to monometallic Pt nanocubes (10%).<sup>158</sup> The high activity was attributed to the high surface concentration of Pt and high-index facets such as (130), whereas the high selectivity was attributed to the steric effects arising from the surface roughness.

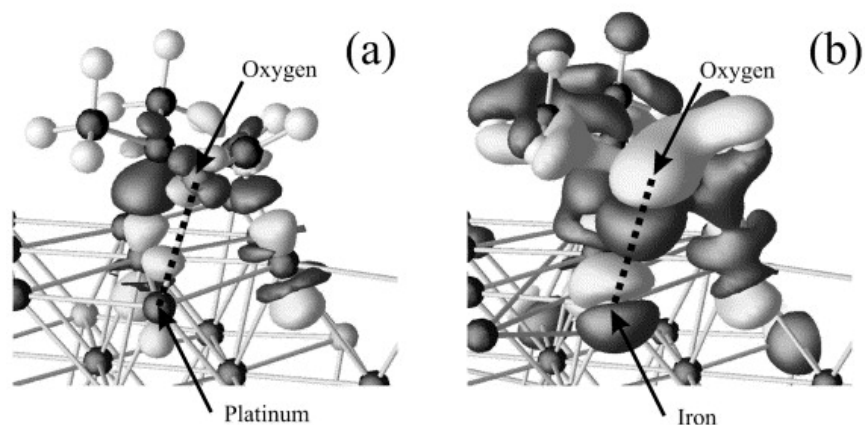


**Figure 12.** Isosurface of the charge density difference of the prenal adsorbed on  $\text{Pt}_4\text{Fe}(111)$  via the  $\eta^3$  configuration, relative to the non-interacting prenal and  $\text{Pt}_4\text{Fe}(111)$ , calculated using DFT: **(a)** clean Pt-segregated surface; **(b)** modified surface with Fe present in the surface layer. Charge gain and loss are represented by dark and light shading, respectively. As evidenced by larger isosurfaces of (b), coordination of Fe to the carbonyl O facilitates the C=O bond activation. Reprinted with permission from ref. 104 (Copyright 2003, Elsevier, Amsterdam).

$\text{Fe}_{0.36}\text{Pt}_{0.64}$  supported on mesoporous carbon had high activity and selectivity to cinnamyl alcohol in cinnamaldehyde hydrogenation.<sup>159</sup> Similar results were obtained with  $\text{Zn}_{0.2}\text{Pt}_{0.8}$ , and the best catalytic performance was given by a ternary alloy  $\text{Zn}_{0.13}\text{Fe}_{0.31}\text{Pt}_{0.56}$ . In  $\text{Fe}_{0.36}\text{Pt}_{0.64}$ , the oxidation state of Fe was not determined; however, the binding energy of  $\text{Pt}^0$  decreased upon alloying, indicating a charge transfer from Fe to Pt. These results are supported by DFT modeling of acrolein and prenal adsorption on  $\text{Pt}_4\text{Fe}(111)$ .<sup>104</sup> The surface segregation profile was modeled using the quasi-chemical approximation,<sup>254</sup> which assumes an equilibrium distribution of the two metal species across the surface layer and the subsurface layer. Pt segregated to the surface in vacuum; in the presence of the adsorbates, however, their preferential adsorption on electropositive Fe over Pt allowed a higher concentration of Fe to be stabilized in the surface layer. Both acrolein and prenal adsorbed via a  $\eta^3$ - $\text{di}\sigma(\text{CC})$ - $\sigma(\text{O})$ -OFe configuration, allowing the carbonyl group to be activated by

Fe (Fig. 12). This study highlights the need for accurate modeling of surface segregation profiles and the dynamic nature of surface composition and morphology under reaction conditions to understand hydrogenation mechanisms.<sup>78–83</sup>

Fe<sub>0.24</sub>Pt<sub>0.76</sub> zigzag nanowires supported on TiO<sub>2</sub> exhibited high selectivity to the unsaturated alcohols in the hydrogenation of crotonaldehyde, cinnamaldehyde, and furfural, with one of the highest selectivity values reported for crotonaldehyde hydrogenation (80.3% selectivity at 80% conversion).<sup>147</sup> However, in contradiction to other studies of FePt, the enhancement was attributed to a charge transfer from Pt to Fe, as indicated by the higher binding energy of Pt observed in X-ray photoelectron spectroscopy.

The effects of 3*d* metal monolayer (M = Fe, Co, Ni, Cu) on Pt(111) – in either surface (M/Pt) or subsurface (Pt/M/Pt) structures – have been investigated for acrolein<sup>94,95,190,255</sup> and furfural,<sup>191</sup> using surface science experiments and DFT. Acrolein hydrogenation occurred readily on Pt/M/Pt(111) but not on M/Pt(111).<sup>190</sup> The allyl alcohol yield was the highest on Pt/Ni/Pt(111), followed by Pt/Co/Pt(111) and Pt/Cu/Pt(111).<sup>94</sup> The yield was further enhanced from 2% to 17% by co-adsorbed H on Pt/Ni/Pt(111). The activity trends were attributed to the electronic modification of the surface in terms of the *d*-band center and the resulting decrease in the adsorption strength of acrolein. Nonetheless, the adsorption of the C=C bond remained stronger than that of the C=O bond, and propanal was the major product. However, NiPt catalysts have not yet been considered in reactor studies, and opportunities exist for the selectivity improvement under reactor conditions.

Furfural underwent hydrodeoxygenation and decarbonylation on M/Pt(111).<sup>191</sup> Compared to Pt(111) or Pt/M/Pt(111), M/Pt(111) exhibited higher activity for furfural hydrodeoxygenation because of a stronger furfural adsorption. Depositing the more oxophilic 3*d* metals (Fe, Co) led to a higher yield of methylfuran, compared to the less oxophilic ones (Ni, Cu) that led to a weaker



furfural adsorption. No hydrogenation products were formed because the H<sub>2</sub> exposure was low. The presence of chemisorbed O decreased the hydrodeoxygenation activity.

#### 4.1.1.3. Concurrent electron transfer and electrophilic site formation

In numerous reactor studies of SnPt alloy catalysts, the selectivity enhancement has been attributed to a charge transfer from Sn to Pt and/or the formation of the electrophilic sites. Surface science and DFT studies have shown that the adsorption of the unsaturated aldehydes is weaker on SnPt surfaces compared to monometallic Pt surfaces, and their adsorption geometries are also modified, except in the case of acrolein.

The selectivity enhancement in furfural hydrogenation has been reported by multiple studies. SnPt/SiO<sub>2</sub> had higher activity and selectivity to furfuryl alcohol, compared to monometallic Pt/SiO<sub>2</sub>.<sup>224</sup> Metallic Pt, metallic Sn (possibly a Pt-Sn alloy phase), and oxidized Sn(II/IV) coexisted in the SnPt sample. The enhancement was attributed to a charge transfer from Sn to Pt. Sn<sub>0.17</sub>Pt<sub>0.83</sub> had the best catalytic performance, exhibiting almost 100% selectivity at 99% conversion. Higher Sn content led to a lower activity due to the blockage of the Pt sites. SnPt/SiO<sub>2</sub> outperformed GePt/SiO<sub>2</sub>, which was attributed to the higher electropositivity of Sn and more favorable C=O bond activation. Sn<sub>0.3</sub>Pt<sub>0.7</sub>/SiO<sub>2</sub> also showed high activity and selectivity (99%) to furfuryl alcohol.<sup>227</sup> Although the authors did not describe the effect of Sn or offered a comparison with monometallic Pt/SiO<sub>2</sub>, they reported high stability and higher activity than the aforementioned study<sup>224</sup> and other reports on similar SnPt/SiO<sub>2</sub> systems. From DFT models of intermetallic SnPt, the selectivity enhancement was attributed to the modification of the furfural binding mode to a vertical  $\eta^1\text{-}\sigma(\text{O})\text{-OSn}$  configuration on SnPt(110) and SnPt(100), compared to a flat orientation on Pt(111).<sup>189</sup>

Pyramidal  $\text{Sn}_{0.25}\text{Pt}_{0.75}$  alloy-metal oxide-graphene hybrids have been shown to have high activity and selectivity to the unsaturated alcohols in the hydrogenation of twelve unsaturated aldehyde species, including crotonaldehyde, furfural, and cinnamaldehyde.<sup>133</sup> These catalysts were comprised of very fine  $\text{Sn}_{0.25}\text{Pt}_{0.75}$  alloy particles (0.6-1.2 nm) fabricated on  $\text{SnO}_2$  nanoparticles (4.8-5.8 nm) supported on reduced graphene oxide (rGO). The remarkable performances were attributed to a synergistic effect between the three components ( $\text{Pt}_3\text{Sn}$ ,  $\text{SnO}_2$ , and rGO).

The selectivity enhancement has also been reported for other unsaturated aldehydes in various studies.  $\text{Sn}_{0.4}\text{Pt}_{0.6}$  nanowires had higher selectivity (90.6%) to the unsaturated alcohols, compared to  $\text{Sn}_{0.4}\text{Pt}_{0.6}$  nanoparticles (86.3%) and monometallic Pt nanoparticles (39.4%), in the hydrogenation of crotonaldehyde, prenal, furfural, and cinnamaldehyde.<sup>134</sup>  $\text{Sn}_{0.4}\text{Pt}_{0.6}$  was found to be the optimal composition: lower Sn content led to a higher activity but a lower selectivity. Two main trends were established: (i) the higher the metallic  $\text{Pt}^0$  content, the higher the conversion; and (ii) the higher the Sn content, the higher the selectivity due to a charge transfer from Sn to Pt. Only oxidized Sn species were present on the surface.

In contrast to these observations from reactor studies, crotonaldehyde hydrogenation in a high pressure reactor exhibited higher activity and lower apparent activation energy on  $\text{SnPt}(111)$  alloys compared to  $\text{Pt}(111)$ .<sup>114</sup> Furthermore, the selectivity remained nearly the same, with butanal as the major product. The increased activity was attributed to a charge transfer from Pt to Sn, contradictory to what would be expected based on the electronegativity difference, reducing the electron density of the Pt sites. On the other hand,  $\text{SnPt}$  alloys supported on carbon showed higher selectivity to crotyl alcohol with increasing Sn concentration, in agreement with reactor studies.<sup>134</sup> To understand the role of the oxidic species,  $\text{SnPt}(111)$  alloys were oxidized to form surface  $\text{SnO}_x$ : the activity for hydrogenation decreased, compared to  $\text{Pt}(111)$  and reduced  $\text{SnPt}(111)$  alloys; the activity was restored upon reducing Sn to its metallic state under  $\text{H}_2$ .

The adsorption energetics of acrolein, crotonaldehyde, and prenal on SnPt(111) alloys have been investigated using surface science experiments<sup>109,110,186</sup> and DFT,<sup>103,109,110,186–188</sup> which showed weaker adsorption on the alloy compared to monometallic Pt(111). Furthermore, the decomposition of crotonaldehyde was reduced by 50% on SnPt(111) alloys compared to Pt(111), in agreement with reactor studies.<sup>113,134</sup> Upon increasing the Sn concentration from Pt<sub>3</sub>Sn(111) to Pt<sub>2</sub>Sn(111), the adsorption of crotonaldehyde was further weakened, and the decomposition products were not formed. Despite the lack of hydrogenation products, the observation is consistent with reactor studies that showed higher selectivity at higher Sn content.

On Pt<sub>3</sub>Sn(111), crotonaldehyde adsorbed in a  $\eta^3$ -di $\sigma$ (CC)- $\sigma$ (O)-OSn configuration with its carbonyl O coordinated to Sn, in direct contrast to the  $\eta^2$ -di $\sigma$ (CC) configuration observed on Pt(111). Upon increasing the Sn coverage to Pt<sub>2</sub>Sn(111), the most stable adsorption geometry shifted to the vertical  $\eta^1$ - $\sigma$ (O)-OSn configuration. These binding modes allowed the C=O bond to be activated by Sn, while weakening the interaction of the C=C bond with the surface. On the other hand, prenal adsorbed via a vertical *trans*- $\eta^1$ - $\sigma$ (O)-OSn configuration on both Pt<sub>3</sub>Sn(111) and Pt<sub>2</sub>Sn(111) (Fig. 13). This binding mode was consistent with a charge transfer from Sn to Pt and the resulting downward shift of the *d*-band center.<sup>103</sup> In contrast to the enhanced selectivity to prenal observed in reactor studies, prenal underwent reversible desorption on SnPt(111) alloys in ultrahigh vacuum, and no hydrogenation or decomposition products were formed.<sup>110</sup> Finally, in the case of acrolein, although the adsorption was weakened, the binding mode remained in the  $\eta^2$ -di $\sigma$ (CC) configuration (Fig. 13), the same as on Pt(111). As such, the selectivity to allyl alcohol remained low.

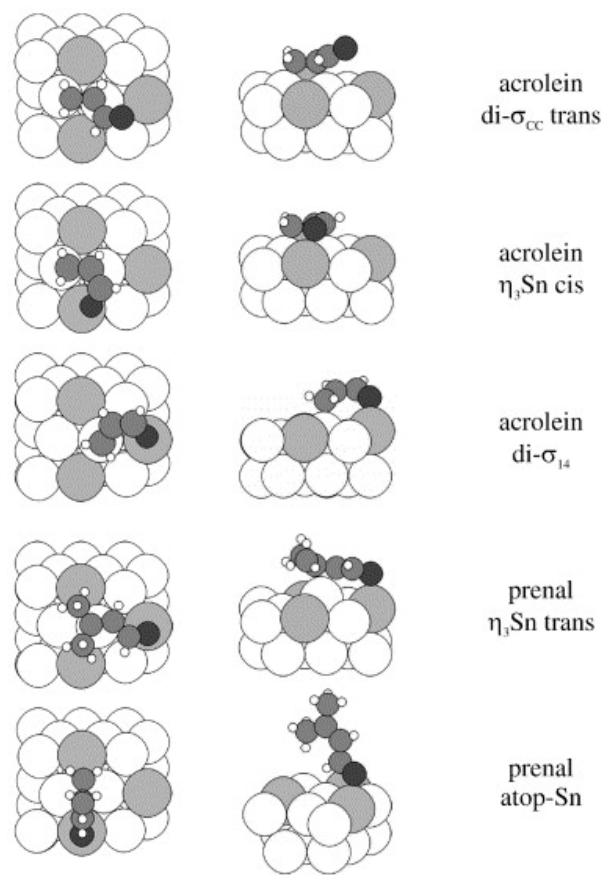


**Figure 13.** Top and side views of the most stable adsorption modes of acrolein and prenal on Pt<sub>2</sub>Sn(111), calculated using DFT. Prenal prefers the vertical atop mode with its carbonyl O coordinated to Sn, whereas acrolein lies flat on the surface (Pt = big white; H = small white; C = grey; O = black). Reprinted with permission from ref. 103 (Copyright 2003, Elsevier, Amsterdam).

#### 4.1.2. Ru and Ru alloys

Monometallic Ru catalysts have generally shown low selectivity to the unsaturated alcohols and a propensity for deactivation in the hydrogenation of crotonaldehyde,<sup>132,140–142,214,228,229,231</sup> cinnamaldehyde,<sup>101,141,214,228,232</sup> and citral<sup>141,234</sup> (Fig. 9b). The only exception is crotonaldehyde hydrogenation on Ru/ZnO containing chlorine residues from the preparation method, but this monometallic catalyst was outperformed by an IrRu alloy catalyst (see below).<sup>140</sup> Ru supported on a metal

organic framework was able to selectively hydrogenate cinnamaldehyde<sup>228</sup> but not crotonaldehyde under the same conditions.

Using DFT and microkinetic modeling, the reactivity of furfural has been shown to be structure-sensitive across various Ru surfaces.<sup>164,169,256</sup> On face centered cubic Ru(001),<sup>169</sup> reduction of the carbonyl group and the furanyl ring opening were both facile and kinetically competitive. Hydrodeoxygenation proceeded after the ring opening, demonstrating the excellent O removal ability of Ru. Pentane was predicted to be the dominant product of the vapor-phase hydrogenation, consistent with experimental studies of bio-oil upgrading on Ru/C.<sup>257</sup> In contrast, on hexagonal close packed Ru(0001),<sup>164</sup> strongly bound species, such as furan and furfuryl alcohol, inhibited the ring opening by site blockage. On oxide-terminated RuO<sub>2</sub>(110),<sup>256</sup> the formation of furfuryl alcohol was facilitated by isopropyl alcohol as the Meerwein-Ponndorf-Verley reagent, where H transfer occurs from the hydroxyl group of isopropyl alcohol to the carbonyl group of furfural. In contrast to Ru(0001), bridge O on RuO<sub>2</sub>(110) acted as the Lewis base sites that prevented the activation of the furanyl ring in furfuryl alcohol, thereby hindering its hydrodeoxygenation. Furthermore, the formation of water was found to be facile and a possible source of surface poisoning.

From DFT modeling of cinnamaldehyde adsorption on Ru fulleride nanospheres (C<sub>60</sub>-Ru<sub>13</sub>-C<sub>60</sub>), the  $\eta^3$ -di $\sigma$ (CC)- $\sigma$ (O) configuration was found to be the most stable, both with and without hydrides on the small Ru cluster.<sup>258</sup> The phenyl ring interacted strongly with one of the cluster facets, but only in the case of clean facets. This binding mode suggests the chemoselective reduction of the C=C bond, in disagreement with the experimentally observed selectivity to cinnamyl alcohol in the presence of a weak base in a methanol solvent. An implicit solvent model was insufficient to shift the adsorption energetics, highlighting the need to model dynamical solvent effects.

Interestingly, promotion of Ru with a secondary metal, such as Fe,<sup>234</sup> Ir,<sup>140,230</sup> Pt,<sup>156</sup> Au,<sup>141</sup> and Sn,<sup>132,233</sup> has led to significant enhancement of the selectivity at high conversions in reactor studies, for the hydrogenation of crotonaldehyde, cinnamaldehyde, furfural, and citral. The enhancements were attributed to an electron transfer to or from Ru and the formation of the electrophilic sites (Fig. 9b). Many promising bimetallic compositions have yet to be investigated for the selective hydrogenation of the unsaturated aldehydes using surface science and DFT methods.

#### 4.1.2.1. Concurrent electron transfer and electrophilic site formation

Because Sn and Fe are more electropositive than Ru, these promoters should donate electron to Ru and thereby favor the adsorption of the C=O bond. Sn<sub>0.3</sub>Ru<sub>0.7</sub>/C had higher activity and selectivity (90%) to furfuryl alcohol in furfural hydrogenation, compared to monometallic Ru/C (47%).<sup>233</sup> The enhancement was attributed to a charge transfer from Sn to Ru, as evidenced by a downward shift in Ru<sup>0</sup> binding energy from X-ray photoelectron spectroscopy, as well as the possible presence of a Ru-Sn alloy phase. The authors also suggested that Sn reduces the adsorption strength of H on Ru, thereby increasing the availability of the Ru active sites. Furthermore, Sn(II/IV) species (coexisting with Sn<sup>0</sup>) could act as the Lewis acid sites, activating the C=O bond and facilitating its reduction. Because the higher Sn content of Sn<sub>0.44</sub>Ru<sub>0.56</sub> catalysts did not improve the catalytic performance, the authors concluded that an optimum exists between the dilution of the Ru active sites and the promoter effect of Sn. In another study of crotonaldehyde hydrogenation, Sn<sub>0.12</sub>Ru<sub>0.88</sub>/SiO<sub>2</sub> had higher selectivity (60%) to crotyl alcohol, compared to monometallic Ru/SiO<sub>2</sub> that only exhibited activity for the C=C bond reduction.<sup>132</sup> The enhancement was attributed to the coexistence of intermetallic RuSn and SnO<sub>x</sub> species, resulting in a charge transfer from Sn to Ru.

$\text{Fe}_{0.36}\text{Ru}_{0.64}$ /graphite had higher selectivity (65%) to geraniol/nerol in citral hydrogenation, compared to monometallic Ru/graphite (35%).<sup>234</sup> The enhancement was attributed to the formation of a Ru-Fe alloy. Fe acted as the Lewis acid site for the C=O bond activation, followed by a facile addition of H chemisorbed on a nearby Ru site.

#### 4.1.2.2. Ru as the Lewis acid site

Promotion of Ru with more electronegative metals, such as Ir, Pt, and Au, have led to higher selectivity via Ru functioning as the Lewis acid sites.  $\text{Ir}_{0.11}\text{Ru}_{0.89}$ /ZnO had higher selectivity to crotyl alcohol (91%) in crotonaldehyde hydrogenation, compared to both monometallic Ir/ZnO (83%) and Ru/ZnO (75%).<sup>140</sup> The enhancement was attributed to a charge transfer from Ru to Ir, based on X-ray photoelectron spectra. Higher Ir content led to a lower selectivity due to the weakening of the overall Lewis acidity of the surface. Although the catalyst was more stable than monometallic Ru/ZnO, it still showed signs of deactivation from surface deposition of organic compounds. Similar findings were reported by the authors for  $\text{Ir}_{0.35}\text{Ru}_{0.65}$ /ZnO, previously reduced at the optimal reduction temperature of 473 K in  $\text{H}_2$ .<sup>230</sup>

$\text{Au}_{0.06}\text{Ru}_{0.94}$ /MCM-41 had higher activity and selectivity to the unsaturated alcohols in the hydrogenation of crotonaldehyde (75%), cinnamaldehyde (73%), and citral (70%), compared to monometallic Ru/MCM-41 (20%, 30%, and 22% respectively).<sup>141</sup> The activity enhancement was attributed to the dispersion of Ru on the support, whereas the selectivity enhancement was attributed to a charge transfer from Ru to Au, as evidenced by X-ray photoelectron spectroscopy. However, no Ru-Au alloy phase was formed; Ru and Au nanoparticles co-existed. The authors hypothesized that Ru nanoparticles in close contact with Au nanoparticles could act as the Lewis acid sites for the C=O bond activation, but no justification was provided.

Pt<sub>0.3</sub>Ru<sub>0.7</sub> supported on carbon nanotubes (CNTs) had higher selectivity (94%) to cinnamyl alcohol in cinnamaldehyde hydrogenation, compared to the same system supported on Al<sub>2</sub>O<sub>3</sub> (52%) or SiO<sub>2</sub> (65%).<sup>156</sup> The enhancement was attributed to (i) the formation of a Ru-rich alloy after high temperature treatment; and (ii) the use of CNTs as a support assisting the cinnamaldehyde adsorption. Here, Ru can act as the Lewis acid site for the C=O bond activation, as well as the electropositive metal that inhibits the C=C bond adsorption by increasing the electron density of Pt. However, the study did not offer any comparison with monometallic Pt or Ru catalysts.

Surface science studies of acrolein hydrogenation on Ru(001) and PtRu(001)<sup>259-261</sup> have demonstrated that the coverages of acrolein and H atoms strongly influence the selectivity. In the absence of H<sub>2</sub>, acrolein decomposed to CO and H<sub>2</sub> on Ru(001), similar to Pt(111).<sup>106,107</sup> Co-adsorption of H<sub>2</sub> and acrolein led to propanal as the major product. The addition of Pt, a reactive metal, formed PtRu near-surface alloys and predominantly led to decomposition on H-covered surfaces. Only 1 ML PtRu(001) alloys exhibited the hydrogenation activity, but the major product was propanal, similar to H-covered Pt(111).<sup>259</sup> Therefore, the addition of Pt increased the reactivity but did not suppress the decomposition.

### 4.1.3. Ir and Ir alloys

Monometallic Ir catalysts have been used for the hydrogenation of crotonaldehyde,<sup>142,146,229,235,236</sup> cinnamaldehyde,<sup>142,153,237</sup> and citral,<sup>262</sup> with moderate to high selectivity to the unsaturated alcohols but rarely at high conversions.

From DFT modeling of crotonaldehyde adsorption on Ir(111), a *cis*- $\eta^4$ - $\sigma$ (C)- $\pi$ (CC)- $\sigma$ (O) configuration was found to be the most stable, with the C=C bond interacting with the surface more strongly than the C=O bond.<sup>263</sup> In the gas phase, the *trans*-configuration was found to be more



stable than the *cis*-configuration. On Ir(111), however, the two configurations were close in energy, suggesting their coexistence. The computed energy barriers for the *cis-trans* isomerization were lower on Ir(111) than in the gas phase.

Although Ir has been used extensively as a promoter for other metals in reactor studies, it has rarely been used as a host metal for the hydrogenation of the unsaturated aldehydes. Promotion of Ir with Fe<sup>145,146</sup> and Ag<sup>144</sup> has led to enhanced catalytic performances (Fig. 9c). In particular, promotion with Re led to an especially selective and active catalyst.<sup>142</sup>

#### 4.1.3.1. Electrophilic sites from promoters

In Ir catalysts, FeO<sub>x</sub> and ReO<sub>x</sub> species have functioned as the electrophilic sites for the preferential adsorption of the C=O bond, with ReIr catalysts exhibiting one of the highest reported selectivity values to crotyl alcohol at high crotonaldehyde conversion. Fe<sub>0.05</sub>Ir<sub>0.95</sub> supported on boron nitride (BN) had higher activity and selectivity (84.4%) to crotyl alcohol than monometallic Ir/BN (55%).<sup>145</sup> Fe<sub>0.05</sub>Ir<sub>0.95</sub> was the optimal composition with the maximum activity, compared to lower Fe loadings. The authors made a note of chlorine residue (~0.05%) from the preparation method that may have influenced the selectivity. The presence of an Ir-Fe alloy phase could not be confirmed due to the low amount of Fe. However, the generation of the active sites at the Ir-FeO<sub>x</sub> interface of contacted Ir and FeO<sub>x</sub> nanoparticles led to a higher intrinsic rate constant and crotonaldehyde adsorption equilibrium. On such sites, the adsorption and the activation of crotonaldehyde is more facile than on a monometallic Ir surface. Similarly, Fe<sub>0.13</sub>Ir<sub>0.87</sub>/SiO<sub>2</sub> had higher activity and selectivity (90.8%) to crotyl alcohol than monometallic Ir/SiO<sub>2</sub> (78.3%).<sup>146</sup> The enhancement was attributed to the interaction between Ir<sup>0</sup> and FeO<sub>x</sub> species coexisting on the support. The catalyst remained stable over 100 hours of reaction. Higher Fe content led to deactivation and loss of

the selectivity due to a strong crotonaldehyde adsorption and the difficulty of the product desorption from the active sites. It should also be noted that Ir supported on bulk  $\text{FeO}_x$  was inactive.

$\text{Re}_{0.25}\text{Ir}_{0.75}/\text{SiO}_2$  catalysts had higher selectivity to crotyl alcohol (91.7%) than  $\text{Ir}/\text{SiO}_2$  (63.7%).<sup>142</sup> They also outperformed  $\text{ReX}/\text{SiO}_2$  ( $X = \text{Rh}, \text{Pd}, \text{Ru}, \text{Pt}$ ) catalysts with the same molar ratio. Increasing the Re content to  $\text{Re}_{0.5}\text{Ir}_{0.5}/\text{SiO}_2$  led to higher activity while preserving the same selectivity. High selectivity was also achieved with other unsaturated aldehydes, including cinnamaldehyde and furfural. The catalyst was comprised of  $\text{Ir}^0$  and  $\text{ReO}_x$  species, and the enhancement was attributed to the preferential adsorption of the  $\text{C}=\text{O}$  bond on  $\text{ReO}_x$ , in close proximity to the  $\text{Ir}-\text{ReO}_x$  interface which functioned as the active site for  $\text{H}_2$  dissociation.

$\text{CoIr}$  alloys have been investigated in surface science studies for furfural hydrogenation.<sup>264</sup> On both  $\text{Ir}(111)$  and  $\text{CoIr}(111)$ , the co-adsorption of furfural and  $\text{H}$  resulted in decomposition to  $\text{CO}$  and  $\text{H}_2$ . No hydrogenation or hydrodeoxygenation products were formed. From high resolution electron energy loss spectroscopy, furfural was adsorbed via its furan ring on  $\text{Ir}(111)$ , and the ring opening occurred below 300 K. On  $\text{CoIr}(111)$ , the ring opening occurred at a lower temperature of 240 K, indicating that the addition of oxophilic  $\text{Co}$  strengthened the adsorption of furfural. As such, although  $\text{CoIr}$  alloys have not been considered in reactor studies, they are not expected to exhibit enhanced selectivity to the unsaturated alcohols under reactor conditions.

#### 4.1.3.2. Other effects

Promotion of  $\text{Ir}$  with  $\text{Ag}$  was investigated for crotonaldehyde hydrogenation on  $\text{Ag}_x\text{Ir}_{1-x}$  ( $x = 0.06-0.31$ ) particles supported on different materials.<sup>144</sup> The use of  $\text{SiO}_2$  and  $\text{Al}_2\text{O}_3$  supports led to very low activity and zero selectivity to crotyl alcohol. Using a mesoporous  $\text{Co}_3\text{O}_4$  support led to a measurable activity, but no conversion was reported. The higher the  $\text{Ag}$  content, the lower the activity. All  $\text{AgIr}$  compositions studied had higher selectivity than monometallic  $\text{Ir}/\text{Co}_3\text{O}_4$ , with

$\text{Ag}_{0.31}\text{Ir}_{0.69}/\text{Co}_3\text{O}_4$  having the highest selectivity of  $\sim 32\%$  to crotyl alcohol. The enhancement was attributed to multiple effects. (i) Weaker H adsorption on more Ag-rich systems was attributed for faster H spillover onto the  $\text{Co}_3\text{O}_4$  support and a closer interaction between crotonaldehyde and the support. (ii) Using DFT, the adsorption of crotonaldehyde was modeled on small Ir ensembles embedded in Ag(111), as well as on  $\text{Co}_3\text{O}_4(110)$  (Fig. 14). While the adsorption occurred through the C=C bond on isolated Ir monomers via a  $\eta^2\text{-}\pi(\text{CC})\text{-CCIr}$  configuration, the  $\eta^4$  binding mode was favored on Ir-rich ensembles and  $\text{Co}_3\text{O}_4(110)$ , allowing the C=O bond reduction to be more feasible. (iii) AgIr nanoparticles were larger than monometallic Ir nanoparticles. This limited the space in mesopores where the reagents can interact with the active sites, thereby hindering the C=C bond adsorption and favoring the C=O bond adsorption instead. The mass transfer limitations increased the overall contact time and the probability of an indirect C=O bond reduction by H atoms that have spilled over onto the support.

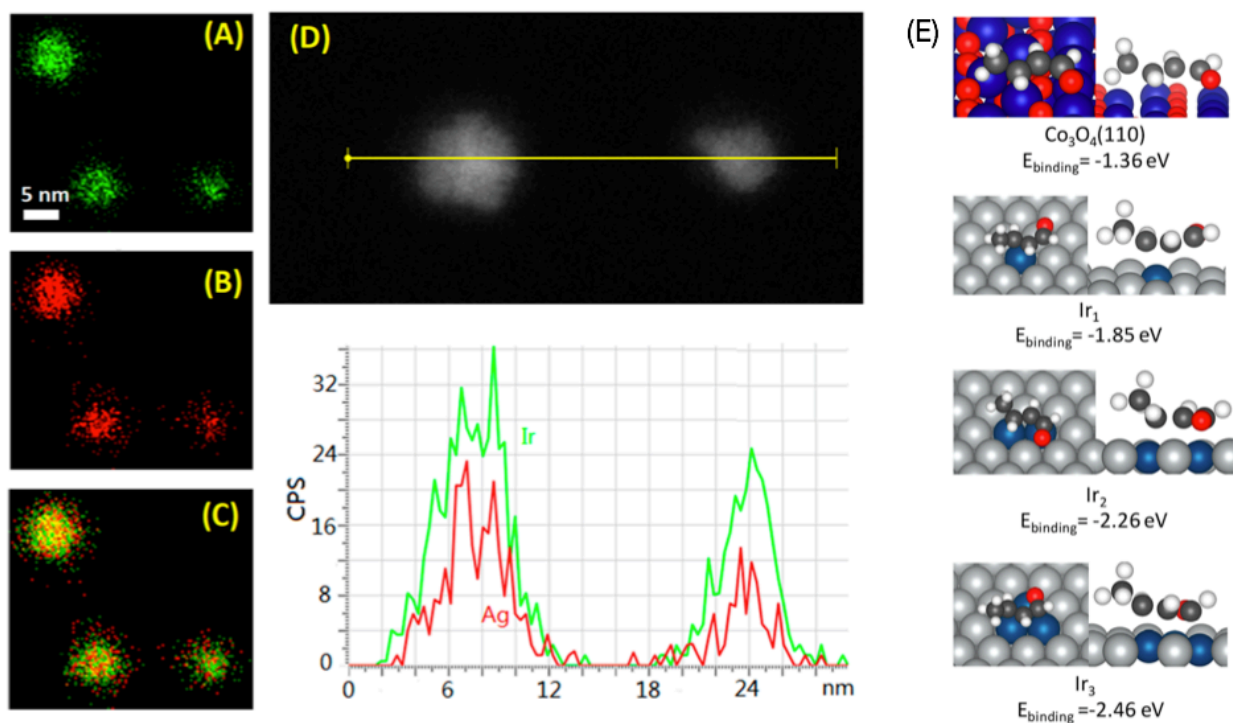


**Figure 14.** 2-dimensional energy dispersive spectroscopy maps of (A) Ir (green), (B) Ag (red), and (C) the overlay map of three  $\text{Ag}_{0.31}\text{Ir}_{0.69}$  nanoparticles. (D) Line-scan elemental profiling of the bottom two  $\text{Ag}_{0.31}\text{Ir}_{0.69}$  nanoparticles with the corresponding elemental counts. (E) The most favorable adsorption modes and binding energies of crotonaldehyde on  $\text{Co}_3\text{O}_4(110)$  as well as  $\text{Ir}_{1-3}$  surface ensembles in  $\text{Ag}(111)$ , calculated using DFT (Ir = turquoise; O = red; C = black; H = white; Co = navy; Ag = gray). Adapted with permission from ref. 144 (Copyright 2018, American Chemical Society, Washington, DC).

#### 4.1.4. Rh and Rh alloys

Monometallic Rh catalysts have exhibited very low selectivity to crotyl alcohol in crotonaldehyde hydrogenation.<sup>139,142</sup> Promotion of Rh with a secondary metal has remained scarce in the literature, with the latest reports using Sn<sup>143</sup> and Ge.<sup>143,239</sup> The selectivity remained low, however (<50%) (Fig. 9d). To the best of our knowledge, Rh has not been investigated by surface science or DFT methods for the hydrogenation of the unsaturated aldehydes.

##### 4.1.4.1. Concurrent electron transfer and electrophilic site formation

$\text{Sn}_{0.32}\text{Rh}_{0.68}/\text{SiO}_2$  had higher selectivity to crotyl alcohol (33.5%) in crotonaldehyde hydrogenation, compared to monometallic Rh/SiO<sub>2</sub> (2.3%).<sup>143</sup> The enhancement was attributed to the formation of a Rh-Sn alloy phase as well as SnO<sub>x</sub> species, with a charge transfer from Sn to Rh facilitating the C=O bond activation.

$\text{Ge}_{0.41}\text{Rh}_{0.59}/\text{TiO}_2$  had higher selectivity to geraniol/nerol (45%) in citral hydrogenation, compared to monometallic Rh/TiO<sub>2</sub> (12%).<sup>239</sup> The enhancement was attributed to the presence of GeO<sub>x</sub> species activating the C=O bond, as well as a strong metal-support interaction with TiO<sub>2</sub> after the reduction at 773 K in H<sub>2</sub>. Higher Ge content led to a higher selectivity at high conversion when reduced at a lower temperature of 573 K.

#### 4.1.5. Pd and Pd alloys

Monometallic Pd catalysts have exhibited low selectivity to the unsaturated alcohols in the hydrogenation of acrolein,<sup>200,241</sup> crotonaldehyde,<sup>142,214,222</sup> and cinnamaldehyde.<sup>151,214,241,242</sup> Saturated aldehydes and saturated alcohols were produced in reactor studies (Fig. 9e).

Pd(111) and Pd nanoparticles have been investigated extensively in surface science studies for the hydrogenation of acrolein,<sup>96,265–268</sup> crotonaldehyde,<sup>112,269</sup> and furfural.<sup>105,270</sup> Decomposition was the predominant pathway for all molecules, producing CO and H<sub>2</sub>, as well as propylene from crotonaldehyde decarbonylation and methylfuran from furfural hydrodeoxygenation.

Remarkably, acrolein on Pd(111) led to ~100% selectivity to allyl alcohol in the presence of a continuous high flux H<sub>2</sub> molecular beam at 250 K.<sup>96</sup> From *in situ* infrared spectroscopy at the maximum conversion, oxopropyl species formed prior to allyl alcohol, whereas propenoxy species formed 16–24 s after the induction period (Fig. 15). This observation indicated that the propenoxy surface intermediates are formed only on the oxopropyl-modified surface, resulting in the geometrically confined adsorption sites for the incoming acrolein molecules to adsorb via their carbonyl O and undergo the chemoselective reduction of the C=O bond.

The particle size had a significant effect on the selectivity of acrolein hydrogenation on Pd/Fe<sub>3</sub>O<sub>4</sub>. The catalyst was studied as a function of the particle size (4, 7, 12 nm) and temperature (220, 250, 270 K).<sup>267,268</sup> On 7 and 12 nm nanoparticles, the rate of the propanal formation was the highest at 220 K with 100% selectivity. No allyl alcohol was formed at any temperature, and no propanal was formed on 4 nm nanoparticles at any temperature. In contrast, the formation of allyl alcohol was observed on Pd(111), with the highest rate and ~100% selectivity at 270 K. At lower temperatures, only a small fraction of acrolein was converted to the oxypopyl intermediate, not

enough to alter the adsorption geometry to form allyl alcohol with 100% selectivity. At higher temperatures, acrolein decomposed to CO and ethylidyne, thereby deactivating the catalyst.

Based on DFT modeling of the hydrogenation pathways of acrolein,<sup>174</sup> crotonaldehyde,<sup>209</sup> and furfural<sup>163,178,271</sup> on Pd(111), similar thermodynamics and kinetics were observed as Pt(111). The formation of allyl alcohol was kinetically favored at a low acrolein coverage because the C=O bond required more space than the C=C bond for the reduction to occur.<sup>174</sup> Similar to Pt(111),<sup>32,160,161</sup> crotonaldehyde adopted the planar  $\eta^4$ -di $\sigma$ (CC)-di $\sigma$ (CO) configuration, and butanal formed indirectly via isomerization of 1-butenol.<sup>209</sup> For all dominant pathways, the first hydrogenation steps were rate-determining.

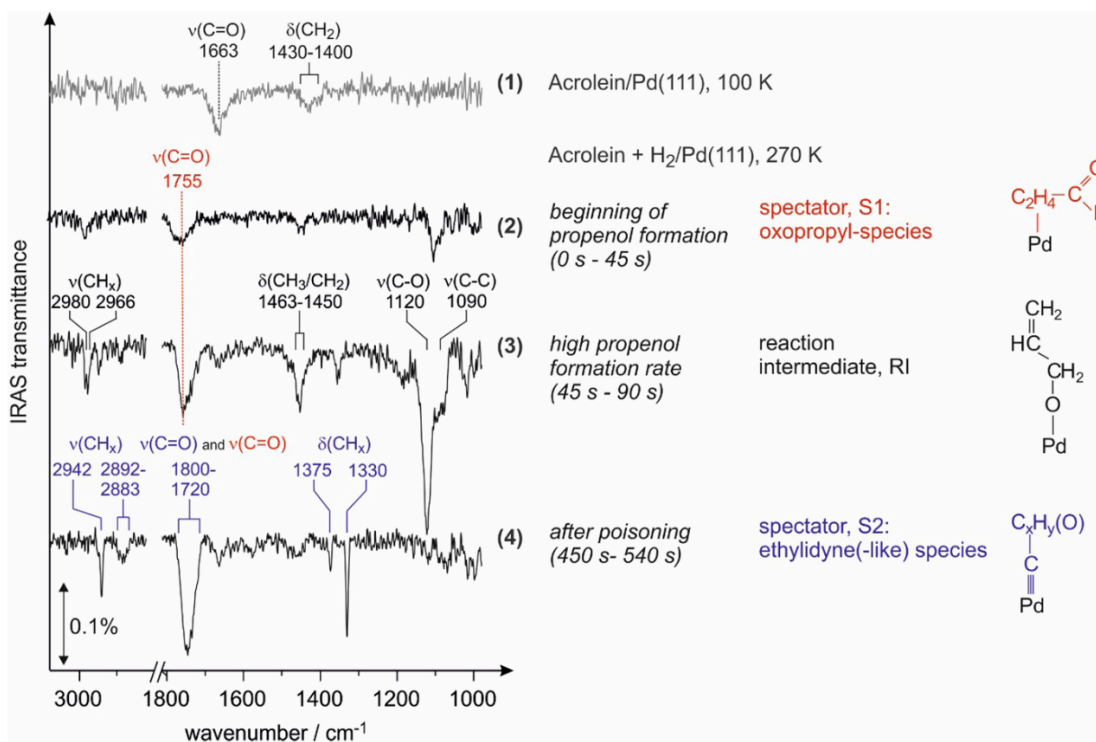


**Figure 15.** *In situ* infrared spectra of 1 ML of acrolein on Pd(111) at 100 K (gray trace, spectrum 1) and of the surface species formed on Pd(111) upon a continuous exposure to acrolein and H<sub>2</sub> at 270 K (black traces, spectra 2–4). The structures of the identified surface species are shown on the right and colored to match

the vibrational bands. Adapted with permission from ref. 267 (Copyright 2017, American Chemical Society, Washington, DC).

DFT modeling of the reduction of furfural on Pd(111) has shown significant changes in the selectivity as a function of the H coverage. On a clean surface,<sup>271</sup> a flat orientation was found to be the most stable, with the furanyl ring lying parallel to the surface. While decarbonylation to furan was favored thermodynamically, hydrogenation to furfuryl alcohol was favored kinetically. However, the dehydration of furfuryl alcohol was also a feasible pathway for hydrodeoxygenation to methylfuran. On a H-covered surface,<sup>163</sup> the furanyl ring was tilted away from the surface, and the effective energy barriers for hydrogenation and decarbonylation increased. From microkinetic modeling based on vdW-DFT, the selectivity reversal was observed upon increasing the H coverage, from furan to furfuryl alcohol (Fig. 16). This study highlights the importance of the operating conditions on the activity and the selectivity shifts induced by the reactant conformational changes.

The selectivity to cinnamyl alcohol in cinnamaldehyde hydrogenation depended strongly on the metal particle size of the Pd catalysts supported on various materials (activated C, SiO<sub>2</sub>, TiO<sub>2</sub>, Al<sub>2</sub>O<sub>3</sub>, SiC, and graphene oxide).<sup>241</sup> Smaller nanoparticles formed hydrocinnamaldehyde, whereas larger nanoparticles formed hydrocinnamyl alcohol. The trend was consistent with DFT calculations: cinnamaldehyde adsorbed via its C=C bond on Pd<sub>4</sub> representative of smaller nanoparticles, whereas the C=O bond adsorption was favored on Pd(111) representative of larger nanoparticles.

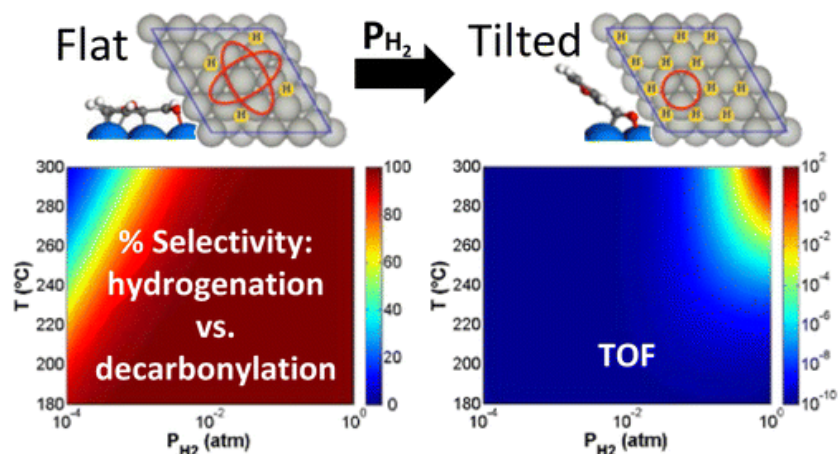


**Figure 16.** Based on DFT modeling, furfural undergoes a conformational change on Pd(111) upon increasing the H coverage, from a flat orientation to a tilted adsorption mode with the furanyl ring tilted away from the surface. The corresponding microkinetic model predicts a shift in the selectivity and the turnover frequency (TOF) from furan to furfuryl alcohol. Reprinted with permission from ref. 163 (Copyright 2015, American Chemical Society, Washington, DC).

In reactor studies, promotion of Pd with a secondary metal has been widely employed for the chemoselective reduction of the C=C bond to produce the saturated aldehydes, while preventing over-hydrogenation to the saturated alcohols. For example, AuPd promoted cinnamaldehyde hydrogenation to hydrocinnamaldehyde while preventing over-hydrogenation to hydrocinnamyl alcohol.<sup>272,273</sup> Similarly, NiPd promoted citral hydrogenation to citronellal while preventing over-hydrogenation to citronellol.<sup>274</sup> Bimetallic Pd catalysts have seldom exhibited high selectivity to the unsaturated alcohols. Promotion of Pd with Ru<sup>151</sup> and Au<sup>150</sup> has led to enhanced selectivity (Fig. 9e).



#### 4.1.5.1. Concurrent electron transfer and electrophilic site formation

$\text{Sn}_{0.6}\text{Pd}_{0.4}$  supported on activated C had higher selectivity (80%) to cinnamyl alcohol in cinnamaldehyde hydrogenation at high conversion (96%), compared to monometallic Pd.<sup>242</sup> The authors observed the formation of a Pd-Sn alloy and a charge transfer from Pd to Sn, in contradiction to what would be expected based on the electronegativity difference. Using DFT models of crotonaldehyde on Pd(111),  $\text{Pd}_3\text{Sn}(111)$ , and  $\text{PdSn}(211)$ , the enhancement was attributed to the preferential adsorption of the C=O bond via a vertical  $\eta^1\text{-}\sigma(\text{O})\text{-OSn}$  configuration.

$\text{Fe}_{0.5}\text{Pd}_{0.5}/\text{SiO}_2$  catalysts had higher selectivity to furfuryl alcohol (~50%) in furfural hydrogenation at a low space time (the catalyst mass divided by the flow rate, commonly called the W/F ratio), compared to monometallic Pd/ $\text{SiO}_2$  where decarbonylation to furan dominated.<sup>275</sup> The dehydration of furfuryl alcohol to methylfuran dominated at higher conversions on  $\text{Fe}_{0.5}\text{Pd}_{0.5}/\text{SiO}_2$ . Changing the support from  $\text{SiO}_2$  to  $\text{Al}_2\text{O}_3$  shifted the selectivity from methylfuran to furan. Using DFT models of PdFe(111) and  $\text{Pd}_3\text{Fe}(111)$  surfaces, these trends were attributed to the following: (i) alloying Pd with Fe weakens the interaction of the furanyl ring with the surface, thereby disfavoring the ring hydrogenation and decarbonylation; (ii) strong interaction of the C=O bond and the -OH group with the oxophilic Fe sites promoted their hydrogenation and dehydration, respectively.

#### 4.1.5.2. Other effects

Several reactor studies, in conjunction with DFT calculations in some cases, did not directly attribute the selectivity enhancement to an electron transfer or the formation of the electrophilic sites.  $\text{Ru}_{0.17}\text{Pd}_{0.83}$  supported on CNTs had higher selectivity to cinnamyl alcohol (67.5%) in cinnamaldehyde hydrogenation, compared to monometallic Pd/CNT samples (20%).<sup>151</sup> The authors did not provide a detailed explanation of the enhancement. Instead, they referred to the previous

literature on a possible synergy between Pd and Ru, which have similar electronegativities (Fig. 8), as well as the interaction of the O-containing functional groups with the CNT surface.

$\text{Cu}_{0.45}\text{Pd}_{0.55}/\text{SiO}_2$  samples had higher yield and selectivity (70%) to furfuryl alcohol in furfural hydrogenation, compared to monometallic Pd/SiO<sub>2</sub> over which decarbonylation to furan dominated.<sup>210</sup> A Pd-Cu alloy was formed, as evidenced by temperature programmed reduction, X-ray photoelectron spectroscopy, and diffuse reflectance infrared Fourier transform spectroscopy. The authors observed an increase in the Pd binding energy upon promotion with Cu, ruling out a direct charge transfer from Cu to Pd. Using a DFT model of PdCu(111), the enhancement was attributed to the weakening of the interaction of the carbonyl C with the surface in the  $\eta^2\text{-di}\sigma(\text{CO})$  configuration, thereby hindering the formyl C-H bond scission required for decarbonylation and promoting the C=O bond reduction instead.

$\text{Re}_{0.5}\text{Pd}_{0.5}/\text{Al}_2\text{O}_3$  catalysts exhibited a surface enrichment of Re ( $\text{Re}_{0.75}\text{Pd}_{0.25}$ ) as well as higher activity and selectivity to furfuryl alcohol in furfural hydrogenation, compared to monometallic Pd/Al<sub>2</sub>O<sub>3</sub>.<sup>276</sup> The catalyst consisted of Re<sup>0</sup> and ReO<sub>x</sub> clusters, in close contact with much larger Pd-rich nanoparticles. The enhancement was attributed to the dispersion of the surface Pd ensembles, inhibiting decarbonylation and promoting the chemoselective reduction of the C=O bond.

$\text{Au}_{0.48}\text{Pd}_{0.52}/\text{SiO}_2$  catalysts had higher selectivity (~50%) to cinnamyl alcohol in cinnamaldehyde hydrogenation, compared to monometallic Pd/SiO<sub>2</sub> (~5%).<sup>150</sup> Conversions were not reported, and the promotion by Au was not examined in detail. In surface science studies of crotonaldehyde hydrogenation, AuPd alloy surfaces did not exhibit any selectivity to crotyl alcohol, but the decomposition pathway was suppressed. In contrast to Pd(111) where decomposition was predominant, crotonaldehyde underwent reversible desorption on 4 ML Au/Pd(111) at 180 K, similar to prenal on SnPt(111).<sup>110</sup> On  $\text{Au}_{0.56}\text{Pd}_{0.44}(111)$ , a saturation exposure of crotonaldehyde led to

decomposition, albeit at a lesser extent than on Pd(111) because Au reduced the number of large Pd ensembles that facilitate the C-C bond cleavage.<sup>269</sup> Such geometric effects have been employed in many other bimetallic systems to enhance the coke resistance and as such warrant further investigation in reactor studies.<sup>277–282</sup>

## 4.2. Active electropositive metals

Co and Ni are Group 9 and 10 metals, respectively, with similar electronegativities (Fig. 8). Although they do exhibit some activity for H<sub>2</sub> dissociation, they are more electropositive and thus not as active as the conventional hydrogenation catalysts described in section 4.1. The activity and/or the selectivity has been enhanced successfully by using Co as an electron donor to Pt, whereas Ni has been promoted with more electropositive metals, such as Fe, Cu, or In (Fig. 17).

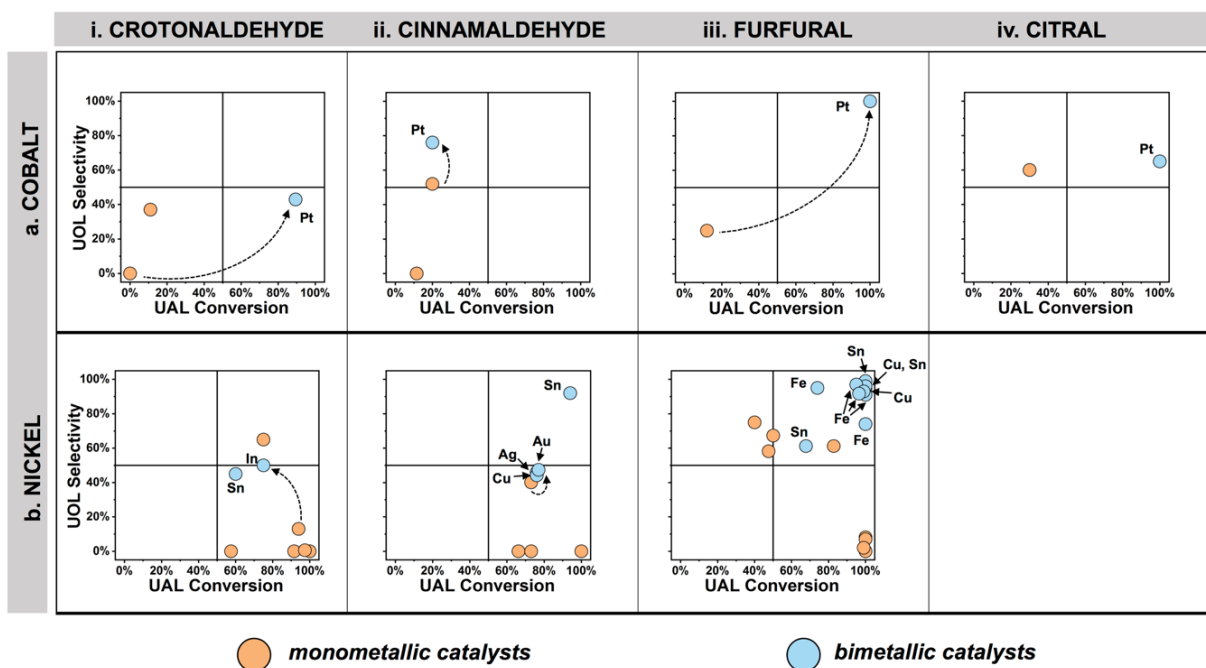


**Figure 17.** Reported selectivity to the unsaturated alcohol (UOL) as a function of the unsaturated aldehyde (UAL) conversion on: **(a)** Co and Co-rich bimetallics for the hydrogenation of crotonaldehyde,<sup>85,283</sup> cinnamaldehyde,<sup>157,215</sup> furfural,<sup>226</sup> and citral;<sup>284,285</sup> **(b)** Ni and Ni-rich bimetallics for the hydrogenation of crotonaldehyde,<sup>135,136,286–289</sup> cinnamaldehyde,<sup>136,152,237,290,291</sup> and furfural.<sup>61,135,136,292–298</sup> Dotted arrows indicate that the data are derived from the same study.

#### 4.2.1. Co and Co alloys

Monometallic Co catalysts have been used for the hydrogenation of crotonaldehyde,<sup>283</sup> cinnamaldehyde,<sup>157,215,299</sup> and citral,<sup>284</sup> and low conversions were reported (<30%) due to the low activity of Co for H<sub>2</sub> dissociation. Promotion of Co with Pt<sup>85,157,226,285</sup> has generally led to higher conversions while also enhancing the selectivity (Fig. 17a). To the best of our knowledge, Co has not been investigated by surface science or DFT methods for the hydrogenation of the unsaturated aldehydes.

##### 4.2.1.1. Electron transfer from Co

Pt<sub>0.1</sub>Co<sub>0.9</sub>/SiO<sub>2</sub> catalysts exhibited higher selectivity (76%) to cinnamyl alcohol in cinnamaldehyde hydrogenation, compared to monometallic Pt/SiO<sub>2</sub> (52%).<sup>157</sup> The enhancement was attributed to the electronic modification of Pt by Co, where the electropositive Co acts as an electron donor to increase the electron density of Pt. The same observations were made in the hydrogenation of citral with Pt<sub>0.15</sub>Co<sub>0.85</sub>/C and Pt<sub>0.3</sub>Co<sub>0.7</sub>/C, which had higher activity compared to more Pt-rich compositions as well as monometallic Pt/C and Co/C.<sup>285</sup> Pt<sub>0.3</sub>Co<sub>0.7</sub>/C catalysts had higher selectivity (65%) to geraniol/nerol than the monometallic samples, which was attributed to the formation of a Co-Pt alloy and a charge transfer from Co<sup>0</sup> to Pt<sup>0</sup>.

Pt<sub>0.23</sub>Co<sub>0.77</sub>/C samples exhibited 100% selectivity to furfuryl alcohol at 100% furfural conversion, outperforming monometallic Pt/C and Co/C.<sup>226</sup> A Co-Pt alloy phase was identified from X-ray diffraction, along with a charge transfer from Co to Pt and the presence of oxidized surface Co from X-ray photoelectron spectroscopy. Based on these observations, the authors proposed the following: H<sub>2</sub> is activated by electron-rich Pt<sup>0</sup>, and the C=O bond is activated by oxophilic Co(II). Lastly, Pt<sub>0.35</sub>Co<sub>0.65</sub>/La<sub>2</sub>O<sub>2</sub>CO<sub>3</sub> catalysts prepared by different impregnation strategies had higher activity and selectivity (34.8%) to crotyl alcohol in crotonaldehyde hydrogenation, compared to monometallic Pt/La<sub>2</sub>O<sub>2</sub>CO<sub>3</sub> (17.7%) and Co/La<sub>2</sub>O<sub>2</sub>CO<sub>3</sub> (0%).<sup>85</sup> Co-impregnation of the metal precursors led to a high degree of alloying between Pt and Co, and a charge transfer from Co to Pt was also demonstrated by X-ray photoelectron spectroscopy.

#### 4.2.2. Ni and Ni alloys

Ni-based catalysts are promising because of their low cost compared to the noble metals, in addition to their ability to activate H<sub>2</sub>. In reactor studies, monometallic Ni catalysts have primarily led to the C=C bond reduction as well as over-hydrogenation to the saturated alcohols in the hydrogenation of cinnamaldehyde,<sup>152,237,290,291</sup> citral,<sup>300</sup> and crotonaldehyde (Fig. 17b).<sup>286–289</sup> An exception was the case of Ni/TiO<sub>2</sub> that exhibited high selectivity (65%) to crotyl alcohol at high crotonaldehyde conversion (75%).<sup>286</sup>

Decarbonylation was the predominant pathway for acrolein<sup>95</sup> and furfural<sup>301–303</sup> on Ni(111) in ultrahigh vacuum. In the presence of pre-adsorbed H, neither the activity nor the selectivity was significantly affected because the intermediates were bound too strongly, preventing the desorption of the desired hydrogenation products. Both the furanyl ring and the carbonyl group of furfural

were oriented parallel to the surface, promoting the C-C and the C-O bond scission to form the decomposition products.<sup>301</sup>

Based on DFT modeling of the acrolein hydrogenation pathways on Ni(111), the formation of allyl alcohol and propanal were found to follow the Langmuir-Hinshelwood mechanism, with the latter favored both thermodynamically and kinetically.<sup>193</sup> Further hydrogenation to n-propanol followed the Eley-Rideal mechanism, in contrast to the results of a separate study that only considered the Langmuir-Hinshelwood mechanism for propanal hydrogenation on Ni(111).<sup>192</sup>

The reduction of furfural was also modeled on Ni(111) and Ni(211), where hydrogenation to furfuryl alcohol was kinetically favored over hydrodeoxygenation to methylfuran, even in the presence of step edges.<sup>168</sup> However, because of the strong interaction of the furanyl ring with the Ni surface, the dehydration of furfuryl alcohol became competitive with its desorption as an alternative route to the formation of methylfuran. Upon increasing the H coverage on Ni(111), the reactivity shifted from the furanyl ring opening to the formation of furfuryl alcohol and furan.<sup>167</sup> This trend is consistent with a previous first-principles microkinetic modeling of the effect of the H coverage on Pd(111).<sup>163</sup>

In reactor studies, promotion of Ni with various secondary metals, such as Fe,<sup>293–295</sup> Co,<sup>293,295</sup> Cu,<sup>152,295,297,298</sup> Ag,<sup>152</sup> Au,<sup>152</sup> In,<sup>135,293</sup> and Sn,<sup>61,136,292</sup> has led to enhanced selectivity to the unsaturated alcohols, which has been attributed to an electron transfer in many cases (Fig. 17b).

#### 4.2.2.1. Electron transfer to Ni

Ni has been promoted with more electropositive metals to increase the electron density of Ni sites and enhance the selectivity to the unsaturated alcohols. In most cases, the observations from reactor studies are supported by surface science experiments and DFT calculations that show

changes in the adsorption geometries as well as the stronger interaction of the C=O bond with the bimetallic surfaces.

Unsupported MNi nanoparticles (M = Fe, Co, In) exhibited higher selectivity to furfuryl alcohol in furfural hydrogenation, compared to monometallic Ni nanoparticles.<sup>293</sup> Fe<sub>0.33</sub>Ni<sub>0.67</sub> was found to be the optimal composition, where a Fe<sub>0.25</sub>Ni<sub>0.75</sub> alloy phase coexisted with a Ni phase, based on X-ray diffraction. From Fourier transform infrared spectroscopy, furfural adsorbed mainly on Fe via its C=O bond, i.e. the  $\eta^1$ - $\sigma$ (O)-OFe configuration. The results are consistent with a charge transfer from Fe to Ni as established in a similar study.<sup>304</sup> Introduction of supports (TiO<sub>2</sub>, Al<sub>2</sub>O<sub>3</sub>, CeO<sub>2</sub>, SiO<sub>2</sub>) did not affect the selectivity, which remained high (>90%), but increased the conversion, except for the case of SiO<sub>2</sub>. On the other hand, the selectivity was very low in the hydrogenation of other unsaturated aldehydes, such as citral and cinnamaldehyde, because of the isomerization of the unsaturated alcohols.

Supported FeNi nanoparticles also outperformed other bimetallic compositions in a study of MNi/SiO<sub>2</sub> (M = Fe, Co, Cu).<sup>295</sup> Fe<sub>0.25</sub>Ni<sub>0.75</sub>/SiO<sub>2</sub> had higher selectivity (91.7%) to furfuryl alcohol at high furfural conversion, compared to monometallic Ni/SiO<sub>2</sub> (67.3%) as well as Fe/SiO<sub>2</sub> which showed no activity. CoNi had the same performance as monometallic Ni. CuNi had high selectivity but low conversions. Fe<sub>0.25</sub>Ni<sub>0.75</sub> was found to be the optimal composition: the lower the Ni content, the lower the activity.

A similar enhancement was observed in Fe<sub>0.38</sub>Ni<sub>0.62</sub>/SiO<sub>2</sub>, which had higher selectivity (74%) to furfuryl alcohol at 100% furfural conversion, compared to monometallic Ni/SiO<sub>2</sub> (2%).<sup>294</sup> After the reduction in H<sub>2</sub> at 973 K, the nanoparticles were found to be an FeNi alloy with the outer shell enriched in Fe. No monometallic Fe nanoparticles were detected.

$\text{Fe}_{0.5}\text{Ni}_{0.5}/\text{SiO}_2$  had higher selectivity to furfuryl alcohol at a low temperature, compared to monometallic  $\text{Ni}/\text{SiO}_2$  over which decarbonylation to furan dominated.<sup>305</sup> However, at higher temperatures and conversions, methylfuran from hydrodeoxygenation became the major product, similar to the results of  $\text{FePd}/\text{SiO}_2$  (section 4.1.5.2).<sup>275</sup> Using a DFT model of  $\text{NiFe}(111)$ , the trends were attributed to the stronger interaction of the  $\text{C}=\text{O}$  bond with the oxophilic Fe, which promoted hydrogenation to furfuryl alcohol and its subsequent dehydration to methylfuran.

Furfural reactivity was investigated on 1 ML  $\text{Fe}/\text{Ni}(111)$  and  $\text{FeNi}/\text{SiO}_2$ .<sup>301</sup> From DFT calculations, furfural adsorbed via its  $\text{C}=\text{O}$  bond with the furanyl ring tilted away from the surface, primarily resulting in hydrodeoxygenation to methylfuran with furfuryl alcohol as the likely intermediate. Surface science experiments also confirmed that the  $\text{C}-\text{C}$  bond cleavage was suppressed on  $\text{Fe}/\text{Ni}(111)$  unlike on  $\text{Ni}(111)$ , thereby forming methylfuran as the major product.

$\text{Cu}_{0.25}\text{Ni}_{0.75}/\text{C}$ , prepared via pyrolysis of a benzene-1,3,5-tricarboxylic acid based metal organic framework, had higher activity and selectivity (93.8%) to furfuryl alcohol, compared to monometallic Cu and Ni catalysts.<sup>297</sup> The formation of a Ni-Cu alloy phase was confirmed by X-ray diffraction. From DFT calculations, the catalytic enhancement was attributed to a downward shift of the  $d$ -band center upon alloying with Cu. This electronic effect offered two benefits: (i) The desorption of  $\text{H}_2$  was facilitated on Ni, promoting the adsorption of furfural and thus the activity; (ii) the tilted adsorption geometry was favored via the  $\text{C}=\text{O}$  bond, promoting the selectivity, in contrast to the flat orientation adopted on monometallic Ni.

$\text{Cu}_{0.08}\text{Ni}_{0.92}/\text{SiO}_2$  with a high metal loading (>50 wt.%) exhibited high selectivity (96%) to furfuryl alcohol at 100% furfural conversion.<sup>298</sup> However, no comparisons were made to monometallic Ni or Cu catalysts. A strong dependence on the catalyst reduction temperature was observed: the best performance was achieved after the reduction at 573 K, resulting in a full reduction of Cu



and a partial reduction of Ni. Lower reduction temperatures resulted in a higher Ni oxide content and led to the formation of isopropyl furfuryl ester.

In surface science studies of furfural hydrogenation, 1 ML Cu/Ni(111) exhibited selectivity to methylfuran, in contrast to the dilute alloys that had high selectivity to furfuryl alcohol in reactor studies. The alloy surfaces were prepared by thermal evaporation of Cu at room temperature; the growth mechanism was previously reported to be layer-by-layer.<sup>306</sup> On Ni(111), the co-adsorption of H<sub>2</sub> and furfural led to the formation of propylene from the ring opening, in addition to CO and H<sub>2</sub> from decomposition.<sup>302,303</sup> On 1 ML Cu/Ni(111), methylfuran formed via hydrodeoxygenation, in addition to ethylene, CO, and H<sub>2</sub>.

Intermetallic In<sub>0.33</sub>Ni<sub>0.67</sub>/Al<sub>2</sub>O<sub>3</sub> catalysts had higher selectivity to the unsaturated alcohols in the hydrogenation of six different unsaturated aldehydes, including crotonaldehyde and furfural,<sup>135</sup> compared to monometallic Ni/Al<sub>2</sub>O<sub>3</sub>. The enhancement was attributed to a charge transfer from In to Ni, which promotes the C=O bond adsorption, as evidenced by DFT calculations.

M<sub>0.1</sub>Ni<sub>0.9</sub>/TiO<sub>2</sub> (M = Cu, Ag, Au) had slightly higher activity and selectivity to cinnamyl alcohol, compared to monometallic Ni/TiO<sub>2</sub>.<sup>152</sup> An alloy phase was formed for CuNi, but not for AgNi and AuNi. The selectivity was similar for the three systems, with AuNi being slightly more selective. The enhancement was attributed to a weaker H adsorption compared to monometallic Ni, as well as a possible charge transfer from Cu, Ag, and Au to Ni, which would destabilize the C=C bond adsorption.

#### **4.2.2.2. Concurrent electron transfer and other effects**

The selectivity enhancement upon promotion of Ni with Sn was attributed to the presence of intermetallic Ni-Sn phases. Sn<sub>0.3</sub>Ni<sub>0.7</sub>/AlOH had higher selectivity to the unsaturated alcohols in the hydrogenation of various unsaturated aldehydes, including crotonaldehyde, cinnamaldehyde,

and furfural, compared to Raney Ni/AlOH.<sup>136</sup> A Ni-Sn alloy phase was formed, facilitating the C=O bond adsorption.

In a similar study, SnNi/Al<sub>2</sub>O<sub>3</sub>, prepared at different Sn/Ni ratios via the layered double hydroxide precursor method, had higher selectivity (61.2%) to furfuryl alcohol in furfural hydrogenation, compared to monometallic Ni/Al<sub>2</sub>O<sub>3</sub> (8.1%).<sup>61,292</sup> Sn<sub>0.4</sub>Ni<sub>0.6</sub> was found to be the optimal composition. The surface composition remained close to Sn:Ni = 1:1, resulting in isolated Ni sites as well as a charge transfer from Sn to Ni. As such, the addition of Sn altered the furfural adsorption geometry to be tilted away from the surface. Due to these geometric and electronic effects promoting an intermediate furfural adsorption, high selectivity at high conversion was achieved on Sn<sub>0.4</sub>Ni<sub>0.6</sub>. Higher Sn content led to a higher selectivity but a lower activity, due to a much weaker furfural adsorption and the furanyl ring tilting farther away from the surface.<sup>292</sup> Using DFT models of various facets and Sn/Ni ratios—including Ni(111), Ni<sub>3</sub>Sn<sub>2</sub>(101), Ni<sub>3</sub>Sn<sub>2</sub>(112), Ni<sub>3</sub>Sn(100), Ni<sub>3</sub>Sn(101), and Ni<sub>3</sub>Sn<sub>4</sub>(40 $\bar{1}$ )—the preferential adsorption via the vertical  $\eta^1$ - $\sigma$ (O)-OSn configuration was confirmed, promoting the chemoselective reduction of the C=O bond.<sup>61</sup>

### 4.3. More noble and selective metals

Because of their full *d*-shells, Au, Ag, and Cu of Group 11 exhibit lower activity for H<sub>2</sub> dissociation than the conventional hydrogenation catalysts described in section 4.1. Nonetheless, moderate to high selectivity to the unsaturated alcohols have been reported, but promotion with more active metals (Pd, Pt, Rh, Ni, Ir) was needed to achieve higher conversions (Fig. 18).

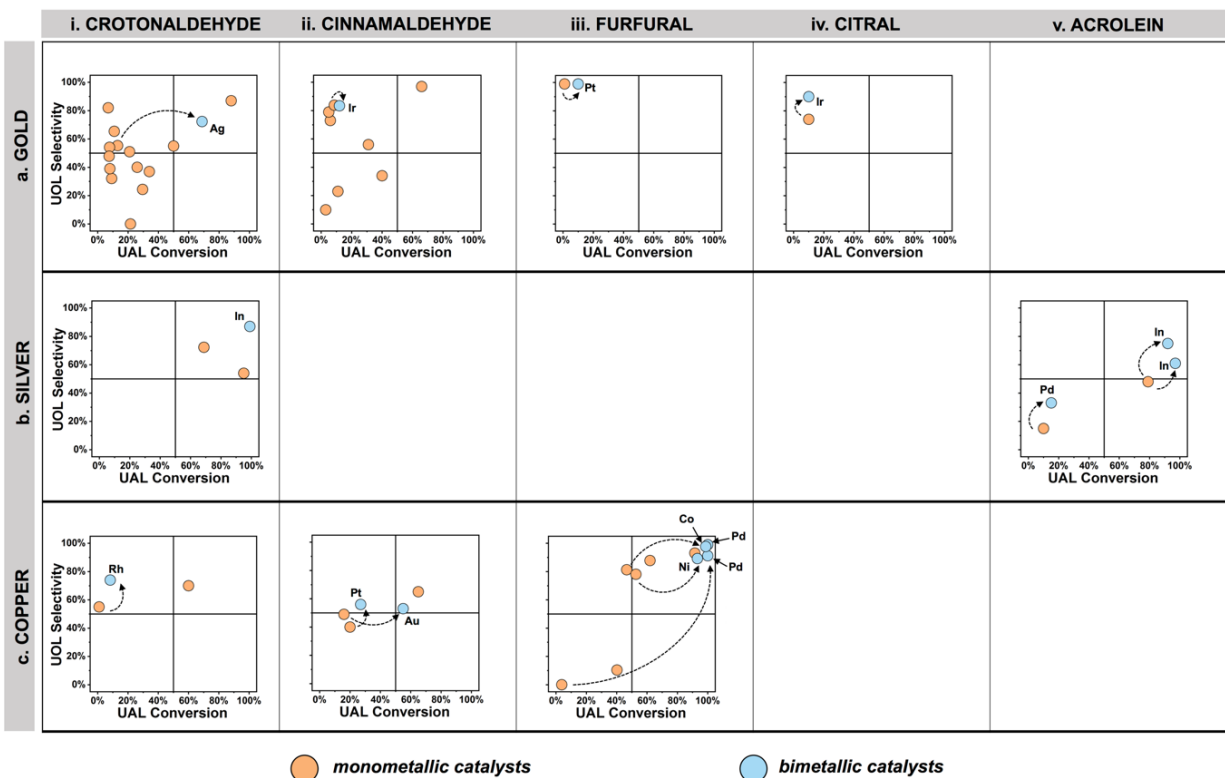


**Figure 18.** Reported selectivity to the unsaturated alcohol (UOL) as a function of the unsaturated aldehyde (UAL) conversion on: **(a)** Au and Au-rich bimetals for the hydrogenation of crotonaldehyde,<sup>137,214,307–312</sup> cinnamaldehyde,<sup>141,153,154,214,217,238,307,313</sup> furfural,<sup>314</sup> and citral;<sup>262</sup> **(b)** Ag and Ag-rich bimetals for the hydrogenation of acrolein<sup>200,315</sup> and crotonaldehyde;<sup>137,138</sup> **(c)** Cu and Cu-rich bimetals for the hydrogenation of crotonaldehyde,<sup>128,139</sup> cinnamaldehyde,<sup>128,154,155</sup> and furfural.<sup>296,297,316–320</sup> Dotted arrows indicate that the data are derived from the same study.

### 4.3.1. Au and Au alloys

Monometallic Au catalysts have been investigated extensively in reactor studies for the hydrogenation of cinnamaldehyde<sup>141,153,154,214,217,238,307,313</sup> and crotonaldehyde,<sup>137,214,307–312</sup> and, to a lesser extent, acrolein<sup>321</sup> and citral<sup>262</sup> (Fig. 18a). While monometallic Au catalysts have exhibited the selectivity to the unsaturated alcohols as high as 80%, the conversions have remained generally

below 50%. High selectivity at high conversions were reported in rare cases when e.g. a CeO<sub>2</sub> support was used.<sup>307</sup> To the best of our knowledge, Au has not been investigated in surface science studies for the hydrogenation of the unsaturated aldehydes.

The adsorption energetics and reactivity on Au have been investigated using DFT, mostly on non-(111) facets and nanoclusters.<sup>b</sup> From *ab initio* thermodynamics,<sup>166</sup> acrolein desorbed from Au(110)-(1×2) at temperatures above ~230 K at 0.15 atm, in contrast to the case of strong adsorption on Pt(110)-(1×2). The weaker adsorption was evidenced by a shift from the  $\eta^4$  to the  $\eta^2$  configuration involving the  $\pi(\text{CC})$  binding mode. The authors highlighted the need to interpret the computed phase diagrams with care, however, given the uncertainties arising from the exchange-correlation functional and the configurational entropy.

On Au(111) and Au(211),<sup>194</sup> the formation of allyl alcohol was kinetically favored, in contrast to 1-propenol formation on Pt(211).<sup>202</sup> Because of the low activity of Au for H<sub>2</sub> dissociation, the non-Horiuti-Polyani mechanisms involving weakly bound molecular H<sub>2</sub> have been proposed to be kinetically favored. The entropic contributions were not assessed in the study, however. Furthermore, the surface residence time of molecular H<sub>2</sub> is expected to be low, given the positive reported adsorption energies of +0.12 and +0.03 eV on Au(111) and Au(211), respectively. On the other hand, the geometric and electronic effects were considered using different structures with simple defects. At the lower-coordination sites, the computed energy barrier for the C=O bond reduction became lower when molecular H<sub>2</sub> was involved, but the opposite was observed when atomic H was involved.

---

<sup>b</sup> Several DFT studies of crotonaldehyde on Au(111)<sup>355–357</sup> and M/Au(111) (M = Co, Ir, Ni, In)<sup>356,358</sup> have been excluded due to inconsistencies in the data. See Table S2 for details.

Modeling of the acrolein adsorption on Au<sub>N</sub> (N = 1-5; 20)<sup>196,322</sup> showed that the  $\eta^2$ - $\pi$ (CC) configuration was favored at the low-coordination sites in all cases, thereby promoting the C=C bond reduction. The hydrogenation pathways were further mapped out on both Au<sub>20</sub> and Au(110).<sup>196</sup> Similar to Pt(111),<sup>203</sup> the reduction of the C=O bond was kinetically favored over that of the C=C bond on Au(110). However, the selectivity to allyl alcohol was achieved kinetically on Au(110) because of the weaker adsorption of allyl alcohol. In contrast, the energy barriers for the C=C and the C=O bond reduction became close to each other on Au<sub>20</sub>, detrimentally affecting the selectivity. Another study modeled the effect of secondary phosphine oxide ligands on Au<sub>55</sub>.<sup>204</sup> The ligands provided a cooperative effect, where heterolytic H<sub>2</sub> dissociation was followed by a concerted H addition into the C=O bond to form allyl alcohol. The activity was correlated to the basicity difference between the ligand and the reactant, as well as the number of the available surface sites.

Modeling of the cinnamaldehyde hydrogenation pathways on Au(111)<sup>323</sup> showed significant differences in the thermodynamics and kinetics compared to Pt. On Pt nanoclusters, the computed energy barriers for the C=O bond reduction were lower than those of the C=C bond reduction;<sup>252,253</sup> the opposite was observed on Au(111), however.<sup>323</sup> Furthermore, the  $\eta^4$  binding mode was favored on Au, in contrast to the  $\eta^2$  configurations on Pt.<sup>249-251</sup> More studies are needed to better understand these discrepancies in the hydrogenation of cinnamaldehyde across Au and Pt model systems.

In reactor studies, promotion of Au with a secondary metal has been widely employed to enhance the activity. However, the selectivity was lower in most cases, producing the saturated aldehydes via the reduction of the C=C bond, albeit without over-hydrogenation to the saturated alcohols. This has notably been the case for Au promoted with Pd.<sup>312,324,325</sup> In other cases of Au

promoted with Ir,<sup>153</sup> Pt,<sup>262</sup> Ag,<sup>137</sup> and In,<sup>321</sup> the activity and/or the selectivity has been enhanced (Fig. 18a). As noted in section 2.1, the strong interaction of Au with metal oxide supports can also promote the activity. However, this factor is not discussed in details below, instead focusing on the promotion effect by a secondary metal.

#### 4.3.1.1. Promotion of activity

Promotion of Au with more reactive metals, such as Ir and Pt, has led to enhanced activity while maintaining high selectivity. An important role of these active metals is to enable the dissociation of H<sub>2</sub>.

Ir<sub>0.13</sub>Au<sub>0.87</sub>/TiO<sub>2</sub> exhibited a rate of hydrogenation five times higher than that of monometallic Au/TiO<sub>2</sub>, while preserving the same level of selectivity (83%) to cinnamyl alcohol in cinnamaldehyde hydrogenation.<sup>153</sup> The enhancement was attributed to the possible promotion of H<sub>2</sub> activation by the strong Au-Ir interaction in the Au-Ir alloy surface, including a charge transfer from Ir to Au. Ir<sub>0.23</sub>Au<sub>0.77</sub>/TiO<sub>2</sub> catalysts had higher activity and selectivity (90%) to geraniol/nerol in citral hydrogenation, compared to monometallic Au/TiO<sub>2</sub> (74%).<sup>262</sup> The samples were not homogeneous; monometallic Ir and bimetallic IrAu nanoparticles coexisted on the support. The enhancement was attributed to the presence of Ir<sup>δ+</sup> species promoting the chemoselective reduction of the C=O bond.

Pt<sub>0.05</sub>Au<sub>0.95</sub>/SiO<sub>2</sub> catalysts exhibited ten times higher activity than monometallic Au/SiO<sub>2</sub>, while preserving the same level of selectivity (>99%) to furfuryl alcohol in furfural hydrogenation.<sup>314</sup> The enhancement was attributed to the presence of surface Pt as the active sites for H<sub>2</sub> dissociation. However, the same catalyst did not exhibit high selectivity to cinnamyl alcohol in cinnamaldehyde hydrogenation. The observed low selectivity is consistent with DFT modeling of cinnamaldehyde hydrogenation pathways on PtAu<sub>19</sub>.<sup>326</sup> The adsorption occurred preferentially on

the Pt dopant through the C=C bond via the  $\eta^2$ - $\pi$ (CC)-Pt configuration. Similar to Au(111),<sup>323</sup> the reduction of the C=C bond was kinetically favored.

#### 4.3.1.2. Other effects

Upon promotion of Au with Ag and In, multiple effects have been proposed to explain the observed selectivity enhancement. Ag<sub>0.1</sub>Au<sub>0.9</sub>/SBA-15 had higher activity and selectivity (72.3%) to crotyl alcohol in crotonaldehyde hydrogenation, compared to monometallic Au/SBA-15 (55.3%).<sup>137</sup> As expected, higher Ag content led to a lower selectivity. The enhancement was attributed to the formation of a Au-Ag alloy phase. The authors hypothesized that H<sub>2</sub> dissociation would mostly occur on the Au sites, followed by H spillover to the neighboring Ag sites where the preferential adsorption and the activation of the C=O bond would occur. However, these effects are not fully understood; in particular, H<sub>2</sub> dissociation is unlikely to occur on Au, as noted in section 2.1.

In<sub>0.05</sub>Au<sub>0.95</sub>/ZnO had high selectivity (60%) to allyl alcohol in acrolein hydrogenation. The conversions were not reported, but the rate of hydrogenation was half that of monometallic Au/ZnO.<sup>321</sup> The observed high selectivity is consistent with DFT modeling of the hydrogenation pathways on In/Au(110).<sup>195</sup> Because of the strong Au-In interaction, In preferentially decorates the terraces rather than the edge sites. Compared to the  $\eta^2$ - $\pi$ (CC) binding mode on Au(110)<sup>166</sup> and the edge sites,<sup>194,202</sup> acrolein adsorbed more strongly on the In dopant through the C=O bond via the  $\eta^2$ -di $\sigma$ (CO)-OIn configuration. As such, In actively stabilized and activated acrolein on the terraces, thereby promoting the chemoselective reduction of the C=O bond.

### 4.3.2. Ag and Ag alloys

Monometallic Ag catalysts have been investigated for the hydrogenation of crotonaldehyde,<sup>137,138,327</sup> acrolein,<sup>200,328,329</sup> and cinnamaldehyde<sup>241,330</sup> in reactor studies (Fig. 18b). Moderate selectivity to the unsaturated alcohols has been reported, e.g. ~54-72% to crotyl alcohol and ~37-48% to allyl alcohol.

In surface science studies of Ag(111), the adsorption geometry strongly influenced the selectivity in the hydrogenation of acrolein<sup>92</sup> and crotonaldehyde<sup>122</sup> (Fig. 19). The co-adsorption of H and acrolein at low coverages led to the formation of allyl alcohol and propanal with 35% and 65% selectivity, respectively. The selectivity to allyl alcohol increased with the acrolein coverage and was the highest at 1.0 ML acrolein coverage (~45% selectivity) due to the steric effect that caused the C=C bond to tilt 12° away from the surface, thereby promoting the reduction of the C=O bond. As such, the adsorption geometry of acrolein and the ensuing selectivity were highly dependent on its coverage on Ag(111), in stark contrast to Pd(111) and Pt(111) where decomposition was dominant at all coverages.

In contrast, the selectivity to crotyl alcohol was higher than that of allyl alcohol at all coverages of H and crotonaldehyde (Fig. 19b). At a low coverage of both H and crotonaldehyde, the C=O bond was nearly parallel to the surface at a tilt angle of 5°, whereas the C=C bond was tilted 31° away from the surface.<sup>122</sup> This adsorption geometry led to 95% selectivity to crotyl alcohol because the C=O bond was activated and accessible to the adsorbed H. At a high crotonaldehyde coverage, the C=C bond became nearly parallel to the surface, resulting in the formation of crotyl alcohol and butanal with 85% and 15% selectivity, respectively. At a high H coverage, the C=C bond remained parallel to the surface, increasing the selectivity to n-butanol.



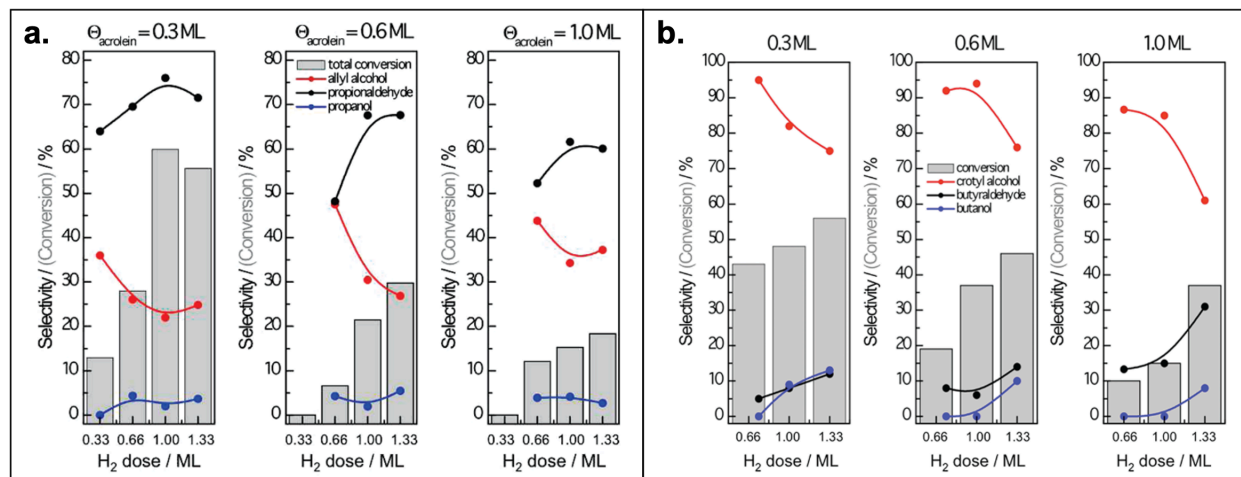


**Figure 19:** Summary of the selectivity to the unsaturated alcohol, the saturated aldehyde, and the saturated alcohol as a function of the H<sub>2</sub> dose for 0.3, 0.6, and 1.0 ML of **(a)** acrolein and **(b)** crotonaldehyde on Ag(111). Adapted with permission from refs. 92 and 122 (Copyright 2009 & 2012, American Chemical Society, Washington, DC).

Based on DFT modeling, acrolein was oriented parallel to the surface of Ag(111) in the  $\eta^2$ - $\pi$ (CC) configuration.<sup>177,197</sup> At a high coverage, however, a complex network of two stable superstructures was obtained, driven by the dipole alignment. The model provided an alternative interpretation of the near edge X-ray absorption fine structure spectroscopy data. On Ag(110) and at the step edges of Ag(221),<sup>199</sup> the computed adsorption energies were in the range of  $-0.10$  to  $-0.25$  eV, with a slight preference for the  $\eta^2$ - $\pi$ (CC) binding mode, but too weak to explain the high selectivity to allyl alcohol reported by reactor studies.

To resolve this, a follow-up study mapped out the acrolein hydrogenation pathways on Ag(110) and O<sub>sub</sub>/Ag(111) surfaces, which demonstrated that the presence of subsurface O species led to enhanced selectivity.<sup>198</sup> The formation of allyl alcohol was kinetically favored on

O<sub>sub</sub>/Ag(111) but not on Ag(110). Both allyl alcohol and propanal desorbed easily from both surfaces at the reaction temperatures of interest, indicating that the selectivity is kinetically controlled. However, the exact nature of the O species responsible for the selectivity enhancement was not examined in the study.

The reactivity of acrolein was also modeled and compared across Ag(111), Ag(100), and at the step edges of Ag(211).<sup>176</sup> The higher-coordination sites led to higher selectivity. Similar to a previous study of Au(111) and Au(211),<sup>194</sup> the non-Horiuti-Polyani mechanisms involving weakly bound molecular H<sub>2</sub> have been proposed to explain the selectivity trend. The entropic contributions were not systematically assessed in the study, however. Free energy barriers were reported for only one elementary step in their Supplementary Information,<sup>176</sup> specifically the second step of 1,4-addition to form the enol via molecular H<sub>2</sub>. Compared to the corresponding internal energy barriers, the entropic contributions more than doubled the barriers (> 1 eV). Moreover, the free energy barriers were not reported for the same elementary step involving atomic H. As such, further systematic analysis is needed to evaluate the viability of the non-Horiuti-Polyani mechanisms.

From DFT calculations, hydrogenation of furfural to furfuryl alcohol was kinetically favored over hydrodeoxygenation to methylfuran on Ag(111) and Ag(211), even in the presence of step edges.<sup>168</sup> Furthermore, in contrast to Ni(111) and Ni(211), the weaker adsorption on Ag favored the desorption of furfuryl alcohol instead of its dehydration to methylfuran.

In reactor studies, promotion of Ag with secondary metals such as Pd enhanced the activity and the selectivity,<sup>200</sup> whereas the addition of In has led to enhanced selectivity.<sup>138,315,331</sup> In particular, promotion with In resulted in one of the highest reported selectivity values to crotyl alcohol at high crotonaldehyde conversion (Fig. 18b).

#### 4.3.2.1. Promotion of activity

$\text{Pd}_{0.001}\text{Ag}_{0.999}/\text{SiO}_2$  catalysts had higher activity and selectivity (33%) to allyl alcohol in acrolein hydrogenation, compared to monometallic  $\text{Ag}/\text{SiO}_2$  (15%).<sup>200</sup> At such a low Pd concentration, the surface consisted of isolated Pd atoms interspersed in Ag, functioning as the active sites for  $\text{H}_2$  dissociation as confirmed by DFT calculations (Fig. 20). However, the Pd dopant strengthened the adsorption of the C=C bond much more so than that of the C=O bond. As such, the selectivity was instead attributed to a possible H spillover to Ag(111). This discrepancy highlights the need for reliable surface model validation, as well as modeling of dynamical and entropic effects that are at play in reactor studies.

#### 4.3.2.2. Electrophilic sites from promoters

Promotion of Ag with In has led to enhanced selectivity at high conversions, which has been attributed to the presence of oxidized In species functioning as the Lewis acid sites.  $\text{In}_{0.07}\text{Ag}_{0.93}/\text{SiO}_2$  had high selectivity to allyl alcohol (61% and 75% in the gas and liquid phase, respectively) at high acrolein conversions (>90%), representing one of the highest reported selectivity values to allyl alcohol at such high conversions.<sup>315</sup> From *in situ* X-ray absorption spectroscopy, In was oxidized under reaction conditions and remained so even in a strongly reducing  $\text{H}_2$  environment. The oxidized In promoted the C=O bond adsorption, in addition to strengthening the interaction of acrolein with Ag and enhancing its coverage.<sup>328</sup>

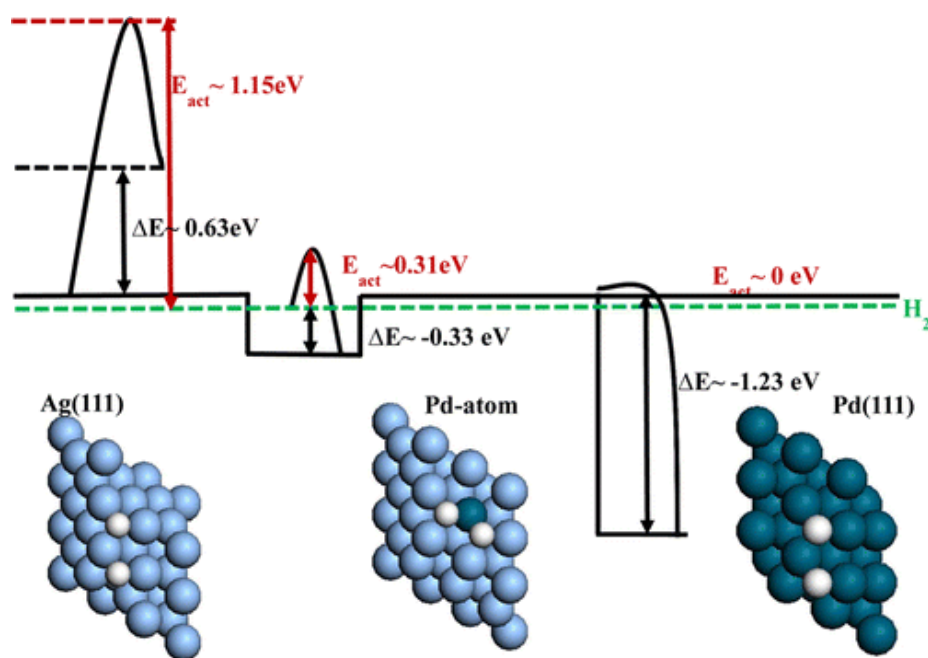


**Figure 20.** The potential energy diagram of H<sub>2</sub> dissociation, calculated using DFT. On Ag(111), the process is significantly activated and endothermic (left). On Pd(111), the process is practically barrierless, but the H atoms are too strongly adsorbed (right). On Pd monomer embedded in Ag(111), both the energy barrier and the resulting adsorption are moderate (center). Reprinted with permission from ref. 200 (Copyright 2015, American Chemical Society, Washington, DC).

In<sub>0.23</sub>Ag<sub>0.77</sub>/SBA-15 catalysts exhibited a remarkable performance for liquid-phase crotonaldehyde hydrogenation.<sup>138</sup> At nearly full conversion, selectivity to crotyl alcohol was 87%, in comparison to 54% on monometallic Ag/SBA-15. The enhancement was attributed to the reduced nanoparticle size of InAg compared to monometallic Ag. This resulted in a larger concentration of the low-coordination sites or the positively charged Ag sites, which favored the adsorption and the activation of the C=O bond as suggested by infrared reflection absorption spectroscopy.<sup>332</sup> In addition, oxidized In in the form of In<sub>2</sub>O<sub>3</sub> functioned as the Lewis acid sites, enhancing the selectivity to the unsaturated alcohol.

$\text{In}_{0.07}\text{Ag}_{0.93}/\text{SiO}_2$  was also selective to geraniol/nerol (76%) in citral hydrogenation, with and without solvent.<sup>331</sup> While the study did not provide a detailed analysis of the catalytic performance, the selectivity and the conversion were comparable to those of the industrial catalysts that require a basic additive.

### 4.3.3. Cu and Cu alloys

Monometallic Cu catalysts have been investigated in reactor studies for the hydrogenation of crotonaldehyde<sup>128,139</sup> and cinnamaldehyde<sup>128,154</sup> which exhibited moderate selectivity (~50%), in addition to furfural<sup>316–318</sup> that showed a wider range of selectivity (0-90%) (Fig. 18c). The highest selectivity to crotyl alcohol was achieved with a reducible  $\text{CeO}_2$  support.<sup>128</sup>

Surface science studies have shown high selectivity in the hydrogenation of crotonaldehyde,<sup>97,98</sup> furfural,<sup>302,303</sup> and cinnamaldehyde<sup>155</sup> on Cu, unlike on the more reactive metals of Groups 8-10. In the presence of sulfur, 100% selectivity to crotyl alcohol was achieved for  $\kappa = 0.16$ , where  $\kappa = 1$  corresponds to the surface atom density of Cu(111) ( $1.77 \times 10^{15}$  Cu atoms/cm<sup>2</sup>). From near edge X-ray absorption fine structure spectroscopy, the C=C and the C=O bond were tilted 36° and 23° away from the surface, respectively. As such, sulfur perturbed the C=O bond while tilting the C=C bond farther away from the surface, promoting the chemoselective reduction of the former.<sup>97</sup> Furthermore, the C=C bond remained tilted even after crotyl alcohol formation, preventing over-hydrogenation to n-butanol. The difference in the selectivity between Ag(111) and Cu(111) was explained by X-ray photoelectron spectroscopy data.<sup>122</sup> Specifically, the 1s binding energies of the carbonyl C in crotonaldehyde were 287.9 and 288.2 eV on Ag(111) and Cu(111), respectively. The larger value on Cu(111) indicated a greater degree of charge transfer from Cu to the C=O  $\pi^*$  orbital, thereby activating the bond for reduction. On Cu(110), 100% selectivity to

cinnamyl alcohol was obtained in cinnamaldehyde hydrogenation, based on both regular (linear temperature ramp) and isothermal (desorption intensity plotted as a function of time at a constant temperature) temperature programmed desorption.<sup>155</sup>

Based on DFT modeling of furfural reduction, hydrodeoxygenation to methylfuran and subsequent desorption were kinetically favored over the dehydration of furfuryl alcohol on Cu(111),<sup>333</sup> similar to Ag(111).<sup>168</sup> As such, the selectivity shifted from furfuryl alcohol to methylfuran only upon increasing the temperature.

In reactor studies, promotion of Cu with a secondary metal, such as Pd,<sup>319</sup> Rh,<sup>139</sup> Ni,<sup>296</sup> and Pt,<sup>155,334</sup> has led to higher activity by providing the active sites for H<sub>2</sub> dissociation, while preserving moderate to high selectivity (Fig. 18c). Promotion with Co<sup>320</sup> and Au<sup>154</sup> has led to enhanced catalytic performances due to a combination of effects described below.

#### 4.3.3.1. Promotion of activity

Pd<sub>0.38</sub>Cu<sub>0.62</sub>/MgO and Pd<sub>0.38</sub>Cu<sub>0.62</sub>/C catalysts had higher activity and selectivity (99% and 91.2%, respectively) for furfuryl alcohol in furfural hydrogenation, compared to monometallic Cu/MgO that exhibited zero selectivity.<sup>319</sup> Pd<sub>0.38</sub>Cu<sub>0.62</sub>/MgO slightly outperformed Pd<sub>0.38</sub>Cu<sub>0.62</sub>/C. Cu(I/II), Pd<sup>0</sup>, and a Pd-Cu alloy phase were found to coexist in Pd<sub>0.38</sub>Cu<sub>0.62</sub>/C, and the enhancement was attributed to the electronic modification of Pd by Cu. In the Pd<sub>0.38</sub>Cu<sub>0.62</sub>/MgO catalyst, no Pd-Cu alloy phase was identified; Pd<sup>0</sup> and Cu<sub>2</sub>O phases coexisted. The enhancement was attributed to the following: (i) Pd<sup>0</sup> provided the active sites for H<sub>2</sub> dissociation; and (ii) Cu(I) functioned as the Lewis acid sites for the preferential adsorption of the C=O bond.

Pt<sub>0.005</sub>Cu<sub>0.995</sub>/SBA-15 catalysts had higher selectivity (56%) to cinnamyl alcohol in cinnamaldehyde hydrogenation, compared to both monometallic Cu/SBA-15 and Pt/SBA-15 (Fig. 21).<sup>155</sup> The enhancement was attributed to the preferential adsorption of the C=O bond on Cu. At

such a low Pt concentration, the Pt atoms remained isolated and interspersed in the Cu nanoparticle. Previous investigations of PtCu single-atom alloys have demonstrated a mechanism by which H<sub>2</sub> is activated on isolated Pt atoms embedded in the Cu surface layer, followed by H spillover and selective hydrogenation on Cu.<sup>335–337</sup> However, the authors of the current study reported that the surface was mainly comprised of a thin oxidized Cu film with no Pt atoms. Two hypotheses were proposed: (i) the active site for H<sub>2</sub> dissociation consists of small ensembles containing Pt, possibly in the subsurface; or (ii) Pt segregates to the surface reversibly during the reaction. A follow-up kinetic study confirmed Pt<sub>0.005</sub>Cu<sub>0.995</sub> as the optimal composition, and the authors concluded that isolated Pt atoms could affect the electronic structure of the entire Cu nanoparticle, or at least that of the ensemble of Cu atoms in close vicinity.<sup>334</sup>

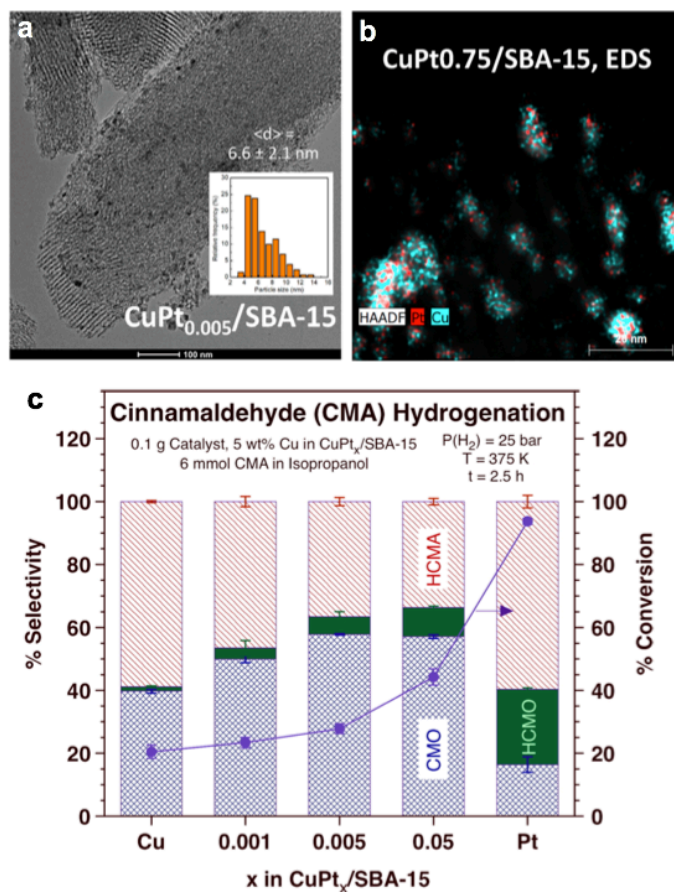


**Figure 21.** (a) Scanning transmission electron microscopy images of Pt<sub>0.005</sub>Cu<sub>0.995</sub>/SBA-15. (b) Energy dispersive spectroscopy image from a Pt<sub>0.75</sub>Cu<sub>0.25</sub>/SBA-15 sample, with Pt and Cu atoms colored in red and blue, respectively. (c) The total conversion after 2.5 hours of reaction (purple circles, right axis) and the selectivity (bars, left axis) for cinnamaldehyde hydrogenation on CuPt<sub>x</sub>/SBA-15 as a function of the catalyst composition (CMO = cinnamyl alcohol; HCMO = hydrocinnamyl alcohol; HCMA = hydrocinnamaldehyde). Adapted with permission from refs. 155 and 334 (Copyright 2019 & 2020, American Chemical Society, Washington, DC).

Ni<sub>0.3</sub>Cu<sub>0.7</sub>/MgAlO catalysts, prepared from the reduction of a spinel, had higher activity and selectivity to furfuryl alcohol in furfural hydrogenation, compared to monometallic Cu/MgAlO and Ni/MgAlO.<sup>296</sup> Ni<sub>0.3</sub>Cu<sub>0.7</sub> was found to be the optimal composition. Catalyst reduction at 573 K led to higher conversion and selectivity compared to the reduction at 493 K, indicating the important role of Cu<sup>0</sup>. Ni oxide species would still have been present, based on a much higher reduction temperature of ~1073 K on Ni/MgAlO; however, the promotion effect of Ni was not analyzed in detail.

In contrast to the reactor studies of dilute NiCu alloys, the formation of furfuryl alcohol was not observed in surface science studies of Cu(111)<sup>303</sup> and 1 ML Ni/Cu(111).<sup>302</sup> Because Cu(111) does not dissociate H<sub>2</sub> in ultrahigh vacuum, no hydrogenation products were formed upon co-dosing H<sub>2</sub> and furfural, and furfural underwent reversible desorption as well as decomposition to CO and H<sub>2</sub>. On 1 ML Ni/Cu(111), furfural underwent decomposition and hydrodeoxygenation to methylfuran. Selectivity to furfuryl alcohol was not observed, possibly due to the presence of large Ni ensembles on the surface where decomposition may still be facilitated. These results were supported by high resolution electron energy loss spectroscopy and DFT calculations showing stronger adsorption of furfural on 1 ML Ni/Cu(111) via the  $\eta^2$ -di $\sigma$ (CO) configuration, compared to Cu(111).



$\text{Rh}_{0.33}\text{Cu}_{0.67}/\text{SiO}_2$  had higher activity and selectivity (74%) to crotyl alcohol in crotonaldehyde hydrogenation, compared to monometallic  $\text{Cu}/\text{SiO}_2$  (55%).<sup>139</sup> The enhancement was attributed to an increased dispersion of Rh and a possible charge transfer from Cu to Rh.

#### 4.3.3.2. Other effects

$\text{Co}_x\text{Cu}_{1-x}/\text{C}$  ( $x = 0-0.5$ ) catalysts, prepared by pyrolysis of benzene-1,3,5-tricarboxylic acid based metal-organic frameworks, had higher selectivity to furfuryl alcohol in furfural hydrogenation, compared to monometallic  $\text{Cu}/\text{C}$ .<sup>320</sup> Both the selectivity and the conversion increased upon promotion with Co.  $\text{Co}_{0.3}\text{Cu}_{0.7}$  was found to be the optimal composition, reaching 97.7% selectivity at nearly full conversion. Metallic Cu, metallic Co, and Co oxide phases coexisted. The enhancement was attributed to the following: (i) the spatial dispersion of Cu and the reduced nanoparticle size of CoCu compared to monometallic Cu, resulting in an increased number of the active sites; and (ii)  $\text{H}_2$  activation on Co and Cu, followed by the preferential adsorption and the reduction of the C=O bond on  $\text{Cu}^0$  and/or  $\text{CoO}_x$ .

$\text{AuCu}/\text{SiO}_2$  catalysts had higher conversion and slightly higher selectivity (55%) to cinnamyl alcohol in cinnamaldehyde hydrogenation, compared to monometallic  $\text{Cu}/\text{SiO}_2$  (49%). It was found that the higher the Au content, the higher the conversion.<sup>154</sup>  $\text{Au}_{0.06}\text{Cu}_{0.94}$  was found to be the optimal composition. The Au sites were postulated to function as the active sites for  $\text{H}_2$  dissociation (enhancing the activity), while  $\text{Cu}^+$  sites promoted the adsorption and the activation of the C=O bond (enhancing the selectivity).

## **5. Conclusions and prospects**

The studies reviewed here demonstrate the great promise of bimetallic and dilute alloy catalysts to achieve high selectivity to the unsaturated alcohols in the hydrogenation of  $\alpha,\beta$ -unsaturated aldehydes. Reactor studies have clearly demonstrated the viability of bimetallic catalysts under reaction conditions, and combined theoretical and surface science studies have provided fundamental understanding of the electronic and geometric effects on adsorption strength, binding modes, and reactivity of these systems.

Aggregate analysis of the published data was used to establish several guidelines for enhancing the selectivity to the unsaturated alcohols over the saturated aldehydes. Promotion of an active electronegative metal (Ru, Rh, Pd, Ir, Pt) with an electropositive metal typically leads to two different electronic effects that may be concurrent. The first is an electron transfer from the promoter to the active metal, which destabilizes the C=C bond adsorption while also strengthening the C=O bond adsorption. The second effect involves the promoter metal functioning as an electrophilic site, sometimes in the form of an oxide species, where the C=O bond can preferentially adsorb in close proximity to the active metal where H<sub>2</sub> dissociation occurs.

On the other hand, promising results have been reported upon promotion of a more noble and selective metal (Au, Ag, Cu) with an active metal (e.g. Ni, Rh, Pd, Ir, Pt), but the mechanisms of H<sub>2</sub> activation and the formation of the unsaturated alcohol are not yet fully understood on most of these systems.

There remains an unmet need for a systematic investigation of effective catalysts for the selective production of the unsaturated alcohols. While high selectivity has been achieved over bimetallic catalysts in the hydrogenation of the unsaturated aldehydes with substituents at the C=C

bond that hinder its reduction, such as cinnamaldehyde, more work is required for smaller molecules such as acrolein and crotonaldehyde. In particular, this review unequivocally highlights the need for more theoretical and surface science studies to advance the rational design of more efficient alloy catalysts. Of all metal combinations investigated in the reactor studies considered in this review, ~40% of the corresponding model surfaces have been investigated with DFT calculations, and only ~20% were investigated using surface science experiments. Furthermore, more than half of these theoretical and surface science studies were dedicated to bimetallic Pt-based surfaces alone, leaving out many compositions that would benefit from fundamental investigations.

Surface science models can provide detailed information about the binding sites, adsorption energies, and reaction mechanisms and kinetics, serving as important benchmarks for theoretical calculations. However, surface science studies have remained scarce for certain metal compositions. One challenge is the construction of extended single crystal models that mimic the high-surface area catalysts with high fractions of edges and defect sites. Another limitation lies with the noble and selective metals (e.g. Au, Ag, Cu) that have high energy barriers for H<sub>2</sub> dissociation—a key step in hydrogenation. As a result, it is difficult to produce a significant coverage of atomic hydrogen on these metals at low pressures (ultrahigh vacuum). Under steady-state conditions of higher pressures and temperatures used for catalysis, sufficient H<sub>2</sub> dissociation may proceed. This limitation in the surface science experiments can be circumvented by using a source of atomic hydrogen. Moreover, the recent development of single-atom alloy catalysts<sup>74,75</sup> has been promising in this regard, in which a reactive minority metal (e.g. Pt, Pd, Ni) is dispersed as isolated atoms in a majority host metal (e.g. Au, Ag, Cu) that exhibits selective chemistry.<sup>335,338–340</sup> The reactive metal acts as the atomic hydrogen source by activating H<sub>2</sub>, which may subsequently migrate to sites on the host metal where selective hydrogenation can occur. These systems not only represent an opportunity for understanding structural and mechanistic fundamentals using surface science studies,

but also as new catalyst architectures in reactor studies as seen in the case of PdAg single-atom alloys for the hydrogenation of acrolein to allyl alcohol.<sup>200</sup>

Carbonaceous deposits have been shown to influence the catalytic performance in hydrogenation reactions, such as olefin hydrogenation and semi-hydrogenation of alkynes. Among various hypotheses, the most widely accepted one is that the presence of these surface species alters the adsorption mode of the reactants by blocking specific active sites, thereby altering the selectivity.<sup>34,341,342</sup> For example, similar to the strongly bound ethynylidyne species that poison the surface in acetylene hydrogenation,<sup>343</sup> prenal has been shown to decompose into highly stable isobutylidyne species on Pt(111).<sup>248</sup> To the best of our knowledge, however, comprehensive and systematic investigation of carbonaceous deposits has yet to be conducted for the hydrogenation of the unsaturated aldehydes. Here, surface science studies can also play a critical role in the design of new catalysts by observing and quantifying the presence of strongly bound carbonaceous deposits, intermediates, and their effect on surface reactions.

Surface science studies face another challenge when the recombination and the desorption of H<sub>2</sub> have a lower energy barrier than the hydrogenation steps. Since there are no reactants in the ambient gas phase in ultrahigh vacuum, hydrogenation may not be observed even when there is a significant amount of hydrogen initially adsorbed on the surface. This challenge can be overcome by investigating crystalline models, especially single-atom alloys, at ambient pressures and higher temperatures. The recent development of ambient pressure methods, including ambient pressure X-ray photoelectron spectroscopy and polarization modulation infrared reflection absorption spectroscopy, provide tools for bridging low-pressure single crystal studies to those of complex catalysts. As such, there exists a clear opportunity to investigate well-defined Au, Ag, and Cu-based dilute and single-atom alloy model systems for the selective hydrogenation of the unsaturated aldehydes.

Theoretical calculations have provided crucial insights on the selectivity enhancement observed in numerous reactor studies, correlating the adsorption modes of the unsaturated aldehydes with their reactivity. However, distinct gaps exist in the types of model systems that have been investigated. Out of all DFT studies considered in this review, the majority have focused on acrolein (~40%) and furfural (~23%) on Pt (~34%), predominantly on monometallic systems with (111) facets (~70%). This imbalance is primarily due to the structural and chemical complexities intrinsic to bimetallic systems, making it challenging to explore the large configurational space. Depending on the miscibility of the constituent metals, the thermodynamically favored structure may range from a random solid solution to more ordered configurations such as core-shell nanoparticles<sup>344</sup> and intermetallics.<sup>345</sup> In particular, due to their well-defined stoichiometry and long-range order, intermetallics are promising model systems as noted in this review (e.g. Sn-Pt, Sn-Pt, Sn-Ru, In-Ni).<sup>50,65,135,189,292</sup> Overall, approaches beyond conventional static methods, such as recent studies using accelerated machine-learning molecular dynamics and automated mechanistic characterization,<sup>83,185</sup> are needed for model validation as well as accurate modeling of entropic and dynamical effects under reaction conditions (see section 3.2 for the discussion of the limitations of DFT modeling).

Assessment of new and emerging catalysts has long been an issue in heterogeneous catalysis due to the lack of both benchmark catalysts and established standard reaction conditions.<sup>346</sup> Rigorous comparison of monometallic and bimetallic catalysts should be carried out with critical factors in mind, such as particle size effects and mass transfer limitations, even when catalysts are evaluated under the same reaction conditions using the same experimental set-up. While it is clear from this review that bimetallic catalysts generally lead to better selectivity than monometallic catalysts, identifying the best bimetallic composition is not straightforward. The large diversity of

metals, molecules, reaction conditions (pressure, temperature, and reactor set-up, i.e. gas/liquid flow or batch) encountered in this review makes comparison of different studies very challenging.

Evaluation of new catalysts against a standard catalyst would greatly benefit the discovery of catalysts for the selective hydrogenation of the unsaturated aldehydes. Unequivocally, the literature lacks this kind of benchmarking. With this in mind, we propose that standard conditions be considered. Based on our review of the literature, a standard for liquid-phase hydrogenation of cinnamaldehyde in batch mode at 20 bar with isopropanol as a solvent is a potential option; a standard for gas flow reactors would be crotonaldehyde hydrogenation at atmospheric pressure with a 20:1 molar ratio of H<sub>2</sub> to crotonaldehyde. A commercial catalyst, 5 wt.% Pt on C, could be used as a benchmark as it should yield a mixture of cinnamyl alcohol and other products.<sup>349</sup> These proposed standards would need to be tested to determine if they are widely applicable; therefore, agreement in the community would need to be established.

Our review highlights an emerging opportunity for Ru-based catalysts. Although Ru is relatively rare and monometallic Ru catalysts are prone to deactivation, reactor studies have demonstrated that combining Ru with other metals such as Ir, Pt, and Au can lead to high selectivity (section 4.1.2.2; Figs. 3 and 9b) as well as enhanced resistance to deactivation in some cases. However, to the best of our knowledge, there have been no theoretical studies of bimetallic Ru surfaces. As such, there exists a tremendous opportunity to investigate the adsorption and reactivity of unsaturated aldehydes on Ru-based materials, as a step toward the development of active, selective, and stable Ru-based bimetallic catalysts.

Contradictions were noted in various instances regarding the effect of electron transfer from one metal to another (e.g. PtCo, PtFe, PtSn in section 4.1.1). Most electron transfer effects in reactor based catalyst studies are investigated only with *ex situ* X-ray photoelectron spectroscopy. Better agreement between studies could be established by recognizing that catalyst supports are well-

known to be prone to charging artifacts that change the binding energy of investigated species.<sup>348,349</sup> Using better references for calibration could lead to less such contradictions. The binding energy of the C 1s electron in the adventitious carbon is commonly used as a reference in the studies considered in this review and the scientific community in general, but this has been shown to result in discrepancies.<sup>348,350</sup> Furthermore, more comprehensive understanding of the electron transfer effect could be achieved by employing a combination of techniques.

While this review highlighted the synergy between reactor studies, surface science, and theory for most metal compositions, discrepancies were noted in some cases as indicated above. A crucial factor in achieving better consistency and agreement between model studies (both theory and surface science) and catalytic experiments is to ensure that the same state of matter is being investigated. Theoretical and surface science studies investigate very well-defined, pristine model surfaces. However, catalytic materials are considerably more complex, and the effects of supports, metal particle size, and solvents are all important factors that should also be studied systematically. Hence, defining the active state of the surface during the reaction is challenging, but of key importance.

In particular, the surfaces of bimetallic and dilute alloy catalysts are highly dynamic, and restructuring has been shown to occur readily during pretreatments and under reaction conditions.<sup>78–84,351–354</sup> Pretreatment is a crucial part of catalytic processes undertaken to transform the catalyst surface into an active—ideally the most active—state. In bimetallic and dilute alloy catalysts, exposure to a reactant feed under high hydrogen pressure and temperature can induce restructuring that considerably changes the surface composition and morphology. Moreover, spectators or modifiers may build up over the course of reaction, as seen historically in the case of acetylene hydrogenation where carbonaceous spectator species such as ethylidyne have been shown to alter

the overall performance of the catalyst.<sup>34</sup> However, in the studies considered in this review, characterization was performed predominantly on *ex situ* samples before pretreatment and reaction. As such, there is an undeniable need for better descriptions of working catalytic surfaces by means of both ambient pressure methods on single crystal models and operando or *in situ* characterization of working catalysts.

In the final analysis, there exists a major opportunity for improving the selectivity of the hydrogenation of the unsaturated aldehydes by using bimetallic and dilute alloy catalysts. Promising future directions would combine advanced characterization of high-surface area catalysts under operating conditions, investigation of single crystal models in ultrahigh vacuum and at ambient pressure and temperature, and theoretical modeling of multicomponent and dynamical systems. Such synergy across the three major research areas would provide a powerful platform for establishing the design principles of bimetallic catalysts for the selective hydrogenation of  $\alpha,\beta$ -unsaturated aldehydes to unsaturated alcohols.

## **6. Supporting information available**

Supplementary data is available for the DFT literature:

1. Acrolein hydrogenation
2. Crotonaldehyde hydrogenation
3. Prenal hydrogenation
4. Cinnamaldehyde hydrogenation
5. Furfural hydrogenation



## Acknowledgment

This work was supported by the Integrated Mesoscale Architectures for Sustainable Catalysis (IMASC), an Energy Frontier Research Center funded by the US Department of Energy, Office of Science, Office of Basic Energy Sciences under Award No. DE-SC0012573. We acknowledge help from N. Molinari with the analysis and plotting of the DFT data, as well as enlightening discussions with K. Duanmu.

## References

- (1) Silva, E. A. P.; Carvalho, J. S.; Guimarães, A. G.; Barreto, R. de S. S.; Santos, M. R. V.; Barreto, A. S.; Quintans-Júnior, L. J. The use of terpenes and derivatives as a new perspective for cardiovascular disease treatment: a patent review (2008-2018). *Expert Opin. Ther. Pat.* **2019**, *29*, 43–53.
- (2) Kimura, H. Progress in One-step Amination of Long-chain Fatty Alcohols with Dimethylamine—Development of Key Technologies for Industrial Applications, Innovations, and Future Outlook. *Catal. Rev. Eng.* **2011**, *53*, 1–90.
- (3) Chen, W.; Viljoen, A. M. Geraniol — A review of a commercially important fragrance material. *S. Afr. J. Bot.* **2010**, *76*, 643–651.
- (4) Schwab, W.; Davidovich-Rikanati, R.; Lewinsohn, E. Biosynthesis of plant-derived flavor compounds. *Plant J.* **2008**, *54*, 712–732.
- (5) Swift, K. A. D. Catalytic Transformations of the Major Terpene Feedstocks. *Top. Catal.* **2004**, *27*, 143–155.

- (6) Pasumansky, L.; Goralski, C. T.; Singaram, B. Lithium Aminoborohydrides: Powerful, Selective, Air-Stable Reducing Agents. *Org. Process Res. Dev.* **2006**, *10*, 959–970.
- (7) Cha, J. S. Recent Developments in Meerwein-Ponndorf-Verley and Related Reactions for the Reduction of Organic Functional Groups Using Aluminum, Boron, and Other Metal Reagents: A Review. *Org. Process Res. Dev.* **2006**, *10*, 1032–1053.
- (8) Ohkuma, T.; Kurono, N.; Arai, N. Development of Asymmetric Reactions Catalyzed by Ruthenium Complexes with Two Kinds of Ligands. *Bull. Chem. Soc. Jpn.* **2019**, *92*, 475–504.
- (9) Fraile, J. M.; García, J. I.; Herrerías, C. I.; Pires, E. Synthetic Transformations for the Valorization of Fatty Acid Derivatives. *SYNTHESIS-STUTTGART* **2017**, *49*, 1444–1460.
- (10) Na, G.; Shoufei, Z. Iron-Catalyzed Hydrogenation Reactions. *Chinese J. Org. Chem.* **2015**, *35*, 1383–1398.
- (11) Lumbroso, A.; Cooke, M. L.; Breit, B. Catalytic Asymmetric Synthesis of Allylic Alcohols and Derivatives and their Applications in Organic Synthesis. *Angew. Chem. Int. Ed.* **2013**, *52*, 1890–1932.
- (12) Joó, F. Aqueous Biphasic Hydrogenations. *Acc. Chem. Res.* **2002**, *35*, 738–745.
- (13) Cornils, B. Bulk and fine chemicals via aqueous biphasic catalysis. *J. Mol. Catal. A Chem.* **1999**, *143*, 1–10.
- (14) Nomura, K. Transition metal catalyzed hydrogenation or reduction in water. *J. Mol. Catal. A Chem.* **1998**, *130*, 1–28.
- (15) Joó, F.; Papp, E.; Kathó, A. Molecular catalysis in liquid multiphase systems. *Top. Catal.* **1998**, *5*, 113–124.
- (16) Klusoň, P.; Červený, L. Ru-Sn Catalyst – A New Promising System for Selective Hydrogenation of a Carbonyl Group. *Chem. Listy* **1997**, *91*, 100–104.

- (17) Ponec, V. On the role of promoters in hydrogenations on metals;  $\alpha,\beta$ -unsaturated aldehydes and ketones. *Appl. Catal. A Gen.* **1997**, *149*, 27–48.
- (18) Gallezot, P.; Richard, D. Selective Hydrogenation of  $\alpha,\beta$ -Unsaturated Aldehydes. *Catal. Rev. Eng.* **1998**, *40*, 81–126.
- (19) Claus, P. Selective hydrogenation of  $\alpha,\beta$ -unsaturated aldehydes and other C=O and C=C bonds containing compounds. *Top. Catal.* **1998**, *5*, 51–62.
- (20) Mäki-Arvela, P.; Hájek, J.; Salmi, T.; Murzin, D. Y. Chemoselective hydrogenation of carbonyl compounds over heterogeneous catalysts. *Appl. Catal. A Gen.* **2005**, *292*, 1–49.
- (21) Stolle, A.; Gallert, T.; Schmöger, C.; Ondruschka, B. Hydrogenation of citral: a wide-spread model reaction for selective reduction of  $\alpha,\beta$ -unsaturated aldehydes. *RSC Adv.* **2013**, *3*, 2112–2153.
- (22) Nakagawa, Y., Tamura, M. & Tomishige, K. Catalytic Reduction of Biomass-Derived Furanic Compounds with Hydrogen. *ACS Catal.* **2013**, *3*, 2655–2668.
- (23) Bailón-García, E.; Maldonado-Hódar, F. J.; Pérez-Cadenas, A. F.; Carrasco-Marín, F. Catalysts Supported on Carbon Materials for the Selective Hydrogenation of Citral. *Catalysts* **2013**, *3*, 853–877.
- (24) Hu, C.; Creaser, D.; Siahrostami, S.; Grönbeck, H.; Ojagh, H.; Skoglundh, M. Catalytic hydrogenation of C=C and C=O in unsaturated fatty acid methyl esters. *Catal. Sci. Technol.* **2014**, *4*, 2427–2444.
- (25) Sánchez, M. A.; Torres, G. C.; Mazzieri, V. A.; Pieck, C. L. Selective hydrogenation of fatty acids and methyl esters of fatty acids to obtain fatty alcohols—a review. *J. Chem. Technol. Biotechnol.* **2017**, *92*, 27–42.
- (26) Watari, R.; Kayaki, Y. Copper Catalysts Unleashing the Potential for Hydrogenation of Carbon-Oxygen Bonds. *Asian J. Org. Chem.* **2018**, *7*, 2005–2014.

- (27) Afeefy, H. Y.; Liebman, J. F.; Stein, S. E. Neutral Thermochemical Data. *NIST Chemistry WebBook, NIST Standard Reference Database Number 69*; National Institute of Standards and Technology: Gaithersburg, MD (retrieved August 31, 2020).
- (28) Burgess Jr., D. R. Thermochemical Data. *NIST Chemistry WebBook, NIST Standard Reference Database Number 69*; National Institute of Standards and Technology: Gaithersburg, MD (retrieved August 31, 2020).
- (29) Acree, W. E.; Chickos, J. S. Phase Transition Enthalpy Measurements of Organic and Organometallic Compounds. *NIST Chemistry WebBook, NIST Standard Reference Database Number 69*; National Institute of Standards and Technology: Gaithersburg, MD (retrieved August 31, 2020).
- (30) Joback, K. G.; Reid, R. C. Estimation of Pure-Component Properties from Group-Contributions. *Chem. Eng. Commun.* **1987**, *57*, 233–243.
- (31) Laref, S.; Delbecq, F.; Loffreda, D. Theoretical elucidation of the selectivity changes for the hydrogenation of unsaturated aldehydes on Pt(111). *J. Catal.* **2009**, *265*, 35–42.
- (32) Delbecq, F.; Sautet, P. A Density Functional Study of Adsorption Structures of Unsaturated Aldehydes on Pt(111): A Key Factor for Hydrogenation Selectivity. *J. Catal.* **2002**, *211*, 398–406.
- (33) Delbecq, F.; Sautet, P. Competitive C=C and C=O Adsorption of  $\alpha$ - $\beta$  Unsaturated Aldehydes on Pt and Pd Surfaces in Relation with the Selectivity of Hydrogenation Reactions: A Theoretical Approach. *J. Catal.* **1995**, *152*, 217–236.
- (34) Zaera, F. The Surface Chemistry of Metal-Based Hydrogenation Catalysis. *ACS Catal.* **2017**, *7*, 4947–4967.
- (35) Cao, S.; Tao, F. (F.); Tang, Y.; Li, Y.; Yu, J. Size- and shape-dependent catalytic performances of oxidation and reduction reactions on nanocatalysts. *Chem. Soc. Rev.* **2016**,

45, 4747–4765.

- (36) McEwan, L.; Julius, M.; Roberts, S.; & Fletcher, J. C. Q. A review of the use of gold catalysts in selective hydrogenation reactions. *Gold Bull.* **2010**, *43*, 298–306.
- (37) Yu, W. W.; Liu, H. Singular modification effects of metal cations and metal complex ions on the catalytic properties of metal colloidal nanocatalysts. *J. Mol. Catal. A Chem.* **2006**, *243*, 120–141.
- (38) Singh, U. K.; Vannice, M. A. Kinetics of liquid-phase hydrogenation reactions over supported metal catalysts — a review. *Appl. Catal. A Gen.* **2001**, *213*, 1–24.
- (39) Coq, B.; Figueras, F. Structure-activity relationships in catalysis by metals: some aspects of particle size, bimetallic and supports effects. *Coord. Chem. Rev.* **1998**, *178*, 1753–1783.
- (40) Moskaleva, L.; Chiu, C.; Genest, A.; Rösch, N. Transformations of Organic Molecules over Metal Surfaces: Insights from Computational Catalysis. *Chem. Rec.* **2016**, *16*, 2388–2404.
- (41) Liu, Y.; Zhao, G.; Wang, D.; Li, Y. Heterogeneous catalysis for green chemistry based on nanocrystals. *Natl. Sci. Rev.* **2015**, *2*, 150–166.
- (42) Hari, T. K.; Yaakob, Z. Recent development of supported monometallic gold as heterogeneous catalyst for selective liquid phase hydrogenation reactions. *Chinese J. Chem. Eng.* **2015**, *23*, 327–336.
- (43) Zang, W.; Li, G.; Wang, L.; Zhang, X. Catalytic hydrogenation by noble-metal nanocrystals with well-defined facets: a review. *Catal. Sci. Technol.* **2015**, *5*, 2532–2553.
- (44) Mitsudome, T.; Kaneda, K. Gold nanoparticle catalysts for selective hydrogenations. *Green Chem.* **2013**, *15*, 2636–2654.
- (45) Pan, M.; Brush, A. J.; Pozun, Z. D.; Ham, H. C.; Yu, W.-Y.; Henkelman, G.; Hwang, G. S.; Mullins, C. B. Model studies of heterogeneous catalytic hydrogenation reactions with gold. *Chem. Soc. Rev.* **2013**, *42*, 5002–5013.

- (46) Cárdenas-Lizana, F.; Keane, M. A. The development of gold catalysts for use in hydrogenation reactions. *J. Mater. Sci.* **2013**, *48*, 543–564.
- (47) Guo, N.; Caratzoulas, S.; Doren, D. J.; Sandler, S. I.; Vlachos, D. G. A perspective on the modeling of biomass processing. *Energy Environ. Sci.* **2012**, *5*, 6703–6716.
- (48) Liao, F.; Lo, T. W. B.; Tsang, S. C. E. Recent Developments in Palladium-Based Bimetallic Catalysts. *ChemCatChem* **2015**, *7*, 1998–2014.
- (49) McCue, A. J.; Anderson, J. A. Recent advances in selective acetylene hydrogenation using palladium containing catalysts. *Front. Chem. Sci. Eng.* **2015**, *9*, 142–153.
- (50) Komatsu, T.; Furukawa, S. Intermetallic Compound Nanoparticles Dispersed on the Surface of Oxide Support as Active and Selective Catalysts. *Mater. Trans.* **2015**, *56*, 460–467.
- (51) Ellert, O. G.; Tsodikov, M. V.; Nikolaev, S. A.; Novotortsev, V. M. Bimetallic nanoalloys in heterogeneous catalysis of industrially important reactions: synergistic effects and structural organization of active components. *Russ. Chem. Rev.* **2014**, *83*, 718–732.
- (52) Cai, S.; Wang, D.; Niu, Z.; Li, Y. Progress in organic reactions catalyzed by bimetallic nanomaterials. *Chinese J. Catal.* **2013**, *34*, 1964–1974.
- (53) Knecht, M. R.; Pacardo, D. B. Employing high-resolution materials characterization to understand the effects of Pd nanoparticle structure on their activity as catalysts for olefin hydrogenation. *Anal. Bioanal. Chem.* **2010**, *397*, 1137–1155.
- (54) Adams, R. D.; Trufan, E. Ruthenium-tin cluster complexes and their applications as bimetallic nanoscale heterogeneous hydrogenation catalysts. *Philos. Trans. R. Soc. A* **2010**, *368*, 1473–1493.
- (55) Guzzi, L.; Boskovic, G.; Kiss, E. Bimetallic Cobalt Based Catalysts. *Catal. Rev. Eng.* **2010**, *52*, 133–203.
- (56) Nikolaev, S. A.; Zhanavskina, L. N.; Smirnov, V. V.; Averyanov, V. A.; Zhanavskina, K. L.

- Catalytic hydrogenation of alkyne and alkadiene impurities from alkenes. Practical and theoretical aspects. *Russ. Chem. Rev.* **2009**, *78*, 231–247.
- (57) Coq, B.; Figueras, F. Bimetallic palladium catalysts: influence of the co-metal on the catalyst performance. *J. Mol. Catal. A Chem.* **2001**, *173*, 117–134.
- (58) Adams, R. D. Metal segregation in bimetallic clusters and its possible role in synergism and bifunctional catalysis. *J. Organomet. Chem.* **2000**, *600*, 1–6.
- (59) Stytsenko, V. D. Surface-modified bimetallic catalysts: Preparation, characterization, and applications. *Appl. Catal. A Gen.* **1995**, *126*, 1–26.
- (60) Luneau, M.; Shirman, T.; Foucher, A. C.; Duanmu, K.; Verbart, D. M. A.; Sautet, P.; Stach, E. A.; Aizenberg, J.; Madix, R. J.; Friend, C. M. Achieving High Selectivity for Alkyne Hydrogenation at High Conversions with Compositionally Optimized PdAu Nanoparticle Catalysts in Raspberry Colloid-Templated SiO<sub>2</sub>. *ACS Catal.* **2020**, *10*, 441–450.
- (61) Marakatti, V. S.; Arora, N.; Rai, S.; Sarma, S. C.; Peter, S. C. Understanding the Role of Atomic Ordering in the Crystal Structures of Ni<sub>x</sub>Sn<sub>y</sub> toward Efficient Vapor Phase Furfural Hydrogenation. *ACS Sustain. Chem. Eng.* **2018**, *6*, 7325–7338.
- (62) Otyuskaya, D.; Thybaut, J. W.; Alexiadis, V.; Alekseeva, M.; Venderbosch, R.; Yakovlev, V.; Marin, G. B. Fast pyrolysis oil stabilization kinetics over a Ni-Cu catalyst using propionic acid as a model compound. *Appl. Catal. B Environ.* **2018**, *233*, 46–57.
- (63) Zhao, J.; Jin, R. Heterogeneous catalysis by gold and gold-based bimetal nanoclusters. *Nano Today* **2018**, *18*, 86–102.
- (64) Goksu, H.; Sert, H.; Kilbas, B.; Sen, F. Recent Advances in the Reduction of Nitro Compounds by Heterogenous Catalysts. *Curr. Org. Chem.* **2017**, *21*, 794–820.
- (65) Furukawa, S.; Komatsu, T. Intermetallic Compounds: Promising Inorganic Materials for Well-Structured and Electronically Modified Reaction Environments for Efficient Catalysis.

*ACS Catal.* **2017**, *7*, 735–765.

- (66) Vilé, G.; Albani, D.; Almora-Barrios, N.; López, N.; Pérez-Ramírez, J. Advances in the Design of Nanostructured Catalysts for Selective Hydrogenation. *ChemCatChem* **2016**, *8*, 21–33.
- (67) Jin, X.; Yin, B.; Xia, Q.; Fang, T.; Shen, J.; Kuang, L.; Yang, C. Catalytic Transfer Hydrogenation of Biomass-Derived Substrates to Value-Added Chemicals on Dual-Function Catalysts: Opportunities and Challenges. *ChemSusChem* **2019**, *12*, 71–92.
- (68) Singh, S. K. Heterogeneous Bimetallic Catalysts for Upgrading Biomass-Derived Furans. *Asian J. Org. Chem.* **2018**, *7*, 1901–1923.
- (69) Kong, X.; Zhu, Y.; Fang, Z.; Kozinski, J. A.; Butler, I. S.; Xu, L.; Song, H.; Wei, X. Catalytic conversion of 5-hydroxymethylfurfural to some value-added derivatives. *Green Chem.* **2018**, *20*, 3657–3682.
- (70) Gupta, K.; Rai, R. K.; Singh, S. K. Metal Catalysts for the Efficient Transformation of Biomass-derived HMF and Furfural to Value Added Chemicals. *ChemCatChem* **2018**, *10*, 2326–2349.
- (71) Sun, D.; Sato, S.; Ueda, W.; Primo, A.; Garcia, H.; Corma, A. Production of C4 and C5 alcohols from biomass-derived materials. *Green Chem.* **2016**, *18*, 2579–2597.
- (72) Yan, K.; Yang, Y.; Chai, J.; Lu, Y. Catalytic reactions of gamma-valerolactone: A platform to fuels and value-added chemicals. *Appl. Catal. B Environ.* **2015**, *179*, 292–304.
- (73) Sankar, M.; Dimitratos, N.; Miedziak, P. J.; Wells, P. P.; Kiely, C. J.; Hutchings, G. J. Designing bimetallic catalysts for a green and sustainable future. *Chem. Soc. Rev.* **2012**, *41*, 8099–8139.
- (74) Giannakakis, G.; Flytzani-Stephanopoulos, M.; Sykes, E. C. H. Single-Atom Alloys as a Reductionist Approach to the Rational Design of Heterogeneous Catalysts. *Acc. Chem. Res.*



2019, 52, 237–247.

- (75) Hannagan, R. T.; Giannakakis, G.; Flytzani-Stephanopoulos, M.; Sykes, E. C. H. Single-Atom Alloy Catalysis. *Chem. Rev.* **2020**, DOI:10.1021/acs.chemrev.0c00078.
- (76) Liu, J.; Bunes, B. R.; Zang, L.; Wang, C. Supported single-atom catalysts: synthesis, characterization, properties, and applications. *Environ. Chem. Lett.* **2018**, 16, 477–505.
- (77) Darby, M. T.; Stamatakis, M.; Michaelides, A.; Sykes, E. C. H. Lonely Atoms with Special Gifts: Breaking Linear Scaling Relationships in Heterogeneous Catalysis with Single-Atom Alloys. *J. Phys. Chem. Lett.* **2018**, 9, 5636–5646.
- (78) Tao, F.; Grass, M. E.; Zhang, Y.; Butcher, D. R.; Renzas, J. R.; Liu, Z.; Chung, J. Y.; Mun, B. S.; Salmeron, M.; Somorjai, G. A. Reaction-Driven Restructuring of Rh-Pd and Pt-Pd Core-Shell Nanoparticles. *Science* **2008**, 322, 932–934.
- (79) Tao, F. (F.); Zhang, S.; Nguyen, L.; Zhang, X. Action of bimetallic nanocatalysts under reaction conditions and during catalysis: evolution of chemistry from high vacuum conditions to reaction conditions. *Chem. Soc. Rev.* **2012**, 41, 7980–7993.
- (80) Zafeiratos, S.; Piccinin, S.; Teschner, D. Alloys in catalysis: phase separation and surface segregation phenomena in response to the reactive environment. *Catal. Sci. Technol.* **2012**, 2, 1787–1801.
- (81) Vignola, E.; Steinmann, S. N.; Le Mapihan, K.; Vandegehuchte, B. D.; Curulla, D.; Sautet, P. Acetylene Adsorption on Pd-Ag Alloys: Evidence for Limited Island Formation and Strong Reverse Segregation from Monte Carlo Simulations. *J. Phys. Chem. C* **2018**, 122, 15456–15463.
- (82) van Spronsen, M. A.; Daunmu, K.; O'Connor, C. R.; Egle, T.; Kersell, H.; Oliver-Meseguer, J.; Salmeron, M. B.; Madix, R. J.; Sautet, P.; Friend, C. M. Dynamics of Surface Alloys: Rearrangement of Pd/Ag(111) Induced by CO and O<sub>2</sub>. *J. Phys. Chem. C* **2019**, 123, 8312–

8323.

- (83) Lim, J. S.; Vandermause, J.; van Spronsen, M. A.; Musaelian, A.; Xie, Y.; Sun, L.; O'Connor, C. R.; Egle, T.; Molinari, N.; Florian, J.; Duanmu, K.; Madix, R. J.; Sautet, P.; Friend, C. M.; Kozinsky, B. Evolution of Metastable Structures at Bimetallic Surfaces from Microscopy and Machine-Learning Molecular Dynamics. *J. Am. Chem. Soc.* **2020**, *142*, 15907–15916.
- (84) Vignola, E.; Steinmann, S. N.; Vandegehuchte, B. D.; Curulla, D.; Sautet, P. C<sub>2</sub>H<sub>2</sub>-Induced Surface Restructuring of Pd-Ag Catalysts: Insights from Theoretical Modeling. *J. Phys. Chem. C* **2016**, *120*, 26320–26327.
- (85) Hou, F.; Zhao, H.; Song, H.; Chou, L.; Zhao, J.; Yang, J.; Yan, L. Effect of impregnation strategy on catalytic hydrogenation behavior of PtCo catalysts supported on La<sub>2</sub>O<sub>2</sub>CO<sub>3</sub> nanorods. *J. Rare Earths* **2018**, *36*, 965–973.
- (86) Guo, Z.; Xiao, C.; Maligal-Ganesh, R. V.; Zhou, L.; Goh, T. W.; Li, X.; Tesfagaber, D.; Thiel, A.; Huang, W. Pt Nanoclusters Confined within Metal–Organic Framework Cavities for Chemoselective Cinnamaldehyde Hydrogenation. *ACS Catal.* **2014**, *4*, 1340–1348.
- (87) Lan, X.; Huang, N.; Wang, J.; Wang, T. Geometric effect in the highly selective hydrogenation of 3-methylcrotonaldehyde over Pt@ZIF-8 core-shell catalysts. *Catal. Sci. Technol.* **2017**, *7*, 2601–2608.
- (88) Stephenson, C. J.; Whitford, C. L.; Stair, P. C.; Farha, O. K.; Hupp, J. T. Chemoselective Hydrogenation of Crotonaldehyde Catalyzed by an Au@ZIF-8 Composite. *ChemCatChem* **2016**, *8*, 855–860.
- (89) Shen, H.; Tang, H.; Yan, H.; Han, W.; Li, Y.; Ni, J. Geometric effect of Ru/HSAG@mSiO<sub>2</sub>: a catalyst for selective hydrogenation of cinnamaldehyde. *RSC Adv.* **2014**, *4*, 30180–30185.
- (90) Kahsar, K. R.; Schwartz, D. K.; Medlin, J. W. Control of Metal Catalyst Selectivity through

Specific Noncovalent Molecular Interactions. *J. Am. Chem. Soc.* **2014**, *136*, 520–526.

- (91) Wu, B.; Huang, H.; Yang, J.; Zheng, N.; Fu, G. Selective Hydrogenation of  $\alpha,\beta$ -Unsaturated Aldehydes Catalyzed by Amine-Capped Platinum-Cobalt Nanocrystals. *Angew. Chem. Int. Ed.* **2013**, *51*, 3440–3443.
- (92) Brandt, K.; Chiu, M. E.; Watson, D. J.; Tikhov, M. S.; Lambert, R. M. Chemoselective Catalytic Hydrogenation of Acrolein on Ag(111): Effect of Molecular Orientation on Reaction Selectivity. *J. Am. Chem. Soc.* **2009**, *131*, 17286–17290.
- (93) Taylor, M. J.; Jiang, L.; Reichert, J.; Papageorgiou, A. C.; Beaumont, S. K.; Wilson, K.; Lee, A. F.; Barth, J. V.; Kyriakou, G. Catalytic Hydrogenation and Hydrodeoxygenation of Furfural over Pt(111): A Model System for the Rational Design and Operation of Practical Biomass Conversion Catalysts. *J. Phys. Chem. C* **2017**, *121*, 8490–8497.
- (94) Murillo, L. E.; Goda, A. M.; Chen, J. G. Selective Hydrogenation of the C=O Bond in Acrolein through the Architecture of Bimetallic Surface Structures. *J. Am. Chem. Soc.* **2007**, *129*, 7101–7105.
- (95) Murillo, L. E.; Chen, J. G. A comparative study of the adsorption and hydrogenation of acrolein on Pt(111), Ni(111) film and Pt-Ni-Pt(111) bimetallic surfaces. *Surf. Sci.* **2008**, *602*, 919–931.
- (96) Dostert, K.; Ivars-Barceló, F.; Schauermann, S.; Freund, H. Spectators Control Selectivity in Surface Chemistry: Acrolein Partial Hydrogenation Over Pd. *J. Am. Chem. Soc.* **2015**, *137*, 13496–13502.
- (97) Chiu, M. E.; Watson, D. J.; Kyriakou, G.; Tikhov, M. S.; Lambert, R. M. Tilt the Molecule and Change the Chemistry: Mechanism of S-Promoted Chemoselective Catalytic Hydrogenation of Crotonaldehyde on Cu(111). *Angew. Chem. Int. Ed.* **2006**, *45*, 7530–7534.
- (98) Chiu, M. E.; Kyriakou, G.; Williams, F. J.; Watson, D. J.; Tikhov, M. S.; Lambert, R. M.

Sulfur, normally a poison, strongly promotes chemoselective catalytic hydrogenation: stereochemistry and reactivity of crotonaldehyde on clean and S-modified Cu(111). *Chem. Commun.* **2006**, 1283–1285.

- (99) Liu, Z.-T.; Wang, C.-X.; Liu, Z.-W.; Lu, J. Selective hydrogenation of cinnamaldehyde over Pt-supported multi-walled carbon nanotubes: Insights into the tube-size effects. *Appl. Catal. A Gen.* **2008**, *344*, 114–123.
- (100) Toebes, M. L.; Zhang, Y.; Hájek, J.; Nijhuis, T. A.; Bitter, J. H.; Jos van Dillen, A.; Murzin, D. Y.; Koningsberger, D. C.; de Jong, K. P. Support effects in the hydrogenation of cinnamaldehyde over carbon nanofiber-supported platinum catalysts: characterization and catalysis. *J. Catal.* **2004**, *226*, 215–225.
- (101) Toebes, M. L.; Prinsloo, F. F.; Bitter, J. H.; Jos van Dillen, A.; de Jong, K. P. Influence of oxygen-containing surface groups on the activity and selectivity of carbon nanofiber-supported ruthenium catalysts in the hydrogenation of cinnamaldehyde. *J. Catal.* **2003**, *214*, 78–87.
- (102) Lan, X.; Wang, T. Highly Selective Catalysts for the Hydrogenation of Unsaturated Aldehydes: A Review. *ACS Catal.* **2020**, *10*, 2764–2790.
- (103) Delbecq, F.; Sautet, P. Influence of Sn additives on the selectivity of hydrogenation of  $\alpha,\beta$ -unsaturated aldehydes with Pt catalysts: a density functional study of molecular adsorption. *J. Catal.* **2003**, *220*, 115–126.
- (104) Hirschl, R.; Delbecq, F.; Sautet, P.; Hafner, J. Adsorption of unsaturated aldehydes on the (111) surface of a Pt-Fe alloy catalyst from first principles. *J. Catal.* **2003**, *217*, 354–366.
- (105) Pang, S. H.; Medlin, J. W. Adsorption and Reaction of Furfural and Furfuryl Alcohol on Pd(111): Unique Reaction Pathways for Multifunctional Reagents. *ACS Catal.* **2011**, *1*, 1272–1283.

- (106) de Jesús, J. C.; Zaera, F. Adsorption and thermal chemistry of acrolein and crotonaldehyde on Pt(111) surfaces. *Surf. Sci.* **1999**, *430*, 99–115.
- (107) de Jesús, J. C.; Zaera, F. Double-bond activation in unsaturated aldehydes: conversion of acrolein to propene and ketene on Pt(111) surfaces. *J. Mol. Catal. A Chem.* **1999**, *138*, 237–240.
- (108) Loh, A. S.; Davis, S. W.; Medlin, J. W. Adsorption and Reaction of 1-Epoxy-3-Butene on Pt(111): Implications for Heterogeneous Catalysis of Unsaturated Oxygenates. *J. Am. Chem. Soc.* **2008**, *130*, 5507–5514.
- (109) Haubrich, J.; Loffreda, D.; Delbecq, F.; Sautet, P.; Krupski, A.; Becker, C.; Wandelt, K. Adsorption of  $\alpha,\beta$ -Unsaturated Aldehydes on Pt(111) and Pt-Sn Alloys: II. Crotonaldehyde. *J. Phys. Chem. C* **2009**, *113*, 13947–13967.
- (110) Haubrich, J.; Loffreda, D.; Delbecq, F.; Sautet, P.; Jugnet, Y.; Krupski, A.; Becker, C.; Wandelt, K. Adsorption and Vibrations of  $\alpha,\beta$ -Unsaturated Aldehydes on Pure Pt and Pt-Sn Alloy (111) Surfaces I. Prenal. *J. Phys. Chem. C* **2008**, *112*, 3701–3718.
- (111) Shi, D.; Vohs, J. M. Deoxygenation of Biomass-Derived Oxygenates: Reaction of Furfural on Zn-Modified Pt(111). *ACS Catal.* **2015**, *5*, 2177–2183.
- (112) Marshall, S. T.; Horiuchi, C. M.; Zhang, W.; Medlin, J. W. Common Decomposition Pathways of 1-Epoxy-3-Butene and 2-Butenal on Pd(111). *J. Phys. Chem. C* **2008**, *112*, 20406–20412.
- (113) Koel, B. E. Structure, Characterization and Reactivity of Pt-Sn Surface Alloys. *Model Systems in Catalysis: Single Crystals to Supported Enzyme Mimics*; Springer: New York, 2010.
- (114) Jerdev, D. I.; Olivas, A.; Koel, B. E. Hydrogenation of Crotonaldehyde over Sn/Pt(111) Alloy Model Catalysts. *J. Catal.* **2002**, *205*, 278–288.

- (115) Handjani, S.; Marceau, E.; Blanchard, J.; Krafft, J.-M.; Che, M.; Mäki-Arvela, P.; Kumar, N.; Wärnå, J.; Murzin, D. Y. Influence of the support composition and acidity on the catalytic properties of mesoporous SBA-15, Al-SBA-15, and Al<sub>2</sub>O<sub>3</sub>-supported Pt catalysts for cinnamaldehyde hydrogenation. *J. Catal.* **2011**, *282*, 228–236.
- (116) Kennedy, G.; Baker, L. R.; Somorjai, G. A. Selective Amplification of C=O Bond Hydrogenation on Pt/TiO<sub>2</sub>: Catalytic Reaction and Sum-Frequency Generation Vibrational Spectroscopy Studies of Crotonaldehyde Hydrogenation. *Angew. Chem. Int. Ed.* **2014**, *53*, 3405–3408.
- (117) Serrano-Ruiz, J. C.; Luettich, J.; Sepúlveda-Escribano, A.; Rodríguez-Reinoso, F. Effect of the support composition on the vapor-phase hydrogenation of crotonaldehyde over Pt/Ce<sub>x</sub>Zr<sub>1-x</sub>O<sub>2</sub> catalysts. *J. Catal.* **2006**, *241*, 45–55.
- (118) Zhou, X.-L.; White, J. M.; Koel, B. E. Chemisorption of atomic hydrogen on clean and Cl-covered Ag(111). *Surf. Sci.* **1989**, *218*, 201–210.
- (119) Hammer, B.; Nørskov, J. K. Electronic factors determining the reactivity of metal surfaces. *Surf. Sci.* **1995**, *343*, 211–220.
- (120) Anger, G.; Winkler, A.; Rendulic, K. D. Adsorption and desorption kinetics in the systems H<sub>2</sub>/Cu(111), H<sub>2</sub>/Cu(110) and H<sub>2</sub>/Cu(100). *Surf. Sci.* **1989**, *220*, 1–17.
- (121) Kammler, T.; Küppers, J. Interaction of H atoms with Cu(111) surfaces: Adsorption, absorption, and abstraction. *J. Chem. Phys.* **1999**, *111*, 8115–8123.
- (122) Brandt, K.; Chiu, M. E.; Watson, D. J.; Tikhov, M. S.; Lambert, R. M. Adsorption Geometry Determines Catalytic Selectivity in Highly Chemoselective Hydrogenation of Crotonaldehyde on Ag(111). *J. Phys. Chem. C* **2012**, *116*, 4605–4611.
- (123) Pan, M.; Gong, J.; Dong, G.; Mullins, C. B. Model Studies with Gold: A Versatile Oxidation and Hydrogenation Catalyst. *Acc. Chem. Res.* **2014**, *47*, 750–760.

- (124) Pan, M.; Flaherty, D. W.; Mullins, C. B. Low-Temperature Hydrogenation of Acetaldehyde to Ethanol on H-Precovered Au(111). *J. Phys. Chem. Lett.* **2011**, *2*, 1363–1367.
- (125) Collins, D. M.; Spicer, W. E. The adsorption of CO, O<sub>2</sub>, and H<sub>2</sub> on Pt: I. Thermal desorption spectroscopy studies. *Surf. Sci.* **1977**, *69*, 85–113.
- (126) Olsen, R. A.; Kroes, G. J.; Baerends, E. J. Atomic and molecular hydrogen interacting with Pt(111). *J. Chem. Phys.* **1999**, *111*, 11155–11163.
- (127) Gdowski, G. E.; Felter, T. E.; Stulen, R. H. Effect of surface temperature on the sorption of hydrogen by Pd(111). *Surf. Sci.* **1987**, *181*, L147–L155.
- (128) Gutiérrez, V.; Nador, F.; Radivoy, G.; Volpe, M. A. Highly selective copper nanoparticles for the hydrogenation of  $\alpha,\beta$ -unsaturated aldehydes in liquid phase. *Appl. Catal. A Gen.* **2013**, *464*, 109–115.
- (129) Bron, M.; Kondratenko, E.; Trunschke, A.; Claus, P. Towards the "Pressure and Materials Gap": Hydrogenation of Acrolein Using Silver Catalysts. *Z. Phys. Chem.* **2004**, *218*, 405–423.
- (130) Keijzer, P. H.; Donoeva, B.; de Jong, K. P.; de Jongh, P. E. Supported silver catalysts prepared via melt infiltration: Synthesis, characterization and performance in selective hydrogenation. *Catal. Today* **2020**, DOI:10.1016/j.cattod.2020.03.017.
- (131) Delbecq, F.; Li, Y.; Loffreda, D. Metal-support interaction effects on chemo-regioselectivity: Hydrogenation of crotonaldehyde on Pt<sub>13</sub>/CeO<sub>2</sub>(111). *J. Catal.* **2016**, *334*, 68–78.
- (132) Riguetto, B. A.; Rodrigues, C. E. C.; Morales, M. A.; Baggio-Saitovitch, E.; Gengembre, L.; Payen, E.; Marques, C. M. P.; Bueno, J. M. C. Ru-Sn catalysts for selective hydrogenation of crotonaldehyde: Effect of the Sn/(Ru + Sn) ratio. *Appl. Catal. A Gen.* **2007**, *318*, 70–78.
- (133) Shi, J.; Zhang, M.; Du, W.; Ning, W.; Hou, Z. SnO<sub>2</sub>-isolated Pt<sub>3</sub>Sn alloy on reduced graphene oxide: an efficient catalyst for selective hydrogenation of C=O in unsaturated

- aldehydes. *Catal. Sci. Technol.* **2015**, *5*, 3108–3112.
- (134) Zhu, M.; Huang, B.; Shao, Q.; Pi, Y.; Qian, Y.; Huang, X. Highly Networked Platinum–Tin Nanowires as Highly Active and Selective Catalysts towards the Semihydrogenation of Unsaturated Aldehydes. *ChemCatChem* **2018**, *10*, 3214–3218.
- (135) Li, C.; Chen, Y.; Zhang, S.; Xu, S.; Zhou, J.; Wang, F.; Wei, M.; Evans, D. G.; Duan, X. Ni–In Intermetallic Nanocrystals as Efficient Catalysts toward Unsaturated Aldehydes Hydrogenation. *Chem. Mater.* **2013**, *25*, 3888–3896.
- (136) Rodiansono; Hara, T.; Ichikuni, N.; Shimazu, S. A Novel Preparation Method of Ni–Sn Alloy Catalysts Supported on Aluminium Hydroxide: Application to Chemoselective Hydrogenation of Unsaturated Carbonyl Compounds. *Chem. Lett.* **2012**, *41*, 769–771.
- (137) Lin, H.; Zheng, J.; Zheng, X.; Gu, Z.; Yuan, Y.; Yang, Y. Improved chemoselective hydrogenation of crotonaldehyde over bimetallic AuAg/SBA-15 catalyst. *J. Catal.* **2015**, *330*, 135–144.
- (138) Tian, L.; Yang, Q.; Jiang, Z.; Zhu, Y.; Pei, Y.; Qiao, M.; Fan, K. Highly chemoselective hydrogenation of crotonaldehyde over Ag–In/SBA-15 fabricated by a modified “two solvents” strategy. *Chem. Commun.* **2011**, *47*, 6168–6170.
- (139) Reyes, P.; Pecchi, G.; Fierro, J. L. G. Surface Structures of Rh-Cu Sol-Gel Catalysts and Performance for Crotonaldehyde Hydrogenation. *Langmuir* **2001**, *17*, 522–527.
- (140) Li, B.; Hong, X.; Lin, J.-J.; Hu, G.-S.; Yu, Q.; Wang, Y.-J.; Luo, M.-F.; Lu, J.-Q. Promoting effect of Ir on the catalytic property of Ru/ZnO catalysts for selective hydrogenation of crotonaldehyde. *Appl. Surf. Sci.* **2013**, *280*, 179–185.
- (141) Li, R.; Zhao, J.; Gan, Z.; Jia, W.; Wu, C.; Han, D. Gold Promotion of MCM-41 Supported Ruthenium Catalysts for Selective Hydrogenation of  $\alpha,\beta$ -Unsaturated Aldehydes and Ketones. *Catal. Letters* **2018**, *148*, 267–276.



- (142) Tamura, M.; Tokonami, K.; Nakagawa, Y.; Tomishige, K. Rapid synthesis of unsaturated alcohols under mild conditions by highly selective hydrogenation. *Chem. Commun.* **2013**, *49*, 7034–7036.
- (143) Reyes, P.; Aguirre, M. C.; Fierro, J. L. G.; Santori, G.; Ferretti, O. Hydrogenation of crotonaldehyde on Rh-Sn/SiO<sub>2</sub> catalysts prepared by reaction of tetrabutyltin on prereduced Rh/SiO<sub>2</sub> precursors. *J. Mol. Catal. A Chem.* **2002**, *184*, 431–441.
- (144) Guo, H.; Li, H.; Jarvis, K.; Wan, H.; Kunal, P.; Dunning, S. G.; Liu, Y.; Henkelman, G.; Humphrey, S. M. Microwave-Assisted Synthesis of Classically Immiscible Ag-Ir Alloy Nanoparticle Catalysts. *ACS Catal.* **2018**, *8*, 11386–11397.
- (145) Ning, X.; Xu, Y.-M.; Wu, A.-Q.; Tang, C.; Jia, A.-P.; Luo, M.-F.; Lu, J.-Q. Kinetic study of selective hydrogenation of crotonaldehyde over Fe-promoted Ir/BN catalysts. *Appl. Surf. Sci.* **2009**, *463*, 463–473.
- (146) Yu, Q.; Bando, K. K.; Yuan, J.-F.; Luo, C.-Q.; Jia, A.-P.; Hu, G.-S.; Lu, J.-Q.; Luo, M.-F. Selective Hydrogenation of Crotonaldehyde over Ir-FeO<sub>x</sub>/SiO<sub>2</sub> Catalysts: Enhancement of Reactivity and Stability by Ir-FeO<sub>x</sub> Interaction. *J. Phys. Chem. C* **2016**, *120*, 8663–8673.
- (147) Bai, S.; Bu, L.; Shao, Q.; Zhu, X.; Huang, X. Multicomponent Pt-Based Zigzag Nanowires as Selectivity Controllers for Selective Hydrogenation Reactions. *J. Am. Chem. Soc.* **2018**, *140*, 8384–8387.
- (148) Tsang, S. C.; Cailuo, N.; Oduro, W.; Kong, A. T. S.; Clifton, L.; Yu, K. M. K.; Thiebaut, B.; Cookson, J.; Bishop, P. Engineering Preformed Cobalt-Doped Platinum Nanocatalysts for Ultrasensitive Hydrogenation. *ACS Nano* **2008**, *2*, 2547–2553.
- (149) Zheng, Q.; Wang, D.; Yuan, F.; Han, Q.; Dong, Y.; Liu, Y.; Niu, X.; Zhu, Y. An Effective Co-promoted Platinum of Co–Pt/SBA-15 Catalyst for Selective Hydrogenation of Cinnamaldehyde to Cinnamyl Alcohol. *Catal. Letters* **2016**, *146*, 1535–1543.

- (150) Pârvulescu, V. I.; Pârvulescu, V.; Eudruschat, U.; Filoti, G.; Wagner, F. E.; Kübel, C.; Richards, R. Characterization and Catalytic-Hydrogenation Behavior of SiO<sub>2</sub>-Embedded Nanoscopic Pd, Au, and Pd–Au Alloy Colloids. *Chem. Eur. J.* **2006**, *12*, 2343–2357.
- (151) Qiu, J.; Zhang, H.; Wang, X.; Han, H.; Liang, C.; Li, C. Selective hydrogenation of cinnamaldehyde over carbon nanotube supported Pd–Ru catalyst. *React. Kinet. Catal. Lett.* **2006**, *88*, 269–275.
- (152) Prakash, M. G.; Mahalakshmy, R.; Krishnamurthy, K. R.; Viswanathan, B. Studies on Ni–M (M = Cu, Ag, Au) bimetallic catalysts for selective hydrogenation of cinnamaldehyde. *Catal. Today* **2016**, *263*, 105–111.
- (153) Zhao, J.; Ni, J.; Xu, J.; Xu, J.; Cen, J.; Li, X. Ir promotion of TiO<sub>2</sub> supported Au catalysts for selective hydrogenation of cinnamaldehyde. *Catal. Commun.* **2014**, *54*, 72–76.
- (154) Yuan, X.; Zheng, J.; Zhang, Q.; Li, S.; Yang, Y.; Gong, J. Liquid-phase hydrogenation of cinnamaldehyde over Cu–Au/SiO<sub>2</sub> catalysts. *AIChE J.* **2014**, *60*, 3300–3311.
- (155) Cao, Y.; Chen, B.; Guerrero-Sánchez, J.; Lee, I.; Zhou, X.; Takeuchi, N.; Zaera, F. Controlling Selectivity in Unsaturated Aldehyde Hydrogenation Using Single-Site Alloy Catalysts. *ACS Catal.* **2019**, *9*, 9150–9157.
- (156) Teddy, J.; Falqui, A.; Corrias, A.; Carta, D.; Lecante, P.; Gerber, I.; Serp, P. Influence of particles alloying on the performances of Pt–Ru/CNT catalysts for selective hydrogenation. *J. Catal.* **2011**, *278*, 59–70.
- (157) Zheng, R.; Porosoff, M. D.; Weiner, J. L.; Lu, S.; Zhu, Y.; Chen, J. G. Controlling hydrogenation of C=O and C=C bonds in cinnamaldehyde using silica supported Co–Pt and Cu–Pt bimetallic catalysts. *Appl. Catal. A Gen.* **2012**, *419*, 126–132.
- (158) Huang, S., Yang, N., Huo, M., Sun, Y. & Zhu, Y. The shape evolution from Pt<sub>x</sub>Co<sub>y</sub>@Co cubes to Pt<sub>x</sub>Co<sub>y</sub> multicubes for selective hydrogenation of  $\alpha,\beta$ -unsaturated aldehyde.

*Nanoscale* **2016**, *8*, 6451–6455.

- (159) Mahata, N.; Gonçalves, F.; Pereira, M. F. R.; Figueiredo, J. L. Selective hydrogenation of cinnamaldehyde to cinnamyl alcohol over mesoporous carbon supported Fe and Zn promoted Pt catalyst. *Appl. Catal. A Gen.* **2008**, *339*, 159–168.
- (160) Cao, X.-M.; Burch, R.; Hardacre, C.; Hu, P. Reaction Mechanisms of Crotonaldehyde Hydrogenation on Pt(111): Density Functional Theory and Microkinetic Modeling. *J. Phys. Chem. C* **2011**, *115*, 19819–19827.
- (161) Cao, X.-M.; Burch, R.; Hardacre, C.; Hu, P. An understanding of chemoselective hydrogenation on crotonaldehyde over Pt(111) in the free energy landscape: The microkinetics study based on first-principles calculations. *Catal. Today* **2011**, *165*, 71–79.
- (162) Cai, Q.-X.; Wang, J.-G.; Wang, Y.-G.; Mei, D. Mechanistic insights into the structure-dependent selectivity of catalytic furfural conversion on platinum catalysts. *AIChE J.* **2015**, *61*, 3812–3824.
- (163) Wang, S.; Vorotnikov, V.; Vlachos, D. G. Coverage-Induced Conformational Effects on Activity and Selectivity: Hydrogenation and Decarbonylation of Furfural on Pd(111). *ACS Catal.* **2015**, *5*, 104–112.
- (164) Mironenko, A. V.; Gilkey, M. J.; Panagiotopoulou, P.; Facas, G.; Vlachos, D. G.; Xu, B. Ring Activation of Furanic Compounds on Ruthenium-Based Catalysts. *J. Phys. Chem. C* **2015**, *119*, 6075–6085.
- (165) Loffreda, D.; Delbecq, F.; Sautet, P. Adsorption thermodynamics of acrolein on Pt (1 1 1) in realistic temperature and pressure from first-principle calculations. *Chem. Phys. Lett.* **2005**, *405*, 434–439.
- (166) Loffreda, D. Theoretical insight of adsorption thermodynamics of multifunctional molecules on metal surfaces. *Surf. Sci.* **2006**, *600*, 2103–2112.

- (167) Banerjee, A.; Mushrif, S. H. Investigating Reaction Mechanisms for Furfural Hydrodeoxygenation on Ni and the Effect of Boron Doping on the Activity and Selectivity of the Catalyst. *J. Phys. Chem. C* **2018**, *122*, 18383–18394.
- (168) Shan, N.; Hanchett, M. K.; Liu, B. Mechanistic Insights Evaluating Ag, Pb, and Ni as Electrocatalysts for Furfural Reduction from First-Principles Methods. *J. Phys. Chem. C* **2017**, *121*, 25768–25777.
- (169) Banerjee, A.; Mushrif, S. H. Reaction Pathways for the Deoxygenation of Biomass-Pyrolysis-Derived Bio-oil on Ru: A DFT Study using Furfural as a Model Compound. *ChemCatChem* **2017**, *9*, 2828–2838.
- (170) Lim, J. S.; Saldana-Greco, D.; Rappe, A. M. Improved pseudopotential transferability for magnetic and electronic properties of binary manganese oxides from DFT+ $U+J$  calculations. *Phys. Rev. B* **2016**, *94*, 165151.
- (171) Gautier, S.; Steinmann, S. N.; Michel, C.; Fleurat-Lessard, P.; Sautet, P. Molecular adsorption at Pt(111). How accurate are DFT functionals? *Phys. Chem. Chem. Phys.* **2015**, *17*, 28921–28930.
- (172) Feibelman, P. J.; Hammer, B.; Nørskov, J. K.; Wagner, F.; Scheffler, M.; Stumpf, R.; Watwe, R.; Dumesic, J. The CO/Pt(111) puzzle. *J. Phys. Chem. B* **2001**, *105*, 4018–4025.
- (173) Medford, A. J.; Wellendorff, J.; Vojvodic, A.; Studt, F.; Abild-Pedersen, F.; Jacobsen, K. W.; Bligaard, T.; Nørskov, J. K. Assessing the reliability of calculated catalytic ammonia synthesis rates. *Science* **2014**, *345*, 197–200.
- (174) Tuokko, S.; Pihko, P. M.; Honkala, K. First Principles Calculations for Hydrogenation of Acrolein on Pd and Pt: Chemoselectivity Depends on Steric Effects on the Surface. *Angew. Chem. Int. Ed.* **2016**, *55*, 1670–1674.
- (175) Pirillo, S.; López-Corral, I.; Germán, E.; Juan, A. Density functional study of acrolein

- adsorption on Pt (111). *Vacuum* **2014**, *99*, 259–264.
- (176) Wang, K.; Yang, B. Theoretical understanding on the selectivity of acrolein hydrogenation over silver surfaces: the non-Horiuti-Polanyi mechanism is the key. *Catal. Sci. Technol.* **2017**, *7*, 4024–4033.
- (177) Ferullo, R. M.; Branda, M. M.; Illas, F. Structure and stability of acrolein and allyl alcohol networks on Ag(111) from density functional theory based calculations with dispersion corrections. *Surf. Sci.* **2013**, *617*, 175–182.
- (178) Liu, B.; Cheng, L.; Curtiss, L.; Greeley, J. Effects of van der Waals density functional corrections on trends in furfural adsorption and hydrogenation on close-packed transition metal surfaces. *Surf. Sci.* **2014**, *622*, 51–59.
- (179) Reece, C.; Luneau, M.; Friend, C. M.; Madix, R. J. Predicting a Sharp Decline in Selectivity for Catalytic Esterification of Alcohols from van der Waals Interactions. *Angew. Chem. Int. Ed.* **2020**, *59*, 10864–10867.
- (180) Xu, Y.; Chen, W.; Kaxiras, E.; Friend, C. M.; Madix, R. J. General Effect of van der Waals Interactions on the Stability of Alkoxy Intermediates on Metal Surfaces. *J. Phys. Chem. B* **2018**, *122*, 555–560.
- (181) Chen, W.; Cubuk, E. D.; Montemore, M. M.; Reece, C.; Madix, R. J.; Friend, C. M.; Kaxiras, E. A Comparative Ab Initio Study of Anhydrous Dehydrogenation of Linear-Chain Alcohols on Cu(110). *J. Phys. Chem. C* **2018**, *122*, 7806–7815.
- (182) Kabeer, F. C.; Chen, W.; Madix, R. J.; Friend, C. M.; Tkatchenko, A. First-Principles Study of Alkoxides Adsorbed on Au(111) and Au(110) Surfaces: Assessing the Roles of Noncovalent Interactions and Molecular Structures in Catalysis. *J. Phys. Chem. C* **2017**, *121*, 27905–27914.
- (183) Karakalos, S.; Xu, Y.; Kabeer, F. C.; Chen, W.; Rodríguez-Reyes, J. C. F.; Tkatchenko, A.;

- Kaxiras, E.; Madix, R. J.; Friend, C. M. Noncovalent Bonding Controls Selectivity in Heterogeneous Catalysis: Coupling Reactions on Gold. *J. Am. Chem. Soc.* **2016**, *138*, 15243–15250.
- (184) Chen, W.; Sun, L.; Kozinsky, B.; Friend, C. M.; Kaxiras, E.; Sautet, P.; Madix, R. J. Effect of Frustrated Rotations on the Pre-Exponential Factor for Unimolecular Reactions on Surfaces: A Case Study of Alkoxy Dehydrogenation. *J. Phys. Chem. C* **2020**, *124*, 1429–1437.
- (185) Lim, J. S.; Molinari, N.; Duanmu, K.; Sautet, P.; Kozinsky, B. Automated Detection and Characterization of Surface Restructuring Events in Bimetallic Catalysts. *J. Phys. Chem. C* **2019**, *123*, 16332–16344.
- (186) Janin, E.; von Schenck, H.; Ringler, S.; Weissenrieder, J.; Åkermark, T.; Göthelid, M. Adsorption and bonding of 2-butenal on Sn/Pt surface alloys. *J. Catal.* **2003**, *215*, 245–253.
- (187) Haubrich, J.; Loffreda, D.; Delbecq, F.; Jugnet, Y.; Sautet, P.; Krupski, A.; Becker, C.; Wandelt, K. Determination of the crotonaldehyde structures on Pt and PtSn surface alloys from a combined experimental and theoretical study. *Chem. Phys. Lett.* **2006**, *433*, 188–192.
- (188) Haubrich, J.; Loffreda, D.; Delbecq, F.; Sautet, P.; Jugnet, Y.; Becker, C.; Wandelt, K. Adsorption and Vibrations of  $\alpha,\beta$ -Unsaturated Aldehydes on Pt(111) and Pt-Sn Alloy (111) Surfaces. 3. Adsorption Energy vs Adsorption Strength. *J. Phys. Chem. C* **2010**, *114*, 1073–1084.
- (189) Maligal-Ganesh, R. V.; Xiao, C.; Goh, T. W.; Wang, L.-L.; Gustafson, J.; Pei, Y.; Qi, Z.; Johnson, D. D.; Zhang, S.; Tao, F. (F.); Huang, W. A Ship-in-a-Bottle Strategy to Synthesize Encapsulated Intermetallic Nanoparticle Catalysts: Exemplified for Furfural Hydrogenation. *ACS Catal.* **2016**, *6*, 1754–1763.
- (190) Murillo, L. E.; Menning, C. A.; Chen, J. G. Trend in the C=C and C=O bond hydrogenation

- of acrolein on Pt–M (M = Ni, Co, Cu) bimetallic surfaces. *J. Catal.* **2009**, *268*, 335–342.
- (191) Jiang, Z.; Wan, W.; Lin, Z.; Xie, J.; Chen, J. G. Understanding the Role of M/Pt(111) (M = Fe, Co, Ni, Cu) Bimetallic Surfaces for Selective Hydrodeoxygenation of Furfural. *ACS Catal.* **2017**, *7*, 5758–5765.
- (192) An, W.; Men, Y.; Wang, J. Comparative study on hydrogenation of propanal on Ni(111) and Cu(111) from density functional theory. *Appl. Surf. Sci.* **2017**, *394*, 333–339.
- (193) Luo, Q.; Wang, T.; Beller, M.; Jiao, H. Acrolein Hydrogenation on Ni(111). *J. Phys. Chem. C* **2013**, *117*, 12715–12724.
- (194) Yang, B.; Gong, X.-Q.; Wang, H.-F.; Cao, X.-M.; Rooney, J. J.; Hu, P. Evidence to Challenge the Universality of the Horiuti-Polanyi Mechanism for Hydrogenation in Heterogeneous Catalysis: Origin and Trend of the Preference of a Non-Horiuti-Polanyi Mechanism. *J. Am. Chem. Soc.* **2013**, *135*, 15244–15250.
- (195) He, X.; Chen, Z.-X.; Kang, G.-J. Theoretical Study of the Role of Indium on the Selectivity of Acrolein Hydrogenation to Propenol on Gold Surfaces. *J. Phys. Chem. C* **2009**, *113*, 12325–12330.
- (196) Li, Z.; Chen, Z.-X.; He, X.; Kang, G.-J. Theoretical studies of acrolein hydrogenation on Au<sub>20</sub> nanoparticle. *J. Chem. Phys.* **2010**, *132*, 184702.
- (197) Ferullo, R.; Branda, M. M.; Illas, F. Coverage Dependence of the Structure of Acrolein Adsorbed on Ag(111). *J. Phys. Chem. Lett.* **2010**, *1*, 2546–2549.
- (198) Lim, K. H.; Mohammad, A. B.; Yudanov, I. V; Neyman, K. M.; Bron, M.; Claus, P.; Rösch, N. Mechanism of Selective Hydrogenation of  $\alpha,\beta$ -Unsaturated Aldehydes on Silver Catalysts: A Density Functional Study. *J. Phys. Chem. C* **2009**, *113*, 13231–13240.
- (199) Lim, K. H.; Chen, Z.-X.; Neyman, K. M.; Rösch, N. Adsorption of acrolein on single-crystal surfaces of silver: Density functional studies. *Chem. Phys. Lett.* **2006**, *420*, 60–64.

- (200) Aich, P.; Wei, H.; Basan, B.; Kropf, A. J.; Schweitzer, N. M.; Marshall, C. L.; Miller, J. T.; Meyer, R. Single-Atom Alloy Pd–Ag Catalyst for Selective Hydrogenation of Acrolein. *J. Phys. Chem. C* **2015**, *119*, 18140–18148.
- (201) Engelhardt, C. M.; Kennedy, R. M.; Enterkin, J. A.; Poepelmeier, K. R.; Ellis, D. E.; Marshall, C. L.; Stair, P. C. Structure Sensitivity of Acrolein Hydrogenation by Platinum Nanoparticles on Ba<sub>x</sub>Sr<sub>1-x</sub>TiO<sub>3</sub> Nanocuboids. *ChemCatChem* **2018**, *10*, 632–641.
- (202) Yang, B.; Wang, D.; Gong, X.-Q.; Hu, P. Acrolein hydrogenation on Pt(211) and Au(211) surfaces: a density functional theory study. *Phys. Chem. Chem. Phys.* **2011**, *13*, 21146–21152.
- (203) Loffreda, D.; Delbecq, F.; Vigné, F.; Sautet, P. Chemo-Regioselectivity in Heterogeneous Catalysis: Competitive Routes for C=O and C=C Hydrogenations from a Theoretical Approach. *J. Am. Chem. Soc.* **2006**, *128*, 1316–1323.
- (204) Almora-Barrios, N.; Cano, I.; van Leeuwen, P. W. N. M.; López, N. Concerted Chemoselective Hydrogenation of Acrolein on Secondary Phosphine Oxide Decorated Gold Nanoparticles. *ACS Catal.* **2017**, *7*, 3949–3954.
- (205) Schweitzer, N.; Xin, H.; Nikolla, E.; Miller, J. T.; Linic, S. Establishing Relationships Between the Geometric Structure and Chemical Reactivity of Alloy Catalysts Based on Their Measured Electronic Structure. *Top. Catal.* **2010**, *53*, 348–356.
- (206) Mavrikakis, M.; Hammer, B.; Nørskov, J. K. Effect of Strain on the Reactivity of Metal Surfaces. *Phys. Rev. Lett.* **1998**, *81*, 2819–2822.
- (207) Hammer, B.; Morikawa, Y.; Nørskov, J. K. CO Chemisorption at Metal Surfaces and Overlayers. *Phys. Rev. Lett.* **1996**, *76*, 2141–2144.
- (208) Ma, Y.; Diemant, T.; Bansmann, J.; Behm, R. J. The interaction of CO with PdAg/Pd(111) surface alloys—A case study of ensemble effects on a bimetallic surface. *Phys. Chem. Chem.*



*Phys.* **2011**, *13*, 10741–10754.

- (209) Shi, W.; Zhang, L.; Ni, Z.; Xiao, X.; Xia, S. Adsorption and hydrogenation mechanism of crotonaldehyde on a Pd(111) surface by periodic DFT calculations. *RSC Adv.* **2014**, *4*, 27003–27012.
- (210) Sitthisa, S.; Pham, T.; Prasomsri, T.; Sooknoi, T.; Mallinson, R. G.; Resasco, D. E. Conversion of furfural and 2-methylpentanal on Pd/SiO<sub>2</sub> and Pd-Cu/SiO<sub>2</sub> catalysts. *J. Catal.* **2011**, *280*, 17–27.
- (211) Shi, J.; Nie, R.; Chen, P.; Hou, Z. Selective hydrogenation of cinnamaldehyde over reduced graphene oxide supported Pt catalyst. *Catal. Commun.* **2013**, *41*, 101–105.
- (212) Rong, H.; Niu, Z.; Zhao, Y.; Cheng, H.; Li, Z.; Ma, L.; Li, J.; Wei, S.; Li, Y. Structure Evolution and Associated Catalytic Properties of Pt–Sn Bimetallic Nanoparticles. *Chem. Eur. J.* **2015**, *21*, 12034–12041.
- (213) Zhao, M.; Yuan, K.; Wang, Y.; Li, G.; Guo, J.; Gu, L.; Hu, W.; Zhao, H.; Tang, Z. Metal-organic frameworks as selectivity regulators for hydrogenation reactions. *Nature* **2016**, *539*, 76–80.
- (214) Ide, M. S.; Hao, B.; Neurock, M.; Davis, R. J. Mechanistic Insights on the Hydrogenation of  $\alpha,\beta$ -Unsaturated Ketones and Aldehydes to Unsaturated Alcohols over Metal Catalysts. *ACS Catal.* **2012**, *2*, 671–683.
- (215) Li, Y.; Li, Z.-G.; Zhou, R.-X. Bimetallic Pt-Co catalysis on carbon nanotubes for the selective hydrogenation of cinnamaldehyde to cinnamyl alcohol: Preparation and characterization. *J. Mol. Catal. A Chem.* **2008**, *279*, 140–146.
- (216) Ji, X.; Niu, X.; Li, B.; Han, Q.; Yuan, F.; Zaera, F.; Zhu, Y.; Fu, H. Selective Hydrogenation of Cinnamaldehyde to Cinnamal Alcohol over Platinum/Graphene Catalysts. *ChemCatChem* **2014**, *6*, 3246–3253.

- (217) Sun, K.-Q.; Hong, Y.-C.; Zhang, G.-R.; Xu, B.-Q. Synergy between Pt and Au in Pt-on-Au Nanostructures for Chemoselective Hydrogenation Catalysis. *ACS Catal.* **2011**, *1*, 1336–1346.
- (218) Guo, Z.; Chen, Y.; Li, L.; Wang, X.; Haller, G. L.; Yang, Y. Carbon nanotube-supported Pt-based bimetallic catalysts prepared by a microwave-assisted polyol reduction method and their catalytic applications in the selective hydrogenation. *J. Catal.* **2010**, *276*, 314–326.
- (219) Bhogeswararao, S.; Srinivas, D. Intramolecular selective hydrogenation of cinnamaldehyde over CeO<sub>2</sub>–ZrO<sub>2</sub>-supported Pt catalysts. *J. Catal.* **2012**, *285*, 31–40.
- (220) Kijeński, J.; Winiarek, P.; Paryjczak, T.; Lewicki, A.; Mikołajska, A. Platinum deposited on monolayer supports in selective hydrogenation of furfural to furfuryl alcohol. *Appl. Catal. A Gen.* **2002**, *233*, 171–182.
- (221) Bidaoui, M.; Especel, C.; Sabour, S.; Benatallah, L.; Saib-Bouchenafa, N.; Royer, S.; Mohammedi, O. Toward the improvement in unsaturated alcohol selectivity during  $\alpha,\beta$ -unsaturated aldehyde selective hydrogenation, using Zn as promoter of Pt. *J. Mol. Catal. A Chem.* **2015**, *399*, 97–105.
- (222) Campo, B. C.; Volpe, A.; Gigola, C. E. Liquid-Phase Hydrogenation of Crotonaldehyde over Platinum- and Palladium-Based Catalysts. *Ind. Eng. Chem. Res.* **2009**, *48*, 10234–10239.
- (223) Silvestre-Albero, J.; Sepúlveda-Escribano, A.; Rodríguez-Reinoso, F.; Anderson, J. A. Influence of Zn on the characteristics and catalytic behavior of TiO<sub>2</sub>-supported Pt catalysts. *J. Catal.* **2004**, *223*, 179–190.
- (224) Merlo, A. B.; Vetere, V.; Ramallo-López, J. M.; Requejo, F. G.; Casella, M. L. Liquid-phase furfural hydrogenation employing silica-supported PtSn and PtGe catalysts prepared using surface organometallic chemistry on metals techniques. *React. Kinet. Mech. Catal.* **2011**,

104, 467–482.

- (225) Chen, B.; Li, F.; Huang, Z.; Yuan, G. Tuning catalytic selectivity of liquid-phase hydrogenation of furfural via synergistic effects of supported bimetallic catalysts. *Appl. Catal. A Gen.* **2015**, *500*, 23–29.
- (226) Dohade, M. G.; Dhepe, P. L. Efficient hydrogenation of concentrated aqueous furfural solutions into furfuryl alcohol under ambient conditions in presence of PtCo bimetallic catalyst. *Green Chem.* **2017**, *19*, 1144–1154.
- (227) O'Driscoll, A.; Curtin, T.; Hernández, W. Y.; Van Der Voort, P.; Leahy, J. J. Hydrogenation of Furfural with a Pt–Sn Catalyst: The Suitability to Sustainable Industrial Application. *Org. Process Res. Dev.* **2016**, *20*, 1917–1929.
- (228) Sawai, T.; Yonehara, T.; Yonezawa, A.; Sano, M.; Suzuki, T.; Miyake, T. Preparation of Pd/MOF and Ru/MOF Catalysts and Catalytic Performance for Hydrogenation and Cross-coupling Reactions. *J. Japan Pet. Inst.* **2014**, *57*, 58–64.
- (229) Gebauer-Henke, E.; Farbotko, J.; Touroude, R.; Rynkowski, J. A Comparative Study of Ir/Ga<sub>2</sub>O<sub>3</sub>, Pt/Ga<sub>2</sub>O<sub>3</sub>, and Ru/Ga<sub>2</sub>O<sub>3</sub> Catalysts in Selective Hydrogenation of Crotonaldehyde. *Kinet. Catal.* **2008**, *49*, 574–580.
- (230) Yu, Q.; Zhang, X.; Li, B.; Lu, J.; Hu, G.; Jia, A.; Luo, C.; Hong, Q.; Song, Y.; Luo, M. Effect of reduction temperature on Ru–Ir/ZnO catalyst for selective hydrogenation of crotonaldehyde. *J. Mol. Catal. A Chem.* **2014**, *392*, 89–96.
- (231) Bachiller-Baeza, B.; Guerrero-Ruiz, A.; Rodríguez-Ramos, I. Role of the residual chlorides in platinum and ruthenium catalysts for the hydrogenation of  $\alpha,\beta$ -unsaturated aldehydes. *Appl. Catal. A Gen.* **2000**, *192*, 289–297.
- (232) Wang, Y.; Rong, Z.; Wang, Y.; Zhang, P.; Wang, Y.; Qu, J. Ruthenium nanoparticles loaded on multiwalled carbon nanotubes for liquid-phase hydrogenation of fine chemicals: An

- exploration of confinement effect. *J. Catal.* **2015**, *329*, 95–106.
- (233) Musci, J. J.; Merlo, A. B.; Casella, M. L. Aqueous phase hydrogenation of furfural using carbon-supported Ru and RuSn catalysts. *Catal. Today* **2017**, *296*, 43–50.
- (234) Bachiller-Baeza, B.; Guerrero-Ruiz, A.; Wang, P.; Rodríguez-Ramos, I. Hydrogenation of Citral on Activated Carbon and High-Surface-Area Graphite-Supported Ruthenium Catalysts Modified with Iron. *J. Catal.* **2001**, *204*, 450–459.
- (235) Chen, P.; Lu, J.-Q.; Xie, G.-Q.; Hu, G.-S.; Zhu, L.; Luo, L.-F.; Huang, W.-X.; Luo, M.-F. Effect of reduction temperature on selective hydrogenation of crotonaldehyde over Ir/TiO<sub>2</sub> catalysts. *Appl. Catal. A Gen.* **2012**, *433*, 236–242.
- (236) Reyes, P.; Aguirre, M. C.; Pecchi, G.; Fierro, J. L. G. Crotonaldehyde hydrogenation on Ir supported catalysts. *J. Mol. Catal. A Chem.* **2000**, *164*, 245–251.
- (237) Lin, W.; Cheng, H.; He, L.; Yu, Y.; Zhao, F. High performance of Ir-promoted Ni/TiO<sub>2</sub> catalyst toward the selective hydrogenation of cinnamaldehyde. *J. Catal.* **2013**, *303*, 110–116.
- (238) Rojas, H.; Díaz, G.; Martínez, J. J.; Castañeda, C.; Gómez-Cortés, A.; Arenas-Alatorre, J. Hydrogenation of  $\alpha,\beta$ -unsaturated carbonyl compounds over Au and Ir supported on SiO<sub>2</sub>. *J. Mol. Catal. A Chem.* **2012**, *364*, 122–128.
- (239) Ekou, T.; Vicente, A.; Lafaye, G.; Especel, C.; Marecot, P. Bimetallic Rh-Ge and Pt-Ge catalysts supported on TiO<sub>2</sub> for citral hydrogenation: II. Catalytic properties. *Appl. Catal. A Gen.* **2006**, *314*, 73–80.
- (240) Nagpure, A. S.; Gurrala, L.; Gogoi, P.; Chilukuri, S. V. Hydrogenation of cinnamaldehyde to hydrocinnamaldehyde over Pd nanoparticles deposited on nitrogen-doped mesoporous carbon. *RSC Adv.* **2016**, *6*, 44333–44340.
- (241) Jiang, F.; Cai, J.; Liu, B.; Xu, Y.; Liu, X. Particle size effects in the selective hydrogenation

- of cinnamaldehyde over supported palladium catalysts. *RSC Adv.* **2016**, *6*, 75541–75551.
- (242) Zhao, J.; Xu, X.; Li, X.; Wang, J. Promotion of Sn on the Pd/AC catalyst for the selective hydrogenation of cinnamaldehyde. *Catal. Commun.* **2014**, *43*, 102–106.
- (243) Kliewer, C. J.; Bieri, M.; Somorjai, G. A. Hydrogenation of the  $\alpha,\beta$ -Unsaturated Aldehydes Acrolein, Crotonaldehyde, and Prenal over Pt Single Crystals: A Kinetic and Sum-Frequency Generation Vibrational Spectroscopy Study. *J. Am. Chem. Soc.* **2009**, *131*, 9958–9966.
- (244) Loffreda, D.; Jugnet, Y.; Delbecq, F.; Bertolini, J. C.; Sautet, P. Coverage Dependent Adsorption of Acrolein on Pt(111) from a Combination of First Principle Theory and HREELS Study. *J. Phys. Chem. B* **2004**, *108*, 9085–9093.
- (245) Janin, E.; Ringler, S.; Weissenrieder, J.; Åkermark, T.; Karlsson, U. O.; Göthelid, M.; Nordlund, D.; Ogasawara, H. Adsorption and bonding of propene and 2-butenal on Pt(1 1 1). *Surf. Sci.* **2001**, *482*, 83–89.
- (246) Urquhart, A. J.; Williams, F. J.; Vaughan, O. P. H.; Cropley, R. L.; Lambert, R. M. Adsorbate conformation determines catalytic chemoselectivity: crotonaldehyde on the Pt(111) surface. *Chem. Commun.* **2005**, 1977–1979.
- (247) Dong, Y.; Zaera, F. Selectivity in Hydrogenation Catalysis with Unsaturated Aldehydes: Parallel versus Sequential Steps. *J. Phys. Chem. Lett.* **2018**, *9*, 1301–1306.
- (248) Haubrich, J.; Loffreda, D.; Delbecq, F.; Sautet, P.; Jugnet, Y.; Krupski, A.; Becker, C.; Wandelt, K. Mechanistic and spectroscopic identification of initial reaction intermediates for prenal decomposition on a platinum model catalyst. *Phys. Chem. Chem. Phys.* **2011**, *13*, 6000–6009.
- (249) Manyar, H. G.; Morgan, R.; Morgan, K.; Yang, B.; Hu, P.; Szlachetko, J.; Sá, J.; Hardacre, C. High energy resolution fluorescence detection XANES – an *in situ* method to study the

- interaction of adsorbed molecules with metal catalysts in the liquid phase. *Catal. Sci. Technol.* **2013**, *3*, 1497–1500.
- (250) Manyar, H. G.; Yang, B.; Daly, H.; Moor, H.; McMonagle, S.; Tao, Y.; Yadav, G. D.; Goguet, A.; Hu, P.; Hardacre, C. Selective Hydrogenation of  $\alpha,\beta$ -Unsaturated Aldehydes and Ketones using Novel Manganese Oxide and Platinum Supported on Manganese Oxide Octahedral Molecular Sieves as Catalysts. *ChemCatChem* **2013**, *5*, 506–512.
- (251) Xiao, X.-C.; Shi, W.; Ni, Z.-M.; Zhang, L.-Y.; Xu, J.-F. Adsorption of Cinnamaldehyde on Icosahedral Au<sub>13</sub> and Pt<sub>13</sub> Clusters. *Acta Phys.-Chim. Sin.* **2015**, *31*, 885–892.
- (252) Li, L.; Wang, W.; Wang, X.; Zhang, L. Investigating the mechanism of the selective hydrogenation reaction of cinnamaldehyde catalyzed by Pt<sub>n</sub> clusters. *J. Mol. Model.* **2016**, *22*, 186.
- (253) Li, L.; Wei, W.; Wang, W.; Wang, X.; Zhang, L.; Tian, A. Selective hydrogenation of cinnamaldehyde catalyzed by Co-doped Pt clusters: a density functional theoretical study. *RSC Adv.* **2016**, *6*, 88277–88286.
- (254) Creemers, C.; Deurinck, P. Platinum Segregation to the (111) Surface of Ordered Pt<sub>80</sub>Fe<sub>20</sub>: LEIS Results and Model Simulations. *Surf. Interface Anal.* **1997**, *25*, 177–190.
- (255) Murillo, L. E.; Chen, J. G. Adsorption and reaction of propanal, 2-propenol and 1-propanol on Ni/Pt(111) bimetallic surfaces. *Surf. Sci.* **2008**, *602*, 2412–2420.
- (256) Jenness, G. R.; Vlachos, D. G. DFT Study of the Conversion of Furfuryl Alcohol to 2-Methylfuran on RuO<sub>2</sub> (110). *J. Phys. Chem. C* **2015**, *119*, 5938–5945.
- (257) Wildschut, J.; Mahfud, F. H.; Venderbosch, R. H.; Heeres, H. J. Hydrotreatment of Fast Pyrolysis Oil Using Heterogeneous Noble-Metal Catalysts. *Ind. Eng. Chem. Res.* **2009**, *48*, 10324–10334.
- (258) Leng, F.; Gerber, I. C.; Axet, M. R.; Serp, P. Selectivity shifts in hydrogenation of

- cinnamaldehyde on electron-deficient ruthenium nanoparticles. *C. R. Chim.* **2018**, *21*, 346–353.
- (259) Esan, D. A.; Trenary, M. Selective Hydrogenation of Acrolein to Propanal on a Pseudomorphic Pt/Ru(001) Bimetallic Surface. *Top. Catal.* **2018**, *61*, 318–327.
- (260) Esan, D. A.; Ren, Y.; Feng, X.; Trenary, M. Adsorption and Hydrogenation of Acrolein on Ru(001). *J. Phys. Chem. C* **2017**, *121*, 4384–4392.
- (261) Esan, D. A.; Trenary, M. Surface chemistry of propanal, 2-propenol, and 1-propanol on Ru(001). *Phys. Chem. Chem. Phys.* **2017**, *19*, 10870–10877.
- (262) Rojas, H. A.; Martínez, J. J.; Díaz, G.; Gómez-Cortés, A. The effect of metal composition on the performance of Ir–Au/TiO<sub>2</sub> catalysts for citral hydrogenation. *Appl. Catal. A Gen.* **2015**, *503*, 196–202.
- (263) Yang, Y.-J.; Teng, B.-T.; Liu, Y.; Wen, X.-D. Crotonaldehyde adsorption on Ir(1 1 1), an interesting *trans*- and *cis*-configuration transformation. *Appl. Surf. Sci.* **2015**, *357*, 369–375.
- (264) Wan, W.; Jenness, G. R.; Xiong, K.; Vlachos, D. G.; Chen, J. G. Ring-Opening Reaction of Furfural and Tetrahydrofurfuryl Alcohol on Hydrogen-Predosed Iridium(1 1 1) and Cobalt/Iridium(1 1 1) Surfaces. *ChemCatChem* **2017**, *9*, 1701–1707.
- (265) Schauermaun, S. Partial Hydrogenation of Unsaturated Carbonyl Compounds: Toward Ligand-Directed Heterogeneous Catalysis. *J. Phys. Chem. Lett.* **2018**, *9*, 5555–5566.
- (266) Dostert, K.-H.; Brien, C. P. O.; Mirabella, F.; Ivars-Barceló, F.; Schauermaun, S. Adsorption of acrolein, propanal, and allyl alcohol on Pd(111): a combined infrared reflection–absorption spectroscopy and temperature programmed desorption study. *Phys. Chem. Chem. Phys.* **2016**, *18*, 13960–13973.
- (267) Dostert, K.-H.; O'Brien, C. P.; Mirabella, F.; Ivars-Barceló, F.; Attia, S.; Spadafora, E.; Schauermaun, S.; Freund, H.-J. Selective Partial Hydrogenation of Acrolein on Pd: A

- Mechanistic Study. *ACS Catal.* **2017**, *7*, 5523–5533.
- (268) O'Brien, C. P.; Dostert, K.-H.; Schauermaun, S.; Freund, H.-J. Selective Hydrogenation of Acrolein Over Pd Model Catalysts : Temperature and Particle-Size Effects. *Chem. Eur. J.* **2016**, *22*, 15856–15863.
- (269) Naughton, J.; Lee, A. F.; Thompson, S.; Vinod, C. P.; Wilson, K. Reactivity of crotonaldehyde and propene over Au/Pd(111) surfaces. *Phys. Chem. Chem. Phys.* **2010**, *12*, 2670–2678.
- (270) Williams, R. M.; Pang, S. H.; Medlin, J. W. Ring-Opening and Oxidation Pathways of Furanic Oxygenates on Oxygen-Precovered Pd(111). *J. Phys. Chem. C* **2014**, *118*, 27933–27943.
- (271) Vorotnikov, V.; Mpourmpakis, G.; Vlachos, D. G. DFT Study of Furfural Conversion to Furan, Furfuryl Alcohol, and 2-Methylfuran on Pd(111). *ACS Catal.* **2012**, *2*, 2496–2504.
- (272) Yang, X.; Chen, D.; Liao, S.; Song, H.; Li, Y.; Fu, Z.; Su, Y. High-performance Pd–Au bimetallic catalyst with mesoporous silica nanoparticles as support and its catalysis of cinnamaldehyde hydrogenation. *J. Catal.* **2012**, *291*, 36–43.
- (273) Cattaneo, S.; Althahban, S.; Freakley, S. J.; Sankar, M.; Davies, T.; He, Q.; Dimitratos, N.; Kiely, C. J.; Hutchings, G. J. Synthesis of highly uniform and composition-controlled gold–palladium supported nanoparticles in continuous flow. *Nanoscale* **2019**, *11*, 8247–8259.
- (274) Liu, C.; Nan, C.; Fan, G.; Yang, L.; Li, F. Facile synthesis and synergistically acting catalytic performance of supported bimetallic PdNi nanoparticle catalysts for selective hydrogenation of citral. *Mol. Catal.* **2017**, *436*, 237–247.
- (275) Pino, N.; Sitthisa, S.; Tan, Q.; Souza, T.; López, D.; Resasco, D. E. Structure, activity, and selectivity of bimetallic Pd-Fe/SiO<sub>2</sub> and Pd-Fe/ $\gamma$ -Al<sub>2</sub>O<sub>3</sub> catalysts for the conversion of furfural. *J. Catal.* **2017**, *350*, 30–40.



- (276) Thompson, S. T.; Lamb, H. H. Palladium–Rhenium Catalysts for Selective Hydrogenation of Furfural : Evidence for an Optimum Surface Composition. *ACS Catal.* **2016**, *6*, 7438–7447.
- (277) Besenbacher, F.; Chorkendorff, I.; Clausen, B. S.; Hammer, B.; Molenbroek, A. M.; Nørskov, J. K.; Stensgaard, I. Design of a Surface Alloy Catalyst for Steam Reforming. *Science* **1998**, *279*, 1913–1915.
- (278) Marcinkowski, M. D.; Darby, M. T.; Liu, J.; Wimble, J. M.; Lucci, F. R.; Lee, S.; Michaelides, A.; Flytzani-Stephanopoulos, M.; Stamatakis, M.; Sykes, E. C. H. Pt/Cu single-atom alloys as coke-resistant catalysts for efficient C–H activation. *Nat. Chem.* **2018**, *10*, 325–332.
- (279) Réocreux, R.; Uhlman, M.; Thuening, T.; Kress, P.; Hannagan, R.; Stamatakis, M.; Sykes, E. C. H. Efficient and selective carbon–carbon coupling on coke-resistant PdAu single-atom alloys. *Chem. Commun.* **2019**, *55*, 15085–15088.
- (280) Zhou, L.; Martirez, J. M. P.; Finzel, J.; Zhang, C.; Swearer, D. F.; Tian, S.; Robotjazi, H.; Lou, M.; Dong, L.; Henderson, L.; Christopher, P.; Carter, E. A.; Nordlander, P.; Halas, N. J. Light-driven methane dry reforming with single atomic site antenna-reactor plasmonic photocatalysts. *Nat. Energy* **2020**, *5*, 61–70.
- (281) Raman, N.; Maise, S.; Grabau, M.; Taccardi, N.; Debuschewitz, J.; Wolf, M.; Wittkämper, H.; Bauer, T.; Wu, M.; Haumann, M.; Papp, C.; Görling, A.; Spiecker, E.; Libuda, J.; Steinrück, H.-P.; Wasserscheid, P. Highly Effective Propane Dehydrogenation Using Ga–Rh Supported Catalytically Active Liquid Metal Solutions. *ACS Catal.* **2019**, *9*, 9499–9507.
- (282) Taccardi, N.; Grabau, M.; Debuschewitz, J.; Distaso, M.; Brandl, M.; Hock, R.; Maier, F.; Papp, C.; Erhard, J.; Neiss, C.; Peukert, W.; Görling, A.; Steinrück, H.-P.; Wasserscheid, P. Gallium-rich Pd–Ga phases as supported liquid metal catalysts. *Nat. Chem.* **2017**, *9*, 862–

867.

- (283) Bailie, J. E.; Hutchings, G. J.; Abdullah, H. A.; Anderson, J. A.; Rochester, C. H. Effects of C5-heterocyclic compounds on CO adsorption and crotonaldehyde hydrogenation over supported Cu and Co catalysts. *Phys. Chem. Chem. Phys.* **2000**, *2*, 283–290.
- (284) Kouachi, K.; Lafaye, G.; Especel, C.; Cherifi, O.; Marécot, P. Effects of support and metal loading on the characteristics of Co based catalysts for selective hydrogenation of citral. *J. Mol. Catal. A Chem.* **2008**, *280*, 52–60.
- (285) Bertero, M.; Trasarti, F.; Moraweck, B.; Borgna, A.; Marchi, A. J. Selective liquid-phase hydrogenation of citral over supported bimetallic Pt–Co catalysts. *Appl. Catal. A Gen.* **2009**, *358*, 32–41.
- (286) Raj, K. J. A.; Prakash, M. G.; Mahalakshmy, R.; Elangovan, T.; Viswanathan, B. Liquid phase hydrogenation of crotonaldehyde over nickel supported on titania. *J. Mol. Catal. A Chem.* **2013**, *366*, 92–98.
- (287) Mahata, N.; Cunha, A. F.; Órfão, J. J. M.; Figueiredo, J. L. Highly selective hydrogenation of C=C double bond in unsaturated carbonyl compounds over NiC catalyst. *Chem. Eng. J.* **2012**, *188*, 155–159.
- (288) Zhao, H.; Song, H.; Chou, L. Nickel nanoparticles supported on MOF-5: Synthesis and catalytic hydrogenation properties. *Inorg. Chem. Commun.* **2012**, *15*, 261–265.
- (289) Numata, M.; Takahashi, R.; Yamada, I.; Nakanishi, K.; Sato, S. Sol–gel preparation of Ni/TiO<sub>2</sub> catalysts with bimodal pore structures. *Appl. Catal. A Gen.* **2000**, *383*, 66–72.
- (290) Chin, S.-Y.; Lin, F.-J.; Ko, A.-N. Vapour Phase Hydrogenation of Cinnamaldehyde over Ni/ $\gamma$ -Al<sub>2</sub>O<sub>3</sub> Catalysts: Interesting Reaction Network. *Catal. Letters* **2009**, *132*, 389–394.
- (291) Gryglewicz, S.; Śliwak, A.; Ćwikła, J.; Gryglewicz, G. Performance of Carbon Nanofiber and Activated Carbon Supported Nickel Catalysts for Liquid-Phase Hydrogenation of

Cinnamaldehyde into Hydrocinnamaldehyde. *Catal. Letters* **2014**, *144*, 62–69.

- (292) Yang, Y.; Chen, L.; Chen, Y.; Liu, W.; Feng, H.; Wang, B.; Zhang, X.; Wei, M. The selective hydrogenation of furfural over intermetallic compounds with outstanding catalytic performance. *Green Chem.* **2019**, *21*, 5352–5362.
- (293) Putro, W.; Kojima, T.; Hara, T.; Ichikuni, N.; Shimazu, S. Selective hydrogenation of unsaturated carbonyls by Ni–Fe-based alloy catalysts. *Catal. Sci. Technol.* **2017**, *7*, 3637–3646.
- (294) Shi, D.; Yang, Q.; Peterson, C.; Lamic-Humblot, A.-F.; Girardon, J.-S.; Griboval-Constant, A.; Stievano, L.; Sougrati, M. T.; Briois, V.; Bagot, P. A. J.; Wojcieszak, R.; Paul, S.; Marceau, E. Bimetallic Fe-Ni/SiO<sub>2</sub> catalysts for furfural hydrogenation: Identification of the interplay between Fe and Ni during deposition-precipitation and thermal treatments. *Catal. Today* **2019**, *334*, 162–172.
- (295) Jia, P.; Lan, X.; Li, X.; Wang, T. Highly Active and Selective NiFe/SiO<sub>2</sub> Bimetallic Catalyst with Optimized Solvent Effect for the Liquid-Phase Hydrogenation of Furfural to Furfuryl Alcohol. *ACS Sustain. Chem. Eng.* **2018**, *6*, 13287–13295.
- (296) Xu, C.; Zheng, L.; Liu, J.; Huang, Z. Furfural Hydrogenation on Nickel-promoted Cu-containing Catalysts Prepared from Hydrotalcite-Like Precursors. *Chin. J. Chem.* **2011**, *29*, 691–697.
- (297) Tang, F.; Wang, L.; Dessie Walle, M.; Mustapha, A.; Liu, Y.-N. An alloy chemistry strategy to tailoring the *d*-band center of Ni by Cu for efficient and selective catalytic hydrogenation of furfural. *J. Catal.* **2020**, *383*, 172–180.
- (298) Khromova, S. A.; Bykova, M. V.; Bulavchenko, O. A.; Ermakov, D. Y.; Saraev, A. A.; Kaichev, V. V.; Venderbosch, R. H.; Yakovlev, V. A. Furfural Hydrogenation to Furfuryl Alcohol over Bimetallic Ni–Cu Sol–Gel Catalyst: A Model Reaction for Conversion of

- Oxygenates in Pyrolysis Liquids. *Top. Catal.* **2016**, *59*, 1413–1423.
- (299) Rudolf, C.; Dragoi, B.; Ungureanu, A.; Chirieac, A.; Royer, S.; Nastro, A.; Dumitriu, E. NiAl and CoAl materials derived from takovite-like LDHs and related structures as efficient chemoselective hydrogenation catalysts. *Catal. Sci. Technol.* **2014**, *4*, 179–189.
- (300) Yang, L.; Jiang, Z.; Fan, G.; Li, F. The promotional effect of ZnO addition to supported Ni nanocatalysts from layered double hydroxide precursors on selective hydrogenation of citral. *Catal. Sci. Technol.* **2014**, *4*, 1123–1131.
- (301) Yu, W.; Xiong, K.; Ji, N.; Porosoff, M. D.; Chen, J. G. Theoretical and experimental studies of the adsorption geometry and reaction pathways of furfural over FeNi bimetallic model surfaces and supported catalysts. *J. Catal.* **2014**, *317*, 253–262.
- (302) Xiong, K.; Wan, W.; Chen, J. G. Reaction pathways of furfural, furfuryl alcohol and 2-methylfuran on Cu(111) and NiCu bimetallic surfaces. *Surf. Sci.* **2016**, *652*, 91–97.
- (303) Xiong, K.; Chen, J. G. Correlating furfural reaction pathways with interactions between furfural and monometallic surfaces. *Catal. Today* **2020**, *339*, 289–295.
- (304) Li, H.; Luo, H.; Zhuang, L.; Dai, W.; Qiao, M. Liquid phase hydrogenation of furfural to furfuryl alcohol over the Fe-promoted Ni-B amorphous alloy catalysts. *J. Mol. Catal. A Chem.* **2003**, *203*, 267–275.
- (305) Sitthisa, S.; An, W.; Resasco, D. E. Selective conversion of furfural to methylfuran over silica-supported Ni–Fe bimetallic catalysts. *J. Catal.* **2011**, *284*, 90–101.
- (306) Myint, M.; Yan, Y.; Chen, J. G. Reaction Pathways of Propanal and 1-Propanol on Fe/Ni(111) and Cu/Ni(111) Bimetallic Surfaces. *J. Phys. Chem. C* **2014**, *118*, 11340–11349.
- (307) Wang, M.-M.; He, L.; Liu, Y.-M.; Cao, Y.; He, H.-Y.; Fan, K.-N. Gold supported on mesostructured ceria as an efficient catalyst for the chemoselective hydrogenation of carbonyl compounds in neat water. *Green Chem.* **2011**, *13*, 602–607.

- (308) Bailie, J. E.; Hutchings, G. J. Promotion by sulfur of gold catalysts for crotyl alcohol formation from crotonaldehyde hydrogenation. *Chem. Commun.* **1999**, 2151–2152.
- (309) Schimpf, S.; Lucas, M.; Mohr, C.; Rodemerck, U.; Brückner, A.; Radnik, J.; Hofmeister, H.; Claus, P. Supported gold nanoparticles : in-depth catalyst characterization and application in hydrogenation and oxidation reactions. *Catal. Today* **2002**, *72*, 63–78.
- (310) Zanella, R.; Louis, C.; Giorgio, S.; Touroude, R. Crotonaldehyde hydrogenation by gold supported on TiO<sub>2</sub>: structure sensitivity and mechanism. *J. Catal.* **2004**, *223*, 328–339.
- (311) Okumura, M.; Akita, T.; Haruta, M. Hydrogenation of 1,3-butadiene and of crotonaldehyde over highly dispersed Au catalysts. *Catal. Today* **2002**, *74*, 265–269.
- (312) Yoshitake, H.; Saito, N. Selective hydrogenation of crotonaldehyde on Au supported on mesoporous titania. *Microporous Mesoporous Mater.* **2013**, *168*, 51–56.
- (313) Hayashi, S.; Ishida, R.; Hasegawa, S.; Yamazoe, S.; Tsukuda, T. Doping a Single Palladium Atom into Gold Superatoms Stabilized by PVP : Emergence of Hydrogenation Catalysis. *Top. Catal.* **2018**, *61*, 136–141.
- (314) Hong, Y.-C.; Sun, K.-Q.; Zhang, G.-R.; Zhong, R.-Y.; Xu, B.-Q. Fully dispersed Pt entities on nano-Au dramatically enhance the activity of gold for chemoselective hydrogenation catalysis. *Chem. Commun.* **2011**, *47*, 1300–1302.
- (315) Lucas, M.; Claus, P. Hydrogenations over Silver: A Highly Active and Chemoselective Ag-In/SiO<sub>2</sub> Catalyst for the One-Step Synthesis of Allyl Alcohol from Acrolein. *Chem. Eng. Technol.* **2005**, *28*, 867–870.
- (316) Manikandan, M.; Venugopal, A. K.; Nagpure, A. S.; Chilukuri, S.; Raja, T. Promotional effect of Fe on the performance of supported Cu catalyst for ambient pressure hydrogenation of furfural. *RSC Adv.* **2016**, *6*, 3888–3898.
- (317) Sitthisa, S.; Sooknoi, T.; Ma, Y.; Balbuena, P. B.; Resasco, D. E. Kinetics and mechanism

- of hydrogenation of furfural on Cu/SiO<sub>2</sub> catalysts. *J. Catal.* **2011**, *277*, 1–13.
- (318) Vargas-Hernández, D.; Rubio-Caballero, J. M.; Santamaría-González, J.; Moreno-Tost, R.; Mérida-Robles, J. M.; Pérez-Cruz, M. A.; Jiménez-López, A.; Hernández-Huesca, R.; Maireles-Torres, P. Furfuryl alcohol from furfural hydrogenation over copper supported on SBA-15 silica catalysts. *J. Mol. Catal. A Chem.* **2014**, *383*, 106–113.
- (319) Fulajtárova, K.; Soták, T.; Hronec, M.; Vávra, I.; Dobročka, E.; Omastová, M. Aqueous phase hydrogenation of furfural to furfuryl alcohol over Pd–Cu catalysts. *Appl. Catal. A Gen.* **2015**, *502*, 78–85.
- (320) Wang, Y.; Miao, Y.; Li, S.; Gao, L.; Xiao, G. Metal-organic frameworks derived bimetallic Cu-Co catalyst for efficient and selective hydrogenation of biomass-derived furfural to furfuryl alcohol. *Mol. Catal.* **2017**, *436*, 128–137.
- (321) Mohr, C.; Hofmeister, H.; Claus, P. Identification of Active Sites in Gold-Catalyzed Hydrogenation of Acrolein. *J. Am. Chem. Soc.* **2003**, *125*, 1905–1911.
- (322) Kang, G.-J.; Chen, Z.-X.; Li, Z. Acrolein Adsorption on Gold Clusters, A Theoretical Study of Conjugation Effect on C=C and C=O Interaction with Au Clusters. *Catal. Letters* **2011**, *141*, 996-1003.
- (323) Xiao, X.-C.; Shi, W.; Ni, Z.-M. Selective Hydrogenation Mechanism of Cinnamaldehyde on Au(111) Surface. *Acta Phys.-Chim. Sin.* **2014**, *30*, 1456–1464.
- (324) Szumelda, T.; Drelinkiewicz, A.; Kosydar, R.; Gurgul, J. Hydrogenation of cinnamaldehyde in the presence of PdAu/C catalysts prepared by the reverse "water-in-oil" microemulsion method. *Appl. Catal. A Gen.* **2014**, *487*, 1–15.
- (325) Zhang, Y.; Yang, X.; Zhou, Y.; Li, G.; Li, Z.; Liu, C.; Bao, M.; Shen, W. Selective hydrogenation of the C=C bond in  $\alpha,\beta$ -unsaturated aldehydes and ketones over ultra-small Pd–Au clusters. *Nanoscale* **2016**, *8*, 18626–18629.

- (326) Cao, Y.; Jiang, J.; Ni, Z.; Xia, S.; Qian, M.; Xue, J. Cluster Properties of Au<sub>19</sub>Pt and Selective Hydrogenation Mechanism of Cinnamaldehyde on Au<sub>19</sub>Pt Cluster Surface. *Chem. J. Chinese U.* **2016**, *37*, 1342–1350.
- (327) Claus, P.; Hofmeister, H. Electron Microscopy and Catalytic Study of Silver Catalysts: Structure Sensitivity of the Hydrogenation of Crotonaldehyde. *J. Phys. Chem. B* **1999**, *103*, 2766–2775.
- (328) Haass, F.; Bron, M.; Fuess, H.; Claus, P. In situ X-ray investigations on AgIn/SiO<sub>2</sub> hydrogenation catalysts. *Appl. Catal. A Gen.* **2007**, *318*, 9–16.
- (329) Osaka, N.; Ishitsuka, M.; Hiaki, T. Infrared reflection absorption spectroscopic study of adsorption structure of self-assembled monolayer film of trithiocyanuric acid on evaporated silver film. *J. Mol. Struct.* **2009**, *921*, 144–149.
- (330) Plessers, E.; De Vos, D. E.; Roeyffers, M. B. J. Chemoselective reduction of  $\alpha,\beta$ -unsaturated carbonyl compounds with UiO-66 materials. *J. Catal.* **2016**, *340*, 136–143.
- (331) Steffan, M.; Lucas, M.; Brandner, A.; Claus, P. Selective Hydrogenation of Citral in an Organic Solvent, in a Ionic Liquid, and in Substance. *Chem. Eng. Technol.* **2007**, *30*, 481–486.
- (332) Fujii, S.; Osaka, N.; Akita, M.; Itoh, K. Infrared Reflection Absorption Spectroscopic Study on the Adsorption Structures of Acrolein on an Evaporated Silver Film. *J. Phys. Chem.* **1995**, *99*, 6994–7001.
- (333) Ren, G.; Wang, G.; Mei, H.; Xu, Y.; Huang, L. Reaction mechanism investigation of furfural conversion to 2-methylfuran on Cu(111) surface. *Chem. Phys. Lett.* **2018**, *703*, 1–7.
- (334) Cao, Y.; Guerrero-Sánchez, J.; Lee, I.; Zhou, X.; Takeuchi, N.; Zaera, F. Kinetic Study of the Hydrogenation of Unsaturated Aldehydes Promoted by CuPt<sub>x</sub>/SBA-15 Single-Atom Alloy (SAA) Catalysts. *ACS Catal.* **2020**, *10*, 3431–3443.

- (335) Kyriakou, G.; Boucher, M. B.; Jewell, A. D.; Lewis, E. A.; Lawton, T. J.; Baber, A. E.; Tierney, H. L.; Flytzani-Stephanopoulos, M.; Sykes, E. C. H. Isolated Metal Atom Geometries as a Strategy for Selective Heterogeneous Hydrogenations. *Science* **2012**, *335*, 1209–1212.
- (336) Lucci, F. R.; Marcinkowski, M. D.; Lawton, T. J.; Sykes, E. C. H. H<sub>2</sub> Activation and Spillover on Catalytically Relevant Pt–Cu Single Atom Alloys. *J. Phys. Chem. C* **2015**, *119*, 24351–24357.
- (337) Lucci, F. R.; Liu, J.; Marcinkowski, M. D.; Yang, M.; Allard, L. F.; Flytzani-Stephanopoulos, M.; Sykes, E. C. H. Selective hydrogenation of 1,3-butadiene on platinum–copper alloys at the single-atom limit. *Nat. Commun.* **2015**, *6*, 8550.
- (338) Lucci, F. R.; Lawton, T. J.; Pronschinske, A.; Sykes, E. C. H. Atomic Scale Surface Structure of Pt/Cu(111) Surface Alloys. *J. Phys. Chem. C* **2014**, *118*, 3015–3022.
- (339) Tierney, H. L.; Baber, A. E.; Kitchin, J. R.; Sykes, E. C. H. Hydrogen Dissociation and Spillover on Individual Isolated Palladium Atoms. *Phys. Rev. Lett.* **2009**, *103*, 246102.
- (340) Patel, D. A.; Kress, P. L.; Cramer, L. A.; Larson, A. M.; Sykes, E. C. H. Elucidating the composition of PtAg surface alloys with atomic-scale imaging and spectroscopy. *J. Chem. Phys.* **2019**, *151*, 164705.
- (341) Simonovis, J.; Tillekaratne, A.; Zaera, F. The Role of Carbonaceous Deposits in Hydrogenation Catalysis Revisited. *J. Phys. Chem. C* **2017**, *121*, 2285–2293.
- (342) Kubota, J.; Ohtani, T.; Kondo, J. N.; Hirose, C.; Domen, K. IRAS study of  $\pi$ -bonded ethylene on a Pt(111) surface in the presence of gaseous ethylene and hydrogen. *Appl. Surf. Sci.* **1997**, *121*, 548–551.
- (343) Vignola, E.; Steinmann, S. N.; Al Farra, A.; Vandegheuchte, B. D.; Curulla, D.; Sautet, P. Evaluating the Risk of C-C Bond Formation during Selective Hydrogenation of Acetylene



- on Palladium. *ACS Catal.* **2018**, *8*, 1662–1671.
- (344) Divi, S.; Chatterjee, A. Generalized nano-thermodynamic model for capturing size-dependent surface segregation in multi-metal alloy nanoparticles. *RSC Adv.* **2018**, *8*, 10409–10424.
- (345) Lotfi, S.; Brgoch, J. Discovering Intermetallics Through Synthesis, Computation, and Data-Driven Analysis. *Chem. Eur. J.* **2020**, *26*, 8689–8697.
- (346) Bligaard, T.; Bullock, R. M.; Campbell, C. T.; Chen, J. G.; Gates, B. C.; Gorte, R. J.; Jones, C. W.; Jones, W. D.; Kitchin, J. R.; Scott, S. L. Toward Benchmarking in Catalysis Science: Best Practices, Challenges, and Opportunities. *ACS Catal.* **2016**, *6*, 2590–2602.
- (347) Rase, H. F. *Handbook of Commercial Catalysts: Heterogeneous Catalysts*; CRC Press: Raton, FL, 2016.
- (348) Greczynski, G.; Hultman, L. X-ray photoelectron spectroscopy: Towards reliable binding energy referencing. *Prog. Mater. Sci.* **2020**, *107*, 100591.
- (349) Radnik, R.; Mohr, C.; Claus, P. On the origin of binding energy shifts of core levels of supported gold nanoparticles and dependence of pretreatment and material synthesis. *Phys. Chem. Chem. Phys.* **2003**, *5*, 172–177.
- (350) Baer, D. R.; Artyushkova, K.; Cohen, H.; Easton, C. D.; Engelhard, M.; Gengenbach, T. R.; Greczynski, G.; Mack, P.; Morgan, D. J.; Roberts, A. XPS guide: Charge neutralization and binding energy referencing for insulating samples. *J. Vac. Sci. Technol. A* **2020**, *38*, 031204.
- (351) Zugic, B.; Wang, L.; Heine, C.; Zakharov, D. N.; Lechner, B. A. J.; Stach, E. A.; Biener, J.; Salmeron, M.; Madix, R. J.; Friend, C. M. Dynamic restructuring drives catalytic activity on nanoporous gold–silver alloy catalysts. *Nat. Mater.* **2017**, *16*, 558–564.
- (352) Doherty, R. P.; Krafft, J.-M.; Méthivier, C.; Casale, S.; Remita, H.; Louis, C.; Thomas, C. On the promoting effect of Au on CO oxidation kinetics of Au-Pt bimetallic nanoparticles

supported on SiO<sub>2</sub>: An electronic effect? *J. Catal.* **2012**, *287*, 102–113.

- (353) Xin, H. L.; Alayoglu, S.; Tao, R.; Genc, A.; Wang, C.-M.; Kovarik, L.; Stach, E. A.; Wang, L.-W.; Salmeron, M.; Somorjai, G. A.; Zheng, H. Revealing the Atomic Restructuring of Pt–Co Nanoparticles. *Nano Lett.* **2014**, *14*, 3203–3207.
- (354) Luneau, M.; Guan, E.; Chen, W.; Foucher, A. C.; Marcella, N.; Shirman, T.; Verbart, D. M. A.; Aizenberg, J.; Aizenberg, M.; Stach, E. A.; Madix, R. J.; Frenkel, A. I.; Friend, C. M. Enhancing catalytic performance of dilute metal alloy nanomaterials. *Commun. Chem.* **2020**, *3*, 46.
- (355) Jiang, J.; Xia, S.; Ni, Z.; Zhang, L. Adsorption and Selective Hydrogenation Mechanism of Crotonaldehyde on Au(111) Surface. *Chem. J. Chinese U.* **2016**, *37*, 693–700.
- (356) Zhang, G.; Zhang, X.; Meng, Y.; Zhou, X.; Pan, G.; Ni, Z.; Xia, S. Experimental and theoretical investigation into visible-light-promoted selective hydrogenation of crotonaldehyde to crotonyl alcohol using Au–Co,Ni alloy nanoparticle supported layered double hydroxides. *J. Mater. Chem. A* **2018**, *6*, 15839–15852.
- (357) Fang, L.; Luo, W.; Meng, Y.; Zhou, X.; Pan, G.; Ni, Z.; Xia, S. Visible-Light-Promoted Selective Hydrogenation of Crotonaldehyde by Au Supported ZnAl-Layered Double Hydroxides: Catalytic Property, Kinetics, and Mechanism Investigation. *J. Phys. Chem. C* **2018**, *122*, 17358–17369.
- (358) Jiang, J.-H.; Qian, M.-D.; Xue, J.-L.; Xia, S.-J.; Ni, Z.-M.; Shao, M.-M. Comparison of Properties of In-Au(111) and Ir-Au(111) Alloy Surfaces, and Their Adsorption to Crotonaldehyde. *Acta Phys.-Chim. Sin.* **2016**, *32*, 2932–2940.

## **Biographies**

Mathilde Luneau received her PhD in Chemistry from the University of Lyon, France under the supervision of Drs Nolven Guilhaume and Frédéric Meunier at the Institute of Researches on Catalysis and Environment of Lyon (IRCELYon). She is currently a postdoctoral researcher in the group of Prof. Cynthia Friend at Harvard University. With an expertise in catalytic reactor studies and design, her research focuses on dilute alloy catalysts for selective oxidation and selective hydrogenation reactions in both the gas phase and the liquid phase.

David (Jin Soo) Lim received B.A. Chemistry and B.S.E. Chemical and Biomolecular Engineering from the University of Pennsylvania in 2016 through the Vagelos Integrated Program in Energy Research. He is currently a Ph.D. candidate in Chemistry at Harvard University, where he pursues computational catalysis research under the joint supervision of Prof. Cynthia Friend and Prof. Boris Kozinsky.

Dipna A. Patel is currently a Chemistry Ph.D. candidate in Prof. Charles Sykes's group at Tufts University working on the design and characterization of model Cu and Ag based single-atom alloys. Using a combination of scanning tunneling microscopy, temperature-programmed desorption, and infrared spectroscopy, she aims to correlate observed reactivity of selective hydrogenation and dehydrogenation reactions with the atomic-scale structure.

E. Charles H. Sykes is the John Wade Professor of Chemistry at Tufts University. Charles received B.S. and M.S. degrees with first class honors from Oxford University in 1998 before moving to Cambridge University for a Ph.D. under the supervision of Professor Richard Lambert. He then relocated to the U.S. for a postdoctoral fellowship with Professor Paul Weiss at Penn State.

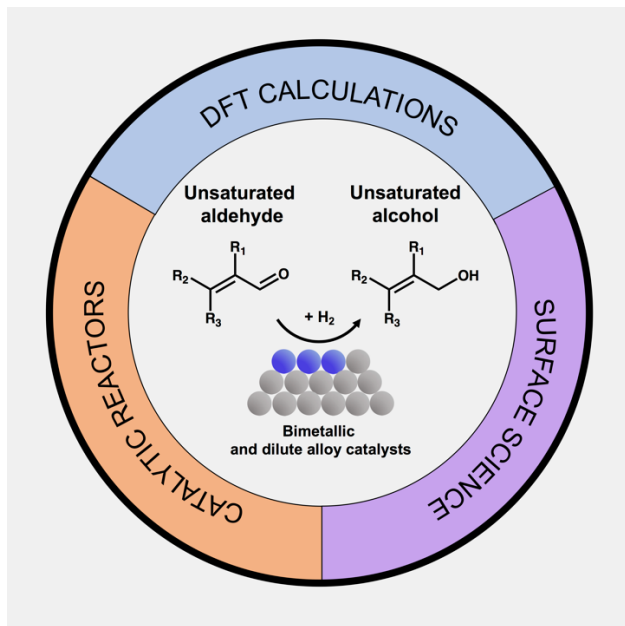
In 2005 Charles began his independent career as an Assistant Professor of Chemistry at Tufts University. He was tenured and promoted to Associate Professor in 2010, promoted Full Professor in 2013, and awarded the John Wade Chair in Chemistry in 2019. Research in the Sykes lab utilizes state of the art scanning probes and surface science instrumentation to study technologically important systems. Early work in the lab lead to the development of the first single-molecule electric motor and the group continue to hold the Guinness World record for the world's smallest electric motor. The major focus of the Sykes lab is now the development of new *single-atom alloy* catalysts which were first discovered by Sykes using surface science and microscopy studies. Sykes was named a Beckman Young Investigator, Research Corporation Cottrell Scholar, IUPAC young observer, and the Usen Family Career Development Professor in 2008. He is also the recipient of a 2009 NSF CAREER award, a 2011 Camille Dreyfus Teacher-Scholar Award and the 2012 AVS Peter Mark Memorial Award. Charles received the Young Talented Scientist Award at Chirality 2014 and was named a Fellow of the Royal Society of Chemistry in 2015. In 2018 Charles was named a Fellow of the AVS and, together with the late Maria Flytzani-Stephanopoulos, was awarded the 2019 ACS Catalysis Lectureship for the Advancement of Catalytic Sciences. He is the author of over 150 peer-reviewed publications and has given over 160 invited talks at conferences and universities.

Cynthia M. Friend is the T.W. Richards Professorship of Chemistry and Professor of Materials Science at Harvard University. Friend joined the Harvard faculty in 1982 after earning her Ph.D. from the University of California, Berkeley in 1981. She graduated from the University of California, Davis in 1977 with a degree in Chemistry and was a postdoctoral fellow at Stanford University in Chemical Engineering. Friend's current research is focused on developing solutions to important problems in energy usage and environmental chemistry. She continues to advance diversity and excellence in scientific research and teaching through her leadership. She is currently

the Director of the IMASC Energy Frontier Research Center at Harvard, which focuses on sustainable production of chemicals, is Vice-Chair of the Basic Energy Sciences Advisory Committee (BESAC) for the U.S. Department of Energy, and is a member of the Board of Directors of Bruker Instruments Corporation. Previously, she was the Director of the Rowland Institute, Associate Dean of the Faculty of Arts and Sciences and the Chair of the Department of Chemistry and Chemical Biology at Harvard. She also served as the Assoc. Director for the Photon Sciences Directorate of SLAC National Laboratory at Stanford, 2011-12. Friend is a fellow of the National Academy of Sciences, American Academy of Arts and Sciences, the American Association of the Advancement of Science, and the American Chemical Society, and a recipient of a Humboldt Senior Research Fellowship in 2007. She is also the recipient of three national American Chemical Society Awards: the 2017 Award in Surface Chemistry, the 2009 George Olah Award in Hydrocarbon Chemistry, and the 1991 Garvan Medal.

Philippe Sautet has studied at “Ecole Polytechnique” in Paris and defended his doctorate in Theoretical Chemistry at Orsay University (Paris XI) in 1989. He then joined the Centre National de la Recherche Scientifique (CNRS) at the Institute of Research on Catalysis in Lyon, where he developed and led a group devoted to the applications of theoretical chemistry to heterogeneous catalysis. He spent a sabbatical at Berkeley University. After being the director of the laboratory of Chemistry at the Ecole Normale Supérieure of Lyon for 8 years, he was the director of the “Institut de Chimie de Lyon,” a cluster of chemistry laboratories in Lyon, from 2007 to 2015. Philippe Sautet is now the Distinguished Professor at the Chemical and Biomolecular Engineering department and at the Chemistry and Biochemistry department of the University of California, Los Angeles (UCLA). He acts as the vice chair for graduate studies of the Chemical and Biomolecular Engineering department and is the deputy director of the IMASC Energy Frontier Research Center. He acts as the associate editor of ACS Catalysis, an international journal published by the American

Chemical Society. His research interests are in the theory of the electronic structure at the interface between a solid surface and molecules and the modeling of elementary steps of heterogeneous catalysis. He received several awards including the silver medal of CNRS in 2007, the Paul Pascal Prize of the French Academy of Science in 2008 and the Pierre Süe Grand Prize of the French Chemical Society in 2012. He was elected at the French Academy of Science in 2010. In addition, France distinguished him in 2011 as “Chevalier de l'Ordre National du Mérite” for his action in research and research organization and in 2015 as “Chevalier de l'ordre des palmes académiques” for his teaching and action towards students.



**Toc graphics**